EFFECTS OF GLASS FIBER CONTENT, 3D-PRINTING AND WEATHERING ON THE PERFORMANCE OF POLYLACTIDE

A THESIS SUBMITTED TO
THE GRADUATE SCHOOL OF NATURAL AND APPLIED SCIENCES
OF
MIDDLE EAST TECHNICAL UNIVERSITY

BY

SAKİNE DENİZ VARSAVAŞ

IN PARTIAL FULFILLMENT OF THE REQUIREMENTS
FOR
THE DEGREE OF MASTER OF SCIENCE
IN
METALLURGICAL AND MATERIALS ENGINEERING

SEPTEMBER 2017

Approval of the thesis:

EFFECTS OF GLASS FIBER CONTENT, 3D-PRINTING AND WEATHERING ON THE PERFORMANCE OF POLYLACTIDE

submitted by **SAKİNE DENİZ VARSAVAŞ** in partial fulfillment of the requirements for the degree of **Master of Science in of Metallurgical and Materials Engineering Department, Middle East Technical University** by,

Prof. Dr. Gülbin Dural Ünver _____
Dean, Graduate School of **Natural and Applied Sciences**

Prof. Dr. Cemil Hakan Gür _____
Head of Department, **Metallurgical and Materials Eng.**

Prof. Dr. Cevdet Kaynak _____
Supervisor, **Metallurgical and Materials Eng. Dept., METU**

Examining Committee Members:

Prof. Dr. Arcan Dericioğlu _____
Metallurgical and Materials Engineering Dept., METU

Prof. Dr. Cevdet Kaynak _____
Metallurgical and Materials Engineering Dept., METU

Assist. Prof. Dr. Şeniz Reyhan Kuşhan Akın _____
Materials Science and Eng. Dept., Çankaya University

Assist. Prof. Dr. Simge Çınar _____
Metallurgical and Materials Engineering Dept., METU

Assist. Prof. Dr. Mert Efe _____
Metallurgical and Materials Engineering Dept., METU

DATE: 07.09.2017

I hereby declare that all information in this document has been obtained and presented in accordance with academic rules and ethical conduct. I also declare that, as required by these rules and conduct, I have fully cited and referenced all material and results that are not original to this work.

Name, Last Name : Sakine Deniz Varsavaş

Signature :

ABSTRACT

EFFECTS OF GLASS FIBER CONTENT, 3D-PRINTING AND WEATHERING ON THE PERFORMANCE OF POLYLACTIDE

Varsavaş, Sakine Deniz

M. S., Department of Metallurgical and Materials Engineering

Supervisor: Prof. Dr. Cevdet Kaynak

September 2017, 116 pages

The purpose of the first part of this thesis was to investigate how optimum mechanical properties (strength-modulus-toughness) of inherently very brittle polylactide (PLA) could be obtained by reinforcing with E-glass fibers (GF) and blending with thermoplastic polyurethane elastomer (TPU). Composites and blends were compounded by twin-screw extruder melt mixing, while specimens were shaped by injection molding. SEM analyses revealed that 15 wt% GF reinforcements and 10 wt% TPU domains, alone or together, could be uniformly distributed in the PLA matrix leading to significant improvements in properties. Mechanical tests indicated that use of TPU blending alone resulted in enormous increases in the ductility and fracture toughness values, while GF reinforcements led to significant increases in strength and elastic modulus values. When GF and TPU were added together, it was observed that crack deflection, debonding and fiber pull-out toughening mechanisms of GF reinforcements were as effective as the rubber toughening mechanism of TPU blending. Additionally, DSC thermograms revealed that crystallinity amount of PLA would be increased almost two times due to especially heterogeneous nucleation site actions of GF reinforcements and fine sized TPU domains.

In the second part of the thesis, the purpose was to compare performance of PLA based materials shaped by the traditional injection molding technique versus 3D-printing additive manufacturing. Comparisons were performed not only for neat PLA but also

for its TPU blend and GF reinforced composites. Performance comparison of the injection molded and 3D-printed specimens were especially conducted to compare their mechanical properties (strength-modulus-toughness) by tensile, flexural and fracture toughness tests. Other comparisons such as their macro-level appearances, fracture surface morphology and thermal behavior were also performed by photographic images, SEM, DSC and TGA analysis. It can be concluded that use of 3D-printing in the shaping of neat PLA and PLA/TPU blend was generally very beneficial; on the other hand, due to the differences in the orientation of the GF reinforcements, there could be certain reductions in the mechanical performance of PLA/GF and PLA/TPU/GF composite specimens.

The objective of the last part of this thesis was to explore the degree of improvement in the resistance of biodegradable PLA structure against atmospheric weathering (outdoor) conditions when reinforced with only 15 wt% GF. For this purpose, both neat PLA and PLA/GF composite specimens were exposed to accelerated weathering conditions of both UV-irradiation and moisture cycles in accordance with ISO 4892-3 standards for various periods till 400 hours. Many characterization techniques revealed that the alterations in the structure and properties of the specimens were due to the drastic decrease in the molecular weight of the PLA matrices via chain scission reactions. It was observed that reductions in the mechanical properties (strength-modulus-toughness) of the neat PLA were much more critical compared to the reductions in the PLA/GF composite. For instance, the reduction in the tensile strength of the neat PLA specimen was as much as 92%; while that reduction for the PLA/GF specimen was only 34%. Because, inorganic strong glass structure of the GF reinforcements having almost no chemical degradation during weathering periods kept their actions in the composite strengthening-stiffening-toughening mechanisms.

Keywords: Polylactide, Glass Fiber, Thermoplastic Polyurethane Elastomer, Injection Molding, 3D-Printing, Accelerated Weathering

ÖZ

CAM ELYAF MİKTARININ, 3D-YAZICI İLE ŞEKİLLENDİRMENİN VE ATMOSFERİK YAŞLANDIRMANIN POLİLAKTİTİN PERFORMANSINA ETKİLERİ

Varsavaş, Sakine Deniz
Yüksek Lisans, Metalurji ve Malzeme Mühendisliği Bölümü
Tez Yöneticisi: Prof. Dr. Cevdet Kaynak
Eylül 2017, 116 sayfa

Bu tez çalışmasının birinci bölümünün amacı, özünde çok kırılgan bir malzeme olan polilaktitin (PLA) E-cam elyafları (GF) ile takviye edilerek ve termoplastik poliüretan elastomer (TPU) ile harmanlanarak optimum mekanik özelliklerinin (mukavemet-modül-tokluk) nasıl elde edilebileceğini araştırmaktır. Kompozitler ve harmanlar, çift vidalı ekstrüder kullanılarak eriyik karıştırma yöntemi ile üretilmiş, numuneler ise enjeksiyon kalıplama yöntemi ile şekillendirilmiştir. SEM analizleri ağırlıkça %15 GF takviyelerinin ve ağırlıkça %10 TPU fazlarının ayrı ayrı veya bir arada PLA matrisinde homojen olarak dağılabildiklerini, dolayısıyla özelliklerde önemli iyileşmelere neden olduklarını ortaya çıkarmıştır. Mekanik testler, tek başına TPU harmanlamanın süneklik ve kırılma tokluğu değerlerinde muazzam artışlarla sonuçlandığını, GF takviyelerinin ise mukavemet ve elastik modül değerlerinde önemli artışlara neden olduğunu göstermiştir. GF ve TPU birlikte eklendiğinde, GF takviyelerinin çatlak sapması (crack deflection), matris-elyaf ayrışması (debonding) ve elyaf çıkması (pull-out) toklaştırma mekanizmalarının en az TPU harmanlamanın elastomerik toklaştırma (rubber toughening) mekanizması kadar etkili olduğu gözlenmiştir. Ek olarak, DSC termogramları, özellikle GF takviyelerinin ve mikron boyutlu TPU fazlarının heterojen çekirdeklendirici gibi davranarak PLA'nın kristallenme miktarını yaklaşık iki kat arttırdığını ortaya koymuştur.

Bu tezin ikinci bölümünün hedefi ise, geleneksel enjeksiyon kalıplama tekniği ile şekillendirilmiş PLA bazlı malzemelerin 3D-yazıcı / eklemeli üretim tekniğine karşı performansını karşılaştırmaktır. Karşılaştırmalar yalnızca saf PLA için değil aynı zamanda TPU harmanı ve GF takviyeli kompozitler için de yapılmıştır. Enjeksiyon kalıplama ve 3D yazıcı teknikleri ile şekillendirilmiş numunelerin performans karşılaştırmaları çekme, eğme ve kırılma tokluğu testleri ile özellikle mekanik özellikleri (mukavemet-modül-tokluk) için yapılmıştır. Diğer karşılaştırmalar, örneğin makro görünüm, kırılma yüzeyi morfolojisi ve ısıl davranış; fotografik görüntüleme, SEM, DSC ve TGA analizleri ile gerçekleştirilmiştir. Sonuç olarak; saf PLA ve PLA/TPU harmanları için 3D-yazıcı tekniği ile şekillendirmenin genel olarak oldukça iyi sonuçlar verdiği; GF takviyelerinin oryantasyonundaki farklılıklardan dolayı ise PLA/GF ve PLA/TPU/GF kompozit numunelerin mekanik performanslarında belirli düşüşlerin olabildiği gözlemlenmiştir.

Bu tezin son bölümünün amacı ise ağırlıkça %15 GF ile takviye edilmiş biyo-bozunur bir polimer olan PLA'nın yapısının atmosferik yaşlanmaya karşı dayanıklılığındaki gelişme derecesini araştırmaktır. Bu amaç için saf PLA ve PLA/GF kompozit numuneleri, ISO 4892-3 standartlarına uygun olarak hem UV irradyasyonu hem de nem döngülerini içeren hızlandırılmış yaşlandırma koşullarına 400 saate kadar maruz bırakılmıştır. Kullanılan birçok karakterizasyon tekniği, numunelerin yapısında ve özelliklerinde oluşan değişikliklerin, zincir kesilme reaksiyonları nedeniyle PLA matrisinin molekül ağırlığındaki önemli düşülerden kaynaklandığını ortaya koymuştur. PLA/GF kompozindeki düşüşlere kıyasla saf PLA'nın mekanik özelliklerindeki (mukavemet-modül-tokluk) düşüşlerin çok daha kritik olduğu gözlenmiştir. Örneğin, saf PLA numunesinin çekme mukavemetindeki azalma %92'ye kadar çıkmışken; PLA/GF numunesi için bu azalma sadece %34'tür. Çünkü, inorganik güçlü cam yapıları nedeniyle GF takviyeleri atmosferik yaşlandırma döngüleri sırasında neredeyse hiç kimyasal bozunmaya uğramadıkları için, kompozit güçlendirme ve toklaştırma mekanizmalarındaki etkinliklerini koruyabilmişlerdir.

Anahtar Kelimeler: Polilaktit, Cam Elyaf, Termoplastik Poliüretan Elastomer, Enjeksiyon Kalıplama, 3D-Yazıcı, Hızlandırılmış Atmosferik Yaşlandırma

in memory of my beloved father

ACKNOWLEDGEMENTS

I would like to thank to my supervisor Prof. Dr. Cevdet Kaynak for his valuable advice, guidance and, patience at each stage of this thesis, and the opportunity to become a TUBITAK project researcher.

I would like to gratefully acknowledge TUBITAK, the Scientific and Technological Research Council of Turkey, for the grant with the Project number 315M556.

I would like to acknowledge all the technical staff and administrative board of the Metallurgical and Materials Engineering Department for supplying all the research facilities required in this dissertation. I would also like to express my sincere gratitude to METU Central Laboratory for SLS analyses.

I want to thank my laboratory mates, Yelda Meyva Zeybek, Burcu Sarı, Ulaş Can and Berk Doğu, for their friendship and support.

My special thanks go to, Cansu Savaş, Gürhan Gümüşsu, Betül Özen, Tuğçe Biçer, Ebru Orhan, Dilara Demir, Özak Durmuş and Berhan Melek for helping me get through the hard time, and for all the support and entertainment.

I would like to express my deepest thankfulness to my father Osman Varsavaş, my mother Seyhan Varsavaş, my lovely sister Evrim Karaman, her husband Onur Karaman, and my lovely little niece Arya. They have been a constant love and encouragement in each step of my life from childhood to adulthood. This dissertation would certainly be not possible without their support.

TABLE OF CONTENTS

LIST OF TABLES

LIST OF FIGURES

NOMENCLATURE

σ_{TS}	:	tensile strength
σ_{Flex}	:	flexural strength
ε_f	:	elongation at break, final strain
ΔH_m	:	heat of melting
ΔH_c	:	heat of crystallization
$\Delta H_m°$	:	melting enthalpy of 100% crystalline PLA
E	:	Young's modulus
E_{Flex}	:	flexural modulus
$G_{ıc}$	:	fracture toughness as critical strain energy release rate
$K_{ıc}$	:	fracture toughness as critical stress intensity factor
ATR-FTIR	:	attenuated total reflectance fourier transform infrared spectroscopy
DSC	:	differential scanning calorimetry
PLA	:	poly(lactic acid) or polylactide
PLLA	:	L-enantiomer of polylactide
PDLA	:	D-enantiomer of polylactide
GF	:	glass fiber
TPU	:	thermoplastic polyurethane elastomer
IM	:	injection molding
3D	:	3D-printing
SEM	:	scanning electron microscopy

TGA	**:**	thermogravimetric analysis
$T_{5wt\%}$	**:**	thermal degradation temperature at 5 wt% mass loss
$T_{10wt\%}$	**:**	thermal degradation temperature at 10 wt% mass loss
$T_{25wt\%}$	**:**	thermal degradation temperature at 25 wt% mass loss
T_c	**:**	cold crystallization temperature
T_g	**:**	glass transition temperature
T_m	**:**	melting temperature
T_{max}, T_d	**:**	thermal degradation temperature of maximum mass loss rate
X_c	**:**	degree of crystallinity

CHAPTER 1

INTRODUCTION

1.1 Polylactides

Engineering polymers both thermoplastics and thermosets have been taking place of many conventional metallic and ceramic materials day by day due to their low weight and ease of processing. Nonetheless, since many of these engineering polymers are petroleum-based, polymer industry has encountered some problems namely difficulty in access to petrochemical resources and rising costs [1]. This situation creates a need for development of bio-based polymers classified as biopolymers. Poly(L-lactic acid), also termed polylactide (PLA) (Figure 1.1), is today one of the most significant thermoplastic biopolymer with aliphatic polyester structure. As first time in 1845 by Peluoze a low molecular weight PLA was produced via the condensation of L-lactic acid (LA) and continuous water removal; however, it was not commercialized at that time until 1990s. In 1992, Cargill Inc. was patented a continuous process to obtain high molecular weight PLA from the direct ring-opening polymerization of renewable LA obtained from corn starch, and the first industrial PLA production plant was founded in 2002 [2].

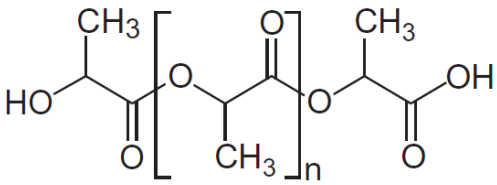

Figure 1.1 Chemical structure of PLA [3]

The main constitutional part of the polylactide macromolecule is lactic acid. Due to the chirality of lactic acid, there are two enantiomers of lactic acid, namely L-lactic acid and D-lactic acid. These two isomers could produce three distinctive forms given in Figure 1.2: optically active L,L-lactide and D,D-lactide and optically inactive D,L-lactide (*meso*-lactide), as well as the mixture of L,L-lactide and D,L-lactide having 50/50 ratio called *racemic*-lactide. Polymerization of these forms creates the poly(L-lactic acid) (PLLA) which is a semi-crystalline material, poly(D-lactic acid) (PDLA) which is a crystallizable material, and *meso*-PLA which is amorphous product of polymerization of *meso*-lactide [4].

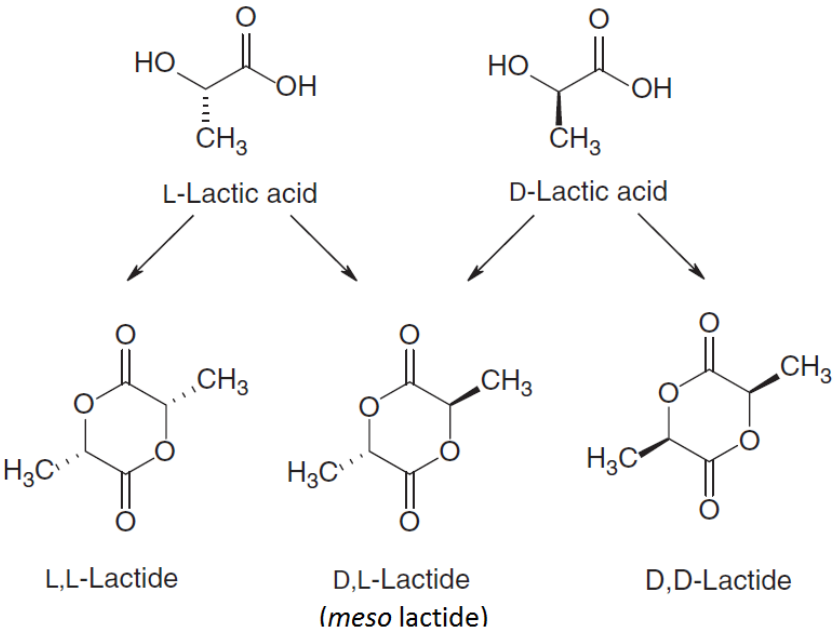

Figure 1.2 Stereoisomers of Lactic Acid [4]

PLLA is the most available type commercially used in the packaging, automobile interiors, electronics cases, etc. On the other hand, for the applications necessitating higher mechanical performance, or higher thermal/hydrolytic stability, apart from the composites making; the stereocomlexation of two different enantiomers (PLLA and PDLA) are the effective approaches used for obtaining high-performance PLA based materials. Because the same enantiomers (PLLA and PLLA, or PDLA and PDLA) have weaker interactions; whereas, in stereocomplexation, there is very strong interactions between PLLA and PDLA polymeric chains resulting in improved performance of polylactide [5].

During synthesis of PLA, high purity monomers are required because the impurities cause the reduced polymer quality. Functional groups like hydroxyl and carboxyl can be regarded as impurities. In the presence of hydroxyl functionalities, although the polymerization rate rises, the molecular weight is reduced and molecular weight distribution of the final product is broadened. On the other hand, the presence of carboxylic functionalities makes complex with the catalyst resulting in decreased polymerization rate; however, molecular weight of the final product is not affected [6]. There are mainly 4 different synthesis routes of PLA given schematically in Figure 1.3.

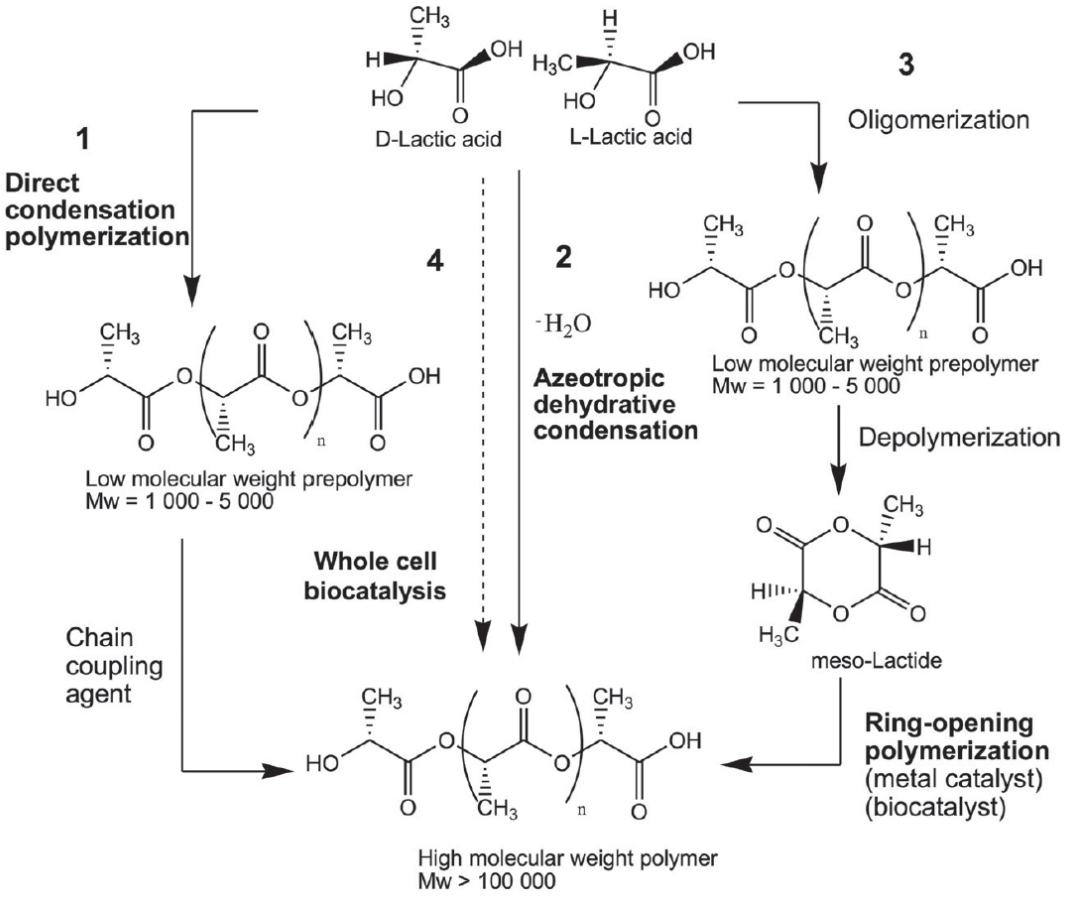

Figure 1.3 Main synthesis routes of PLA [7]

The first route to synthesize PLA is the "direct condensation polymerization" (*route 1* in Figure 1.3) which is the cheapest route and yielding low molecular weight products. Properties are deficient for most applications; therefore, by using chain coupling

agents (anhydrides, epoxides or isocyanates) the higher molecular weight products are achieved. Yet, this creates a need for purification step to remove the unreacted coupling agents [7].

"Azeotropic dehydrative condensation polymerization" is another route which yields directly high molecular weight PLA (*route 2* in Figure1.3). The process comprises of the elimination of the condensation water of lactic acid, then the addition of high amount of catalyst and diphenyl ester, and heating up the mixture to reflux for 30-40h at 103°C. Lastly, purification process of PLA to remove catalyst residues is applied [7].

Today, the most preferred route to produce high molecular weight polylactide is the "ring-opening polymerization" (ROP) (*route 3* in Figure 1.3). In this process, first of all a low molecular weight prepolymer is produced by oligomerization, and then this prepolymer is depolymerized into dehydrated cyclic dimers to obtain lactides (3,6-dimethyl-1,4-dioxane- 2,5-dione) which is the starting material of ROP. This crude lactide contains high amount of impurities causing low molecular weight products with high racemization. Therefore, before polymerization lactide is purified and by ROP the high molecular weight PLA is obtained [6, 7].

The last route "whole-cell biocatalysis" (*route 4*, Figure 1.3) is a relatively new process and continue to progress. In 2008 a new lactate-polymerizing enzyme was discovered. This enzyme creates a lactide enrich polymer, a PLA homopolymer [7].

Semicrystalline PLA has quite remarkable mechanical properties compared to many common use polymers such as PE, PP, PS and PET. Thanks to its Young's modulus, for example, it is an alternative to general-use polymers in applications such as short-time packaging processes. In addition, environmental friendly profile, biocompatibility, suitability to be traditionally processed, and relatively affordable prices are the reasons for increased use from day to day.

1.2 Glass Fibers

In composite industry glass fibers have been used for a variety of application by using different fabrication technologies. The first use of glass fiber was in ancient Egypt to produce containers by drawing glass fibers from a hot glass. More recently, in 1930s the first continuous glass fibers were produced for the high temperature electrical equipment. From then on, glass fibers have become widespread in many industries, namely electrical, automotive, aviation, civil, etc. [8]. There are several types of glass fibers available which have different chemical compositions related to desired properties. The classification scheme of glass fibers is given in Figure 1.4 while their chemical compositions are given in Table 1.1 as defined in the American Society for Testing and Materials (ASTM) D578: Standard Specification for Glass Fiber Strands and International Organization for Standardization (ISO) 2078: Textile Glass - Yarns - Designation.

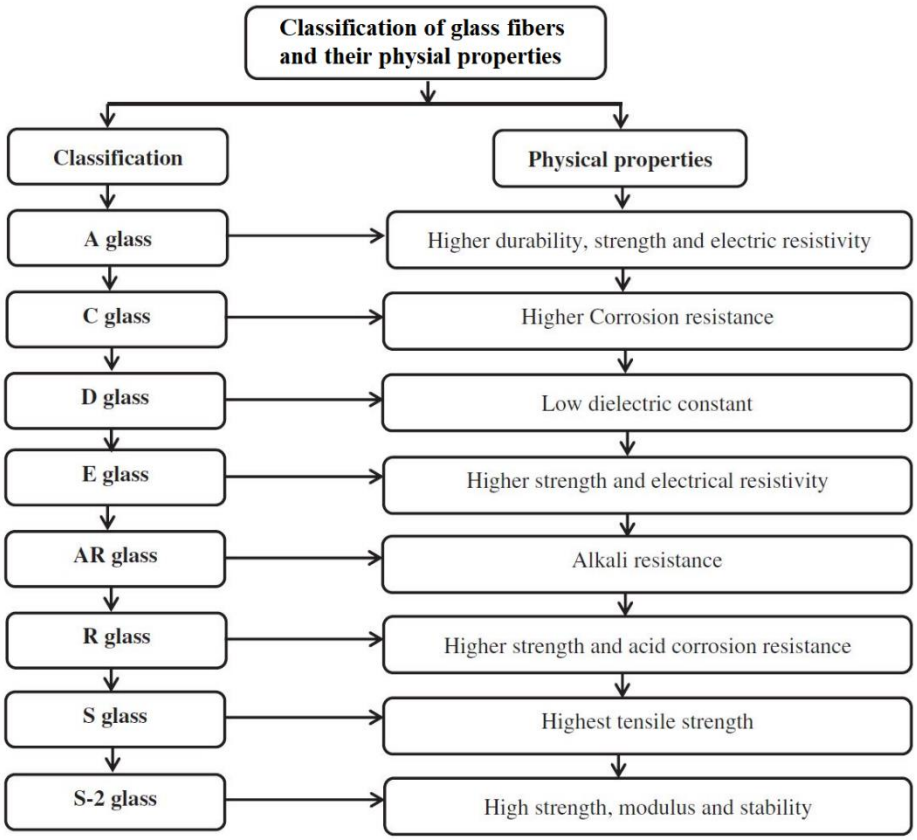

Figure 1.4 Classification and physical properties of glass fibers [8]

The most commonly used glass fiber in industry is E-glass fibers due to its availability and low cost. Aside from its brittleness, it has very high effective tensile strength, i.e. approximately 1700 MPa. Although the bulk glasses suffer from the microscopic surface defects acting as crack initiation and propagation sites resulting in lower strength, glasses in fiber forms have very low possibility of defects (due to their low volume under load); thus, they can reach much higher strength levels. Moreover, their surfaces are coated (sized) to keep them away the damages. The "size" is applied on the surface of the glass fibers just after their exit from the bushings. Sizing material is an aqueous solution containing a polymeric binder to protect against the friction of other fibers during processing, and a coupling agent, generally an "organo-silane". While the organic part of this molecule makes bonds with the polymeric matrices, silane part attaches itself to glass fiber surfaces acting as a bridge between the glass fiber and polymeric matrices [9].

To produce glass fibers, the batch, containing the ingredients of desired glass fiber composition given in Table 1.1, is transferred to the heated furnace to melt. During the motion of the molten glass along a channel, it starts to cool down. Once the molten glass reaches the multiple forehearts, where it gets ready to fiberize with multiple fiberizing positions, fibers are pulled through microscopic orifices which located on the metal bushing. Pulled from the bushing out fibers are fast cooled, gathered, and sized. If the fibers are to be used in continuous form, they fed to a winder; otherwise, i.e. short glass fibers, they fed to a chopper [10]. These processes are illustrated in Figure 1.5.

Table 1.1 Chemical compositions of glass fiber types in wt% [8]

Type	**SiO_2**	**Al_2O_3**	**TiO_2**	**B_2O_3**	**CaO**	**MgO**	**Na_2O**	**K_2O**	**Fe_2O_3**
E-glass	55.0	14.0	0.2	7.0	22.0	1.0	0.5	0.3	-
C-glass	64.6	4.1	-	5.0	13.4	3.3	9.6	0.5	-
S-glass	65.0	25.0	-	-	-	10.0	-	-	-
A-glass	67.5	3.5	-	1.5	6.5	4.5	13.5	3.0	-
D-glass	74.0	-	-	22.5	-	-	1.5	2.0	-
R-glass	60.0	24.0	-	-	9.0	6.0	0.5	0.1	-
EGR-glass	61.0	13	-	-	22.0	3.0	-	0.5	-
Basalt	52.0	17.2	1.0	-	8.6	5.2	5.0	1.0	5.0

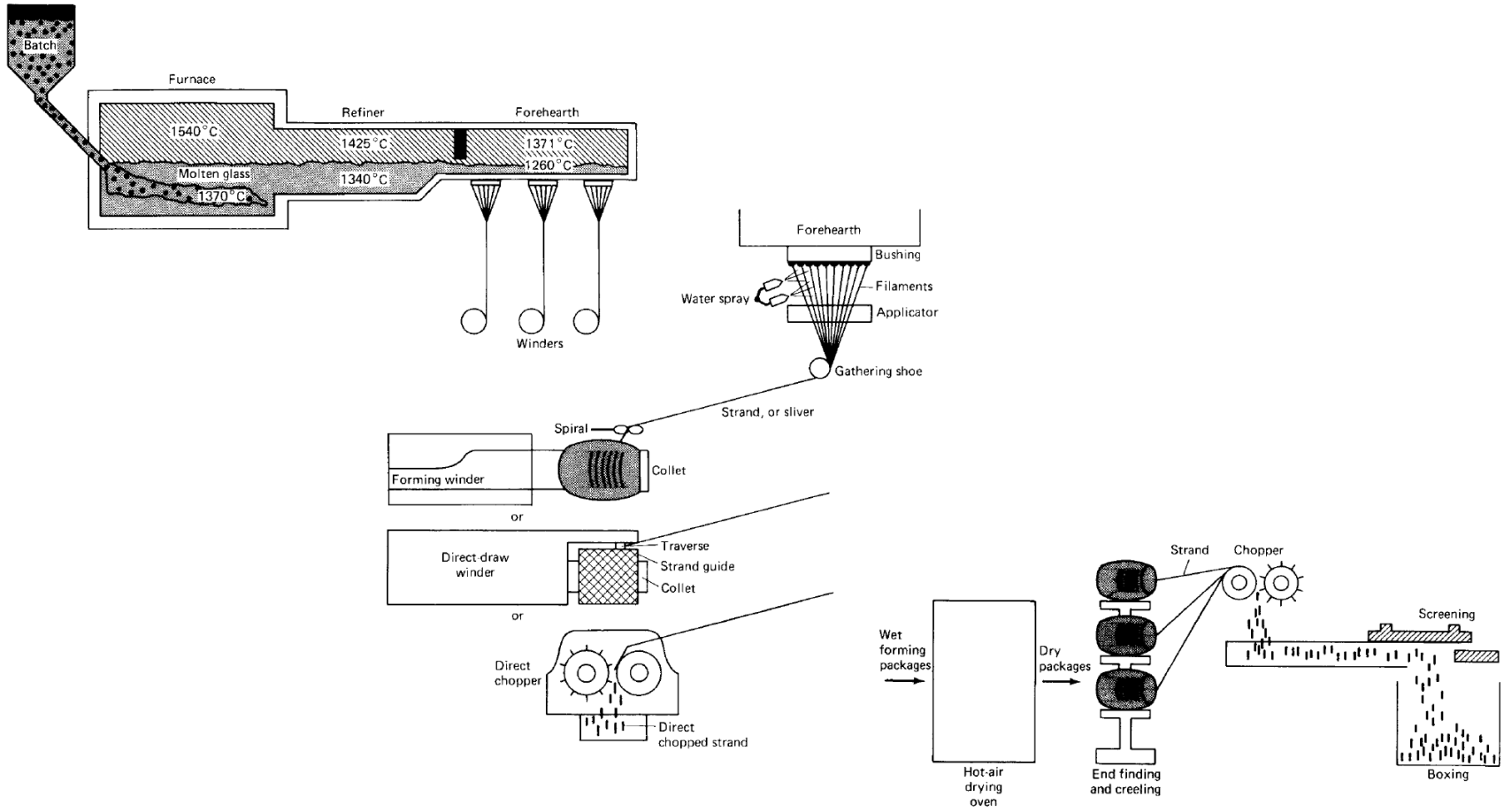

Figure 1.5 Typical glass fiber production route [11]

After the production of continuous glass fibers, they are transformed into several forms according to their composite applications. Commercially important glass fiber forms are:

- *Roving* is a single large strand composed of packs of strands wound of a cylinder. Multi-end rovings are used in the production of bath tubs, shower trays, and many marine products by spray-up fabrication process; and several glass fiber reinforced polymer automobile parts produced by sheet molding compound. On the other hand, single-end rovings are used to produce structural composites parts such as tanks and pipes via filament winding and pultrusion.
- *Woven roving* is a form of fiberglass rovings weaved into fabric. This is used in glass fiber reinforced polymer products manufactured by panel molding and hand lay-up processes.
- *Mats* can be continuous or chopped strand mats forms. Short glass fibers are randomly bound onto a belt or chain by a chemical binder to produce chopped strand mats; similarly, if the continuous fibers are used to bind onto belt or chain, continuous strand mats are produced.
- *Combination of a mat and woven roving* is a recent product used for specific purposes obtained by lay-up process of alternating fiberglass mat and woven roving layers.
- *Textile yarns* are produced from fine fiber strands by air-drying on the forming tubes.
- *Chopped strands / short glass fibers* manufactured by either wet forming or direct chop processes shown in Figure 1.5. In the wet forming process, wet forming packages are firstly dried. Then, these packages are gathered and fed to a chopper. Chopped fibers are screened and packaged to ship. On the other hand, in direct chop process, wet strands formed at the bushing are directly chopped after the sizing. Then chopped fibers are gathered, dried, screened and packaged to ship. These products are mostly used for thermoplastics in injection molding industry. However, they can also be used for reinforcing thermosets in bulk molding compounds [11].

1.3 Thermoplastic Polyurethane Elastomers

The very first homogenous elastomeric materials having the processability of thermoplastics was the thermoplastic polyurethane (TPU) elastomers. The production of TPU elastomers pioneered the rising trend of thermoplastic elastomers [12]. Nowadays, the TPU elastomers has been widely used in automotive interiors, footwear, flexible hose and tubing, cellphone buttons, closures, seals and o-rings, adhesives, cable jacketing, sport and leisure items, textiles and textile coatings, photovoltaic cell encapsulation, and wastewater treatment equipment, etc. [13].

Thermoplastic polyurethane elastomers are linear, block copolymers consisting of alternating soft segment (long chain diols) and hard segments (diisocyanates and short-chain extender) as given in Figure 1.6. The majority of the elastic properties of TPU elastomers are due to the soft segments which act as an elastomeric matrix; while the roles of the hard segments are crosslinking, and reinforcing as fillers. Additionally, this crosslinking is not a chemical crosslinking. The action of heat or solvents can break down the crosslinks in the hard segments, but this effect is recoverable by removing the heat or solvent [12].

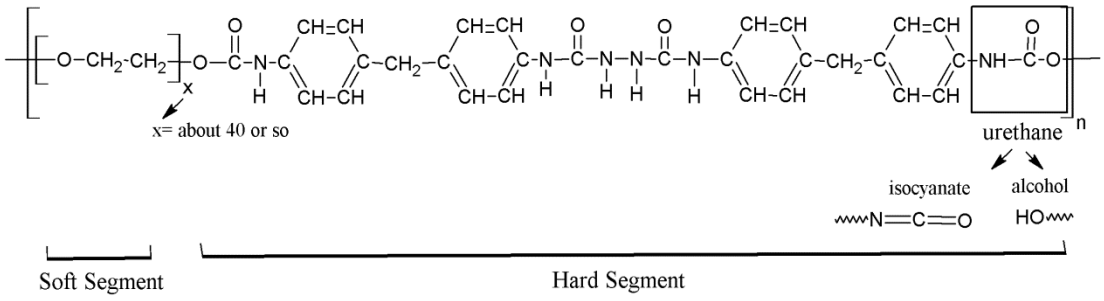

Figure 1.6 Chemical structure of TPU elastomers

The secret of the remarkable mechanical properties and the thermoplastic nature of TPU elastomers is the micro phase separation of the soft and hard segments due to incompatibility at room temperature resulting in a nanoscale texture formed by soft and hard domains [13]. In the hard segments crystallization is observed to some extent; in addition, the polarity and melting temperature of soft segments is lower than that of

the hard segments significantly. These factors are the driving force of the phase separation. Above the melting temperature of hard segments, a homogeneous viscous melt is obtained which enables processability; on the other hand, as it cools to room temperature, soft and hard segment domains are regained leading to elastic properties (Figure 1.7) [12]. This phase separated morphology originates the higher toughness and tensile strength than that of other elastomeric materials having covalent crosslinks. Moreover, lacking of the chemical crosslinking results in processability via extrusion, injection molding, compression molding, etc. [14].

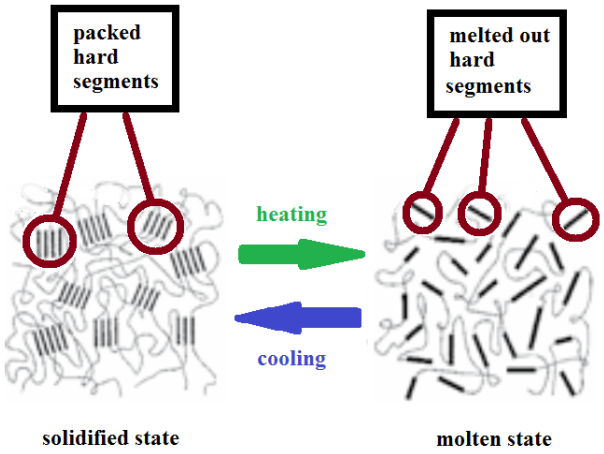

Figure 1.7 Graphical illustration of the morphology of TPU elastomers

1.4 3D-Printing

3D-Printing technology is a form of additive manufacturing defined as the transformation of a digital model of an object in the computer media into a real product by adding a proper material layer-by-layer [15]. In Figure 1.8 [16] the evolution of this technology in time and also futuristic expectations are given. The first patented 3D-printer was invented in 1986 by Charles Hull, which was named as Stereo Lithography (SLA). After that, in 1989 "Fused Deposition Modelling" (FDM) and "Selective Laser Sintering" (SLS) technologies were developed. Starting from 2007, the "RepRap Movement", which was an open source low cost 3D-printer trend introduced by Dr. Adrian Bowyer, spread to the world. RepRap is based upon the FDM process which produce its own components to replicate itself. Since the expiration of the patents of

FDM and SLS technologies in 2014, 3D-printing has become more and more popular as prototyping and manufacturing technique in various sectors as given in Figure 1.9, the results of the survey conducted by the marketing research company IDC (International Data Corporation) showing the market distribution of 3D-printing use in 2016 [17].

3D printing technology can be categorized into three main classes and their subgroups as listed in Figure 1.10. The first one is "Fused Deposition Modelling" (FDM) process. In this process, the 3D object is manufactured in a laying down fashion by fusing a thermoplastic material layer by layer. Secondly, in "Stereo Lithography" (SLA) process photo curing action of UV blue light is used to transform a of liquid thermoset resin into solid 3D objects. On the other hand, in the "Selective Laser Sintering" (SLS) process, powders of a metal, or a ceramic or an alloy as first layer laying thin layers are sintered selectively. After sintering the completely, another powder layer is spread and this process continues until the 3D object is formed [18]. According to a survey conducted by *Sculpteo*, a French 3D-printing company, and published in *Forbes*, an American business magazine, given in Figure 1.11, the most preferred 3D-Printing technologies in the world by 2016 were Selective Laser Sintering (SLS) and Fused Deposition Modelling (FDM) by 38% and 31%, respectively [19].

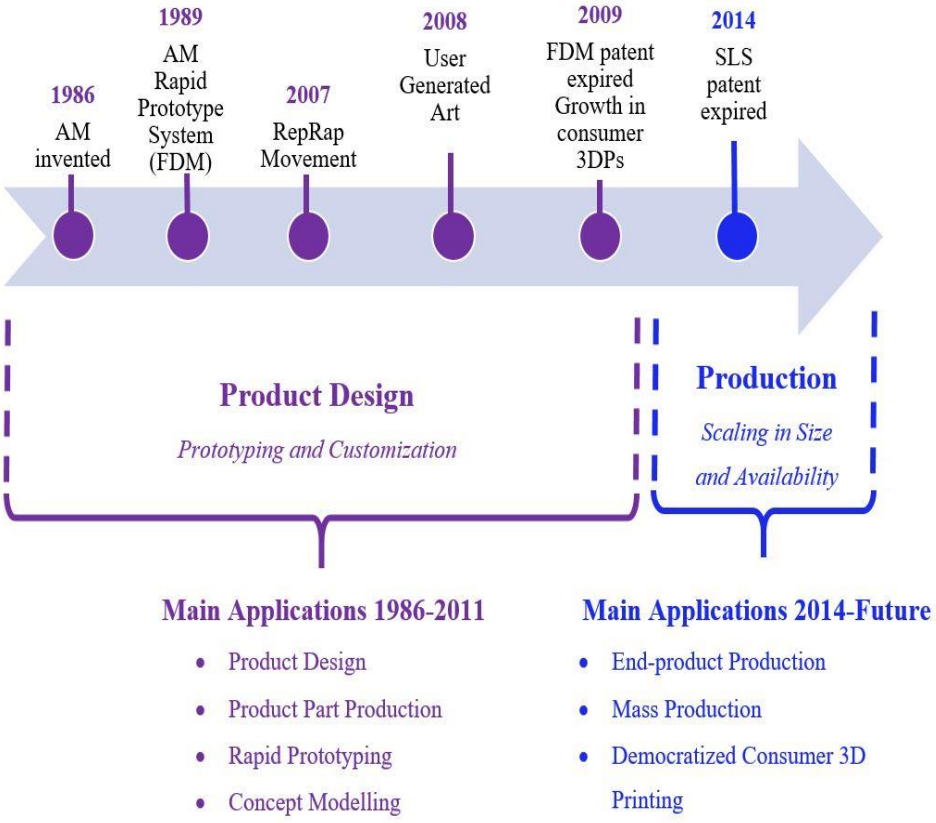

Figure 1.8 Evolution of 3D-Printing technology [16]

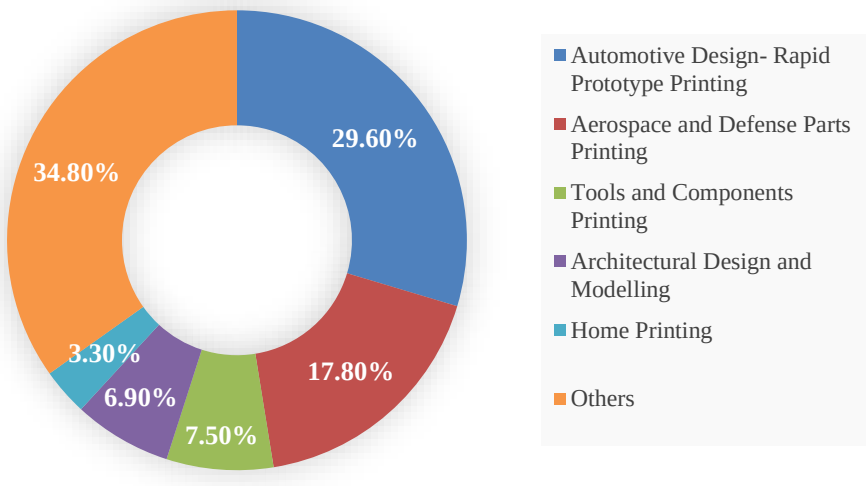

Figure 1.9 3D-Printing Market Distribution Worldwide in 2016, by use case [17]

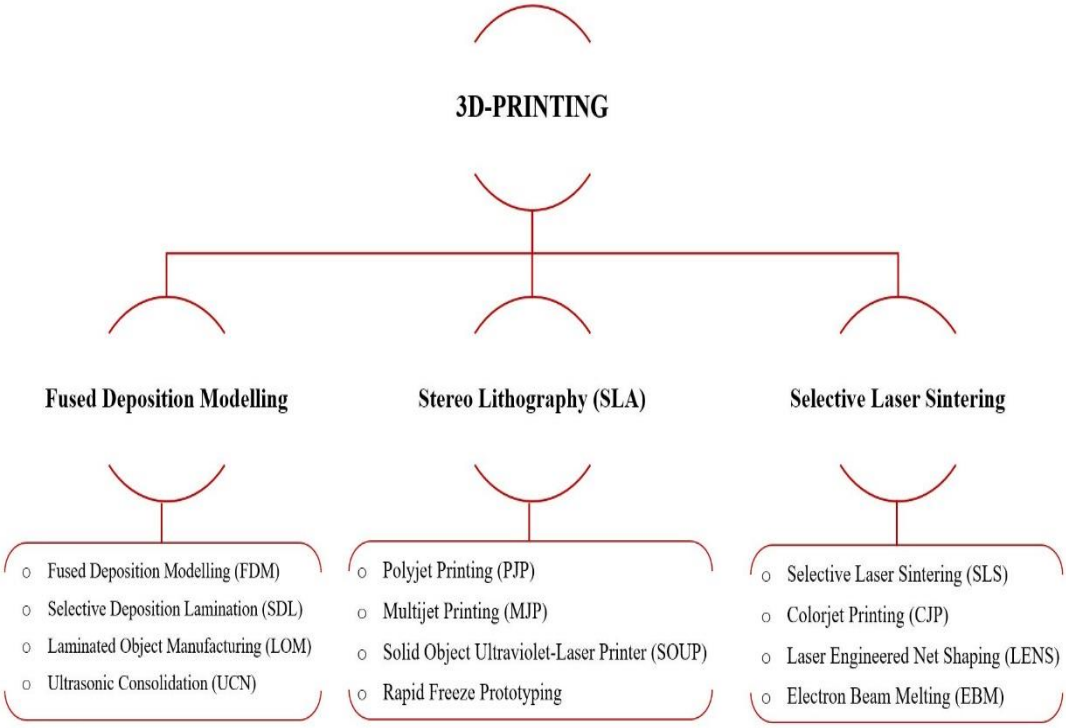

Figure 1.10 Classification of 3D-printing processes

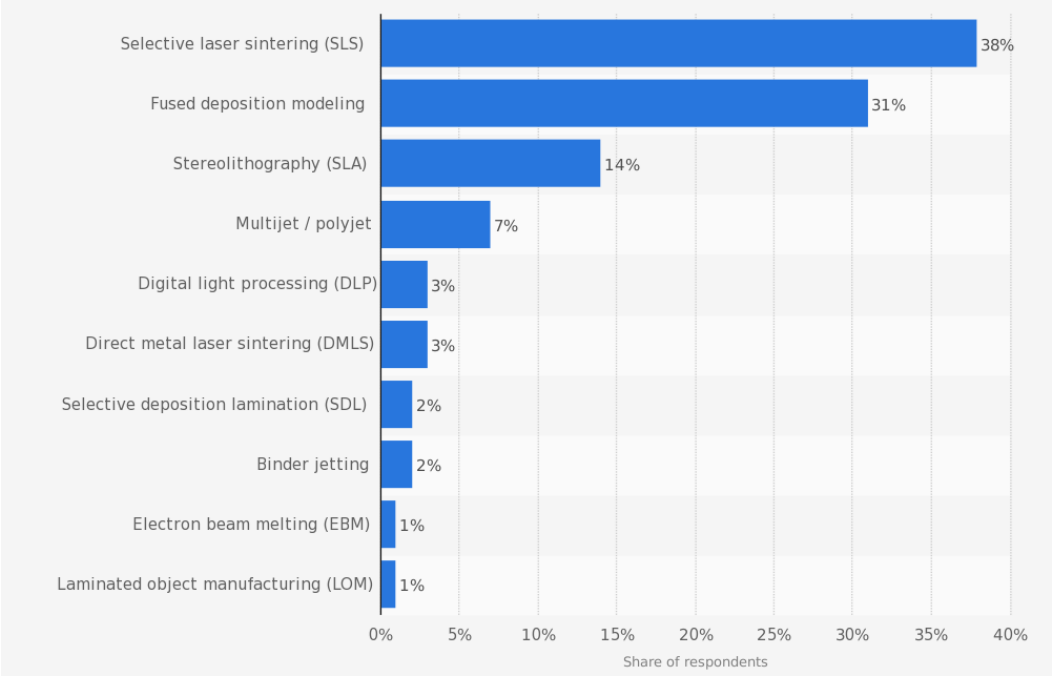

Figure 1.11 Preferred 3D-technologies, as of early 2016 [19]

The FDM method has the highest potential for final product production compared to other Additive Manufacturing (AM) technologies. In this process, as shown in Figure 1.12, a thermoplastic filament material is smoothly passed through the extrusion system and then softened in the heater core to a temperature above the melting temperature, then the fluidized material is pushed out of the nozzle head and solidification takes place layer by layer. This head system operates by computer control, creating the wall of the object and then filling the inner part in each layer [20]. Today, as the filament raw materials for FDM process, many thermoplastics such as PLA (polylactide), ABS (acrylonitrile-butadiene-styrene), PC (polycarbonate), PA (polyamide) etc. are used. According to the latest data reported in July 2017 [21] (Figure 1.13), among these thermoplastics, PLA and ABS filaments dominate the market. Since PLA is produced from renewable sources like corn starch, its sustainability and environmentally friendly nature makes it stand out against other petroleum-based alternatives. In addition, PLA has lower melting temperature than ABS; therefore, it allows less energy consumption during production and higher dimensional stability preventing warping. All these advantages make the PLA the most preferred filament material in 3D-printing market.

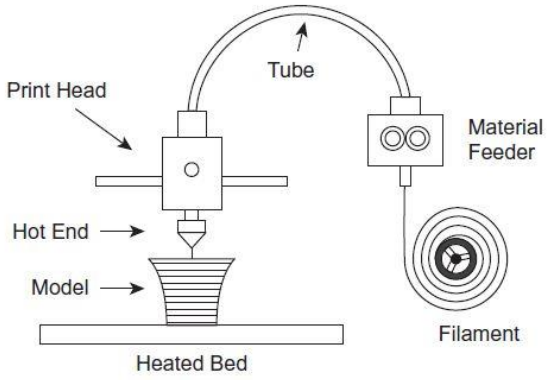

Figure 1.12 Schematic representation of the FDM process [18]

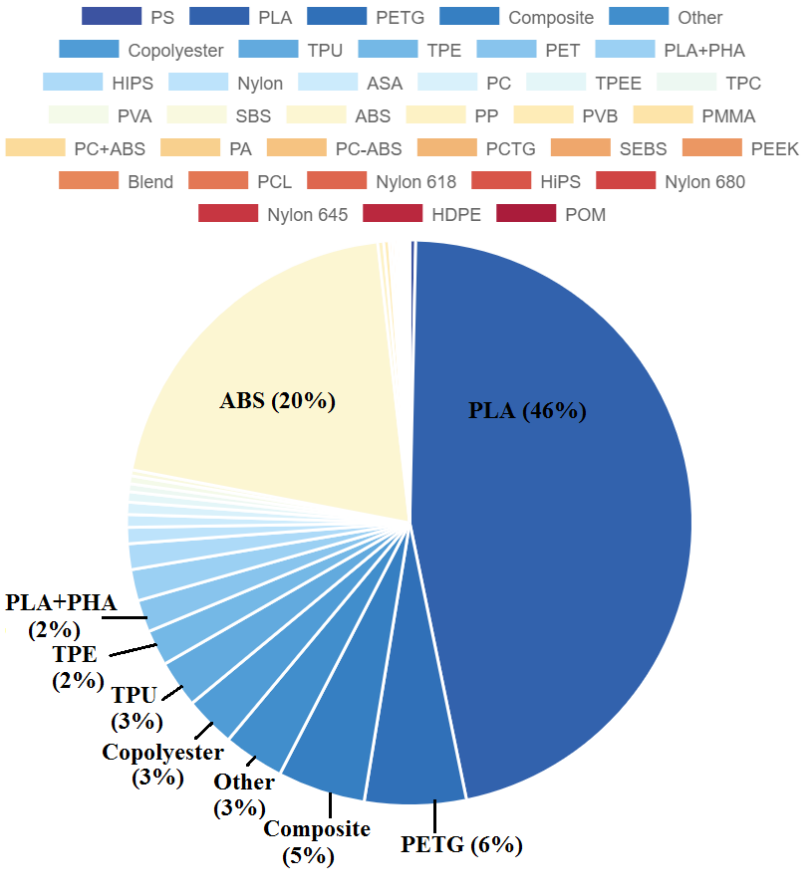

Figure 1.13 Thermoplastic filament materials used in FDM process by July 2017 [21]

In the polymer industry, it is known that for the fabrication of thermoplastic parts the most advantageous production technique is injection molding due to its rather low labor cost, high design flexibility, and high product quality with tight dimensional control. This technique consists of basically three steps of “filling”, “packing” and “cooling”; where the melted polymer is injected into a cold closed mold cavity by the action of pressure leading to solidification of the polymer melt into a rigid solid component. On the other hand, shaping of polymer parts with injection molding requires high initial cost of tooling and machinery. Therefore, for the small batch size production, the overall manufacturing cost could be very high. Moreover, the molds should withstand so several types of loads and pressures to provide high reproducibility of the component. Thus; mold design features, mold making processes, molding equipment and part design are all very critical to assure quality and reproductivity of the polymer parts; which all result in significant cost increase for the small batch size production. In this respect, shaping by 3D-printing today appears to

be an alternative. 3D-printing technology, also called “additive manufacturing” or “rapid prototyping”, uses the 3-dimensional CAD model of a component to produce it layer-by-layer. In the FDM technique, 3D-printers generally use thermoplastic filaments which can easily melt and then solidify to fabricate the model. Contrary to traditional subtractive manufacturing techniques, 3D-printing is not only faster and cheaper, but also there is no loss of material.

1.5 Weathering Mechanisms of PLA

It is known that almost all polymeric materials are susceptible to the UV radiation of sunlight leading to certain level of changes in the chemical structure of their macromolecular chains, such as chain scissions in the backbone, crosslinking, oxidation, bond cleavage, resulting in discoloration, or decreased viscosity, molecular weight, mechanical strength and increased brittleness. However, PLA has more delicacy compared to other polymers due to its biodegradable nature. This sensitivity gains acceleration in the outdoor applications because of the very high UV irradiation energy of the sun. Therefore, PLA needs resistance to all types of weathering degradation during structural outdoor applications.

According to the literature, the first photodegradation mechanism proposed for PLA via UV irradiation was “ photolysis” by McNeill and Leiper [22]. They indicated that, just like the thermal decomposition mechanism, PLA decomposes by UV irradiation at the C-O bond of ester linkages, especially at the broken bond position “b” as shown in Figure 1.14 [23].

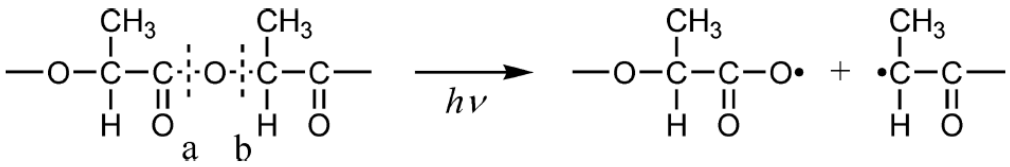

Figure 1.14 Typical photolysis reaction of PLA [23]

After that Ikada [24] proposed another mechanism for the photodegradation of PLA. They attributed the increased number of C=C double bonds and OH groups seen in IR-spectra after weathering to the random main chain scission occurring especially by Norrish type II reaction given in Figure 1.15 [23]. It can be seen that although the decomposition mechanisms are different, the products of the reactions are the same.

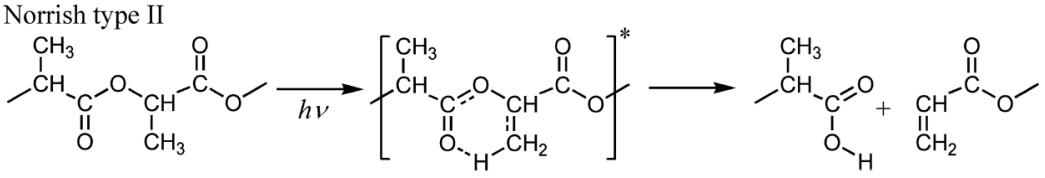

Figure 1.15 Typical Norrish type II reaction of PLA [23]

Moreover, Janorkar *et.al.* [25] proposed two more mechanisms for the UV irradiation-induced photodegradation: photolysis and photooxidation reactions as given in Figure 1.16 [23]. During the former reaction (a) photolysis in C=O backbone causes the dehydrogenation, while in the latter (b), hydroperoxide derivatives are formed and followed by decomposition into carboxylic acid and diketones. Yet this does not explain the increased number of C=C bonds in IR spectra after weathering as proposed by Ikada [24].

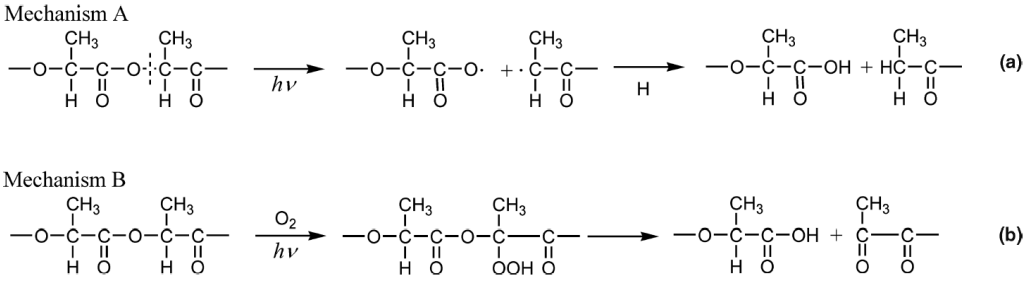

Figure 1.16 Typical photolysis (a) and photooxidation (b) reactions of PLA [23]

In addition, the moisture uptake from the environment causes hydrolyses in the ester linkages. PLA is much more sensitive to hydrolysis in humid or aqueous environments compared to for example PET. The hydrolysis reaction of PLA is a two-stage reaction as given in Figure 1.17 [25]. It starts with the water intake causing the random chain

scission in the amorphous region of the polyester chains. Because the amorphous parts are more susceptible of the humidity due to ease of water penetration in unorganized parts. Above T_g the hydrolysis accelerates. Once the most of the amorphous parts are degraded, the second stage of hydrolysis starts at the crystalline parts [26].

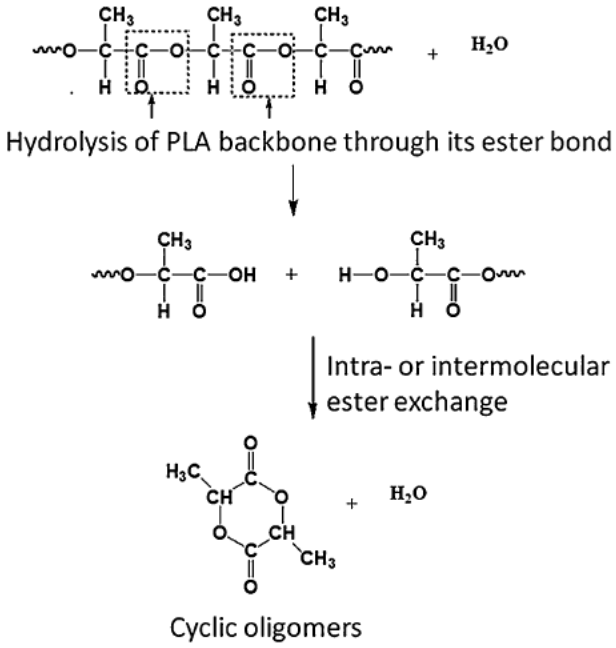

Figure 1.17 Typical hydrolysis reaction of PLA [25]

It should be also pointed out that, the decreased molecular weight and the plasticizing effect of the water uptake result in the increased mobility of chains and ultimately degradation-induced crystallization during weathering. Because as the degradation proceeds, the chains become short enough to rearrange spatially of the amorphous parts in crystalline regions [23].

1.6 Literature Survey

1.6.1 Studies on the Engineering Performance of Glass Fiber Reinforced and Thermoplastic Elastomer Blended PLA

In the literature, it was observed that the majority of the studies [27–38] did not use E-glass fibers; instead, they used phosphate glass fibers. Because, the composition and structure of bone and phosphate glass are similar and the main purpose of these biomedical studies was to develop a biodegradable and biocompatible implant material via tissue engineering. They particularly investigate the bone fixation which would be bio-absorbable without any harmful or toxic effect; and have a slow degradation rate that allows slow transformation of load to bone to heal. These tissue engineering studies were focused on the quality of the interface between phosphate glass fibers and PLA matrix, cyto-compatibility and mechanical properties of the composites, and the levels of degradation and retention of these properties under *in vitro* conditions.

The studies reported in literature on the use of E-glass fiber (GF) reinforcement of PLA seems to be very limited. In one of these studies, Lin *et al.* [39] used GF reinforcements not for neat PLA, but for a PLA/PC (70/30) blend. Compounding of PLA/PC with 10, 20, 30 wt% GF was done by melt mixing via twin-screw extruder. Mechanical tests of the injection molded specimens indicated that 30 wt% GF reinforcement resulted in 84%, 73% and 200% increases in tensile strength, flexural strength and notched Izod impact strength, respectively; while ductility of the blend decreased by 71%.

Similarly, Lu *et al.* [40] used 5, 10, 20, 30 wt% GF reinforcements for the blend of PLA/HDPE (60/40). It was found that addition of 30 wt% GF resulted in 75% increase in tensile strength of the blend, while it decreases its impact strength and ductility by 57% and 83%, respectively.

In the work of Huda *et al.* [41] use of 30 wt% GF in PLA matrix, again via twin-screw extruder compounding and injection molding shaping; tensile strength and flexural

strength were increased by 28% and 10%, respectively. In addition, elastic tensile modulus, flexural modulus and notched Izod impact strength values were also raised by 145%, 152% and 53%, respectively.

In another similar study, Jaskiewicz *et al.* [42] found that tensile modulus and notched Charpy impact strength of PLA having 30 wt% GF were 188% and 531% higher than that of neat PLA, respectively.

Literature survey indicated that in order to overcome inherent brittleness of PLA, rubber toughening could be used. In this respect, researches especially focused on the blending of PLA with an elastomeric material such as natural and synthetic rubbers [43–46] and also thermoplastic polyurethane elastomer (TPU) [47–63]. These studies generally revealed that, due to the effective rubber toughening mechanisms, significant increases in toughness and ductility would be attained; of course, with certain degree of losses in strength and modulus values of PLA.

1.6.2 Studies on the 3D-Printing of PLA and Other Polymers

Today, 3D-printing techniques are particilarly used in the production of health care and medical devices, while their use in other sectors are rapidly emerging in other sectors. According to the analysts Shanler and Basiliere [64] from an American research company Gartner, additive manufacturing techniques will reach a peak in 5-10 years in both automotive and aerospace industries. Similarly, analyst Cotteleer [16] from Deloitte LLP reported that by 2030-2050, end product production by 3D-printing technologies will amplify in all industries.

Consequently, academic researches on the use of various thermoplastic polymers in 3D-printing techniques are also emerging. On the other hand, literature survey indicated that, apart from the biomedical field, the number of 3D-printing studies about polylactide (PLA) based materials were not more than ten to the best of our knowledge. These studies [65–72] particularly investigate the effects of the process parameters of 3D-printing on the mechanical and other properties of PLA blends and composites.

If 3D-printing methods would be considered as an alternative shaping technique, then the properties of samples shaped by 3D-printing and conventional injection molding technique should be compared. However, our literature survey revealed that there seems to be only four studies [73–76] comparing the behavior of certain thermoplastic specimens (not PLA based) shaped by 3D-printing and injection molding.

In the first one, Franchetti *et. al.* [73] performed a comparative cost analysis of 3D-printing and injection molding for various batch sizes. They determined "break-even points" of batch sizes above which injection molding would be cost effective. It was concluded that 3D-printing type additive manufacturing was only cost effective for the small batch size productions, i.e. approximately 200 units.

Huber *et. al*. [74] investigating the magnetic hysteresis behavior of 3D-printed and injection molded polyamide 11 (PA11) samples filled with isotropic NdFeB powder revealed that layered structure of the 3D-printed samples have no adverse effect in terms of isotropy.

In the study of Miller *et. al.* [75], thermoplastic polycarbonate urethane (PCU) specimens were shaped by both injection molding and 3D-printing to compare their mechanical properties. They indicated that due to proper printing parameters and high toughness of PCU; tensile, compressive, shear and fatigue strength of the 3D-printed samples were matched with the injection molded samples.

Weng *et. al.* [76] compared the tensile mechanical properties of neat acrylonitrile butadiene styrene (ABS) and its 1, 3, 5 wt% montmorillonite (MMT) nanocomposite specimens shaped by 3D-printing and injection molding. They indicated that tensile strength and modulus of the 3D-printed samples were all lower than the injection molded ones. For instance, tensile strength of 3D-printed ABS samples was 45% lower, while 3D-printed ABS/5 wt% MMT nanocomposite was 39% lower. Possible reasons of these reductions were also discussed in the manuscript.

1.6.3 Studies on the Weathering Performance of PLA-based Materials

Poly(L-lactic acid), simply known as polylactide (PLA) is recently becoming one of the most important thermoplastic biopolymer having aliphatic polyester structure that could be polymerized from fully renewable resources. It has already found large application areas in the field of textile, food packaging, and biomedical sectors. Today it is being considered to replace traditional petroleum-based engineering thermoplastics in the outdoor structural applications such as in automotive industry. In these applications, the performance of PLA based materials including its blends and composites should be thoroughly determined not only for standard conditions but also under degradative weathering conditions.

In the literature, there are several studies investigating the effects of either natural weathering conditions or accelerated weathering conditions for neat PLA [77–86], for PLA blends [87–91], and for micro or nano-particle filled PLA composites [92–114]. Some of these researches exposed only UV-irradiation, some of them only moisture; but in the majority of these studies accelerated weathering conditions of both UV-irradiation and moisture were applied together in consecutive cycles.

These studies generally revealed that prolonged weathering conditions could be very deteriorative in the properties of PLA based materials. They indicated that reductions in the many properties of the specimens were due to the degradation mechanisms of UV radiation in the form of photolysis via Norrish II type photo-cleavage or photodegradation reactions; and also, due to the hydrolysis reaction of moisture, all leading to significant levels of main chain scissions in PLA matrix.

It is known that for structural engineering applications of traditional thermoplastics are normally reinforced with E-glass type fiber (GF) reinforcements; therefore, PLA should be also reinforced with these fibers in order to gain sufficient strength-modulus-toughness values to be used in these structural applications. In the literature, there are certain number of studies [39–42, 115, 116] investigating the increased mechanical

and other properties of PLA with GF reinforcement. Unfortunately, none of them explored the influences of weathering conditions on these composites.

1.7 Purpose of the Study

Although compared to other biopolymers PLA has rather higher level of mechanical and thermal properties, this is not the case if compared to conventional engineering thermoplastics. Therefore, mechanical properties of PLA; not only strength and modulus, but due to its inherent brittleness, toughness should be also improved. It is known that strengthening of polymer matrices can be achieved by fiber reinforcements, while toughening can be achieved by elastomer blending.

In order to compare mechanical behavior of PLA with traditional engineering thermoplastics, it would be wise to consider effects of fiber strengthening and rubber toughening together. However, to the best of our knowledge, there is no study reported on the effects of both GF reinforcement and TPU blending, yet. Therefore, the first purpose of this thesis was, as the first time in literature, to investigate not only strengthening level of PLA with increasing GF reinforcement content but also toughening level of PLA by TPU blending with and without GF.

Since biopolymer PLA is considered as a significant alternative for the petroleum based thermoplastics not only for biomedical applications, but also for structural engineering applications; it would be very crucial to compare the mechanical performance of PLA based samples shaped by 3D-printing and the conventional injection molding. However, to the best of our knowledge, there seems to be no study cited in the literature. Therefore, the second aim of this thesis was, as the first time, to compare mechanical performance of neat PLA, glass fiber (GF) reinforced PLA and thermoplastic polyurethane elastomer (TPU) blended PLA samples shaped by 3D-printing and injection molding.

For the long term outdoor structural applications, the performance of the polymer matrix composites should be determined under various weathering conditions.

Although there are a few studies investigating the mechanical and other properties of PLA/GF composites under normal conditions, however, to the best of our knowledge, none of them explored the influences of weathering conditions on the behavior of PLA/GF composites. Therefore, the third objective of this thesis was, as the first time, to investigate engineering performance of PLA and PLA/GF composites under outdoor conditions via exposing different periods of accelerated weathering conditions of both UV-irradiation and moisture cycles.

CHAPTER 2

EXPERIMENTAL WORK

2.1 Materials Used

In this study, PLA matrix material was commercial L-lactic acid type polylactide supplied from NaturePlast (France) with an extrusion grade (PLE 001). As it is indicated in its technical data sheet, it melts between 145°-155°C and degrades in the range of 240°-250°C; its melt flow index range at 190°C under 2.16 kg is 2-8 g/10 min, as well as a density of 1.25 g/cm^3.

GF reinforcement used was E-glass type chopped fibers (CamElyaf Glass Fiber, PBT2) with the average length and diameter of 4.5 mm and 10.5 μm, respectively. The producer indicates that fibers have silane sizing compatible with thermoplastic polyesters of PBT and PET.

As the rubber toughening agent, polyurethane type thermoplastic elastomer was chosen. This TPU (Interplast, Epaflex EL 392 A 25) has a density of 1.19 kg/dm^3, hardness of 93 Shore A, tensile strength of 40 MPa, and elongation at break of 550%.

2.2 Compounding of PLA with GF and TPU Elastomer

Composites and blends of PLA with GF and TPU were all produced by “twin-screw extrusion melt-compounding” with a laboratory size equipment. As the first step, PLA powders and TPU granules were pre-dried for 15 hours and 4 hours, respectively; in a vacuum oven at 60°C. Then according to the formulation, PLA, GF and TPU particles were pre-mixed manually, and these mixtures were melt compounded via Rondol

Microlab 300 laboratory size (D=10 and L/D=20) twin-screw extruder. Typical temperature profile used from feeder to die were 115°-170°-180°-175°-145°C, while the typical screw speed used was 75 rpm throughout the compounding stage.

In the first part of this thesis, GF reinforced PLA matrix composites were produced with the loadings of 5, 10, 15 and 20 wt%. These composites were designated by using the format of "PLA/*x* GF", where *x* denotes wt% of GF used. In the case of toughening with TPU, blending was applied only with 10 wt% TPU; because in the former study of our group [117] conducted for a different grade of PLA, use of 10 wt% TPU resulted in optimum toughness values almost without any decrease in the strength values. This specimen is designated as PLA/10 TPU. As would be discussed in the following results and discussion section, since use of 15 wt% GF revealed the optimum mechanical properties; use of TPU blending with GF reinforcement was applied only with this GF content. Thus, this specimen is designated as PLA/10 TPU/15 GF.

2.3 Shaping by Injection Molding

Before shaping of the test specimens by injection molding; continuous strands coming out from the twin-screw extruder die were cut into 2-3 mm granules by using a four-blade cutter. Then, pellets were dried for 15 hours in a vacuum oven at 60°C. Standard sized specimens required for testing and analyses were melt-shaped via laboratory scale DSM Xplore Micro injection molder. Typical barrel and mold temperatures used were 160°C and 35°C, respectively; while the melting time in the barrel was approximately 7 minutes, with the subsequent three-step pressure-time profile determined as 13 bar for 4 s, 13 bar for 5 s, and 12 bar for 5 s.

In the second part of this thesis, in order to differentiate these specimens shaped by injection molding, an italic suffix of "*IM*" was used; i.e. PLA-*IM*, PLA/GF-*IM*, PLA/TPU-*IM*, PLA/TPU/GF-*IM*.

2.4 Shaping by 3D-Printing

Before shaping of the test specimens by 3D-printing; continuous strands coming out from the twin-screw extruder die were carefully air cooled and wound on empty filament spools keeping their diameter approximately as 2 mm. Then, these filaments were used to shape test specimens via Ultimaker 2+ (Ultimaker B.V.) a "Fused Deposition Modelling" (FDM) type 3D-printer. It is an open source code equipment with changeable nozzles and many process parameters. Its build chamber size is 223 x 223 x 205 mm; while the nozzle and built plate temperature ranges are 180 º-260 ºC and 50 º-100 ºC, respectively.

After drawing the standard size geometries of the test specimens by a CAD software (SolidWorks), Cura 2.3.1 slicing software of the printer was used to generate G-code of the specimen geometries. Since the printer used is an open code equipment, there are so many software parameters to be used. In this thesis, the most important software parameters were determined after several trials to get the optimum mechanical properties of the specimens. The parameters used are tabulated in Table 2.1.

On the hardware of the 3D-printer, the nozzle diameter and temperature were chosen as 4 mm and 180ºC, respectively; while the built plate was set at 65ºC. Specimens were printed in a "laying down fashion" with alternating ±45º printing orientation.

Again, in the second part of this thesis, in order to differentiate these specimens shaped by 3D-printing, this time an italic suffix of "*3D*" was used; i.e. PLA-*3D*, PLA/GF-*3D*, PLA/TPU-*3D*, PLA/TPU/GF-*3D*.

Table 2.1 The most important 3D-printer software parameters chosen in this study

Parameter Name	Parameter Definition	Used Value
Layer Height	The height of each layer in mm. Higher values produce faster prints in lower resolution and vice versa.	0.06 mm
Wall Thickness	The thickness of the outside wall in horizontal direction. This value divided by the wall line width defines number of walls.	0.6 mm
Top/Bottom Thickness	The thickness of the top and bottom layers in the print. This value divided by the layer height defines the number of top/bottom layers.	0.72 mm
Infill Density	Adjust the density of infill of the print.	100%
Print Speed	The speed at which printing happens.	50 mm/s
Travel Speed	The speed at which travel moves are made.	120 mm/s
Print Cooling	The fans improve the print quality on layers with short layer times and bridging/overhangs.	Yes
Build Plate Adhesion Type	BRIM adds a single layer flat area around the base of your model to prevent warping. RAFT adds a thick grid with a roof below the model. SKIRT is a line printed around the model, but not connected to the model.	Skirt

2.5 SEM Analyses

In order to observe morphology of all specimen groups in terms of distribution of GF and TPU domains in PLA matrix and the interface between them, scanning electron microscopy analysis (SEM) were carried out for the gold sputtered fracture surface of the fracture toughness specimens under FEI Nova Nano 430.

2.6 Mechanical Tests

In order to determine the mechanical performance of all the specimen groups, first their strength and modulus values were determined both with tension tests according to ISO 527-2 standard, and also with flexural tests in terms of three-point bending

according to ISO 178 standard. These tests were carried out under 5 kN Instron 5565A universal testing system. Apart from tension and flexural tests; fracture toughness tests were also carried out to compare K_{IC} and G_{IC} fracture toughness of the specimens. These tests were conducted for single-edge-notched-bending specimens according to ISO 13586 standard under Instron 5565A system. Notches and pre-cracks on the injection molded specimens were created by Ceast Notchvis system as defined in the standard. For each specimen group, all mechanical tests were repeated 5 times; and the properties were determined as the average values including their standard deviations.

2.7 Thermal Analyses

In order to determine the thermal behavior of all specimen groups, differential scanning calorimetry (DSC) analyses were conducted. The heating profile used for the materials was -80° to 220°C with 10°C/min rate under SII X-DSC 700 Exstar system. In addition to DSC, for the determination of the thermal degradation temperatures of all specimen groups, thermogravimetric analyses (TGA) were also carried out. This time the heating profile was 30° to 550°C under SII TG/DTA 7300 Exstar system.

2.8 Weathering of PLA and PLA/GF Specimens

Outdoor performance of neat PLA and PLA/GF composite specimens were measured by using Q-LAB QUV/se model accelerated weathering test system. The weathering conditions applied were in accordance with the Cycle-C of the SAE J2020, ASTM G154-05 and ISO 4892-3 standards. Fluorescent lamps (UVB-313) with 0.49 W/m^2 irradiance (at 310 nm) were used with cycles of 8 h UV irradiation at 70°C, followed by 4 h dark condensation at 50°C. These consecutive cycles were applied to the specimens attached to the test panels without any interruption. Effects of accelerated weathering were investigated for six periods: 50, 100, 150, 200, 300 and 400 hours. Specimens for each period were designated as PLA-x h or PLA/GF-x h, where x denotes the accelerated weathering period; e.g. PLA-400h and PLA/GF-400h.

Effects of each period of accelerated weathering on the performance of the neat PLA and PLA/GF composite specimens were investigated by comparing the changes in the results of the following tests and analyses conducted.

2.9 Characterization for the Changes After Weathering

2.9.1 Changes in the Color

After each accelerated weathering period, not only visual but also quantitative inspection of changes in the color of the specimens were carried out. Visual inspection was made by photographing the images of the weathered specimens and comparing their color with the unweathered one.

The quantitative analysis for the color change was conducted by determining the CIELAB color space parameters (L*, a*, b*) of the specimens before and after each accelerated weathering period. For this purpose, diffused reflectance analysis (DRA) was utilized via DRA unit of Agilent Cary 60 UV-vis spectrophotometer in accordance with CIE 1976 standards.

2.9.2 Changes in the Chemical Structure

In this respect, the first analysis was to observe the decreases in the molecular weight of PLA matrix after each accelerated weathering period. For this purpose, static light scattering (SLS) spectrometry (Malvern CGS-3) was conducted to determine the weight-average molecular weight (M_w) of the specimens by using the results of Guiner plots of four different concentrations of PLA samples dissolved in chloroform.

The second analysis was attenuated total reflectance-Fourier transform infrared spectroscopy (ATR-FTIR) to observe the changes in the chemical bonds of the specimens after each accelerated weathering period. Spectra were taken via ATR unit of Bruker ALPHA with signal-averaged 32 scans at a resolution of 4 cm^{-1} within the wavenumber range of 400 to 4000 cm^{-1}.

2.9.3 Changes in the Morphology, Mechanical and Thermal Properties

The alterations in the fracture surface morphology, tensile strength and modulus, flexural strength and modulus, ductility, fracture toughness, transition temperatures along with the thermal degradation temperatures of neat PLA and 15 wt%GF reinforced PLA composite specimens before and after each accelerated weathering period were assessed by SEM analyses, mechanical tests and thermal analyses as explained in detail above in the Sections 2.5, 2.6 and 2.7.

CHAPTER 3

RESULTS AND DISCUSSION

As stated before, since this dissertation has three different parts, their results are presented and discussed successively in the following three subsections.

3.1 Effects of GF Content and TPU Elastomer Blending

3.1.1 Distribution and Morphology of GF and TPU in the PLA Matrix

Even distribution of the fiber reinforcements is one of the key factor to obtain enhanced mechanical properties of polymer composites. Thus, SEM analysis on the fracture surfaces of fracture toughness test specimens were conducted first to observe the effects of silane sized GF content in the neat PLA matrix, and then also in the matrix of PLA/TPU blend.

Lower magnification SEM images in Figure 3.1 shows that 5, 10, 15 wt% GF reinforcements were rather uniformly distributed in the neat PLA matrix. On the other hand, use of 20 wt% GF content resulted in decreased uniformity of GF distribution; thus, as would be discussed in the next section, with this content, mechanical properties started to decrease. Figure 3.1 also indicates that there was no uniformity problem of 15 wt% GF distribution in the matrix of PLA/10 TPU blend.

It is known that due to the immiscibility of TPU and PLA, when blended they lead to a two-phase structure, where round shaped TPU domains form in the matrix of PLA. Since these TPU domains are micron sized, it was possible to observe them only in the higher magnification SEM images of Figure 3.2. Due to the certain degree of

compatibility between PLA and TPU domains, Figure 3.2 also shows that micron-sized TPU domains were also uniformly distributed in the PLA matrix. The reason of this partial compatibility is the certain interactions between the carboxyl, hydroxyl end groups and ester carbonyl groups of PLA and polar groups of the hard segments of TPU.

Figure 3.2 also shows that there were certain levels of "debonding" and "pull-out" of GF reinforcements in each matrix. As would be discussed later, these phenomena lead to additional toughening mechanisms.

3.1.2 Effects of GF and TPU on the Strength and Modulus of PLA

Tension tests and three-point bending tests were conducted to investigate the effects of GF reinforcement and TPU blending on the strength and elastic modulus of PLA. While "tensile stress-strain" curves and "flexural stress-strain" curves of specimens are given separately in Figure 3.3, the values of "Tensile Strength (σ_{TS})" and "Tensile Modulus (E)" determined by tension tests; and the values of "Flexural Strength (σ_{Flex})" and "Flexural Modulus (E_{Flex})" determined by bending tests are all tabulated in Table 3.1. Moreover, influences of increasing GF content on the strength and elastic modulus values of PLA/GF composites were compared in Figure 3.4. Additionally, effects of TPU blending with and without 15 wt% GF reinforcement on the strength and modulus values are also compared in Figure 3.5.

Figures 3.3, 3.4 and Table 3.1 simply show that use of GF reinforcement was very effective to improve strength and modulus values of PLA matrix. Because, it is known that strengthening in composites is induced basically by the decreased mobility of macromolecular chains of polymer matrix, and the applied load transfer from the matrix to the reinforcement material. The necessary condition for these strengthening mechanisms to be effective is the presence of sufficient degree of interfacial adhesion between the matrix and reinforcement surfaces; which was achieved by the use of silane sized GF reinforcements.

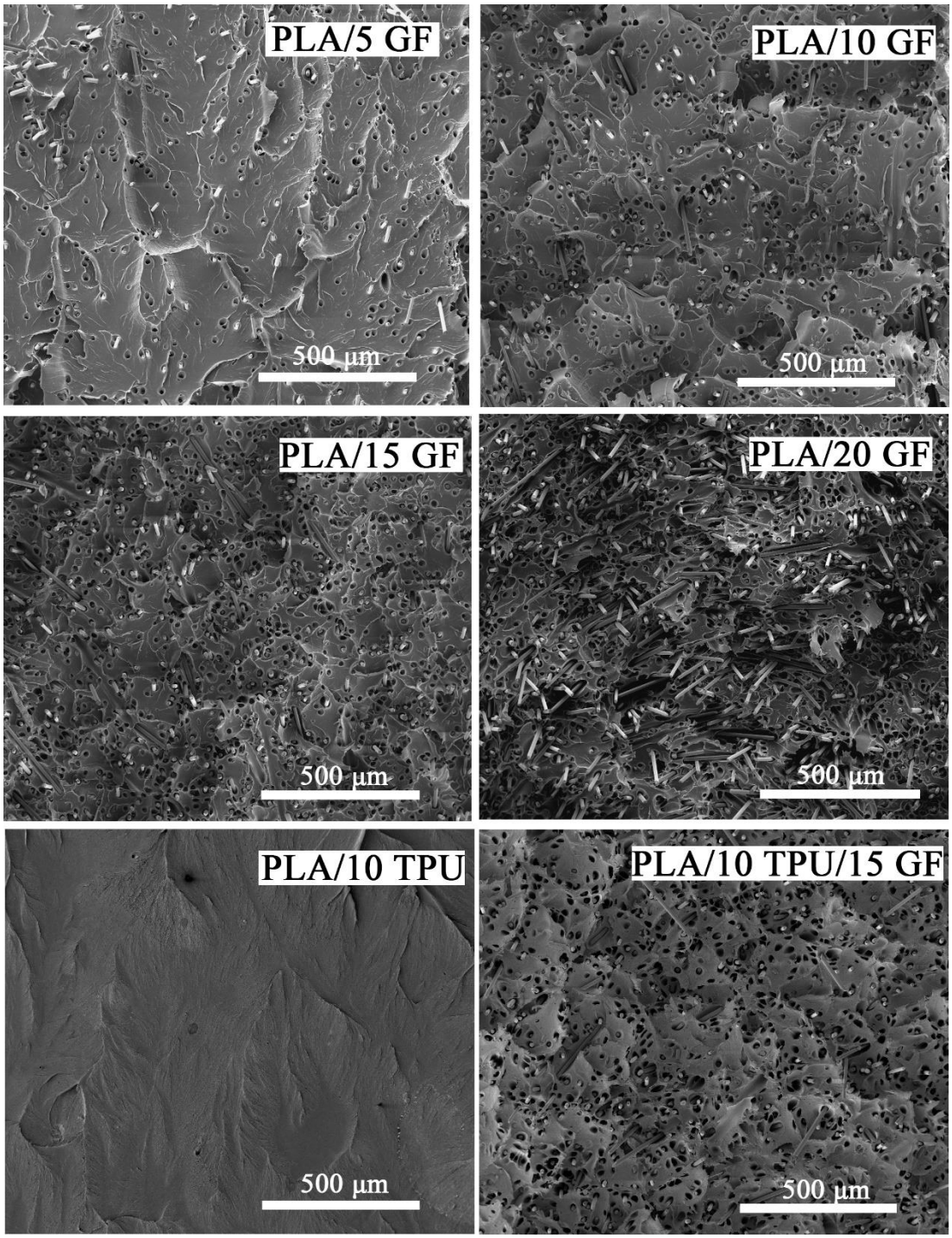

Figure 3.1 Low magnification SEM fractographs showing distribution of GF in the matrix of neat PLA and PLA/TPU blend

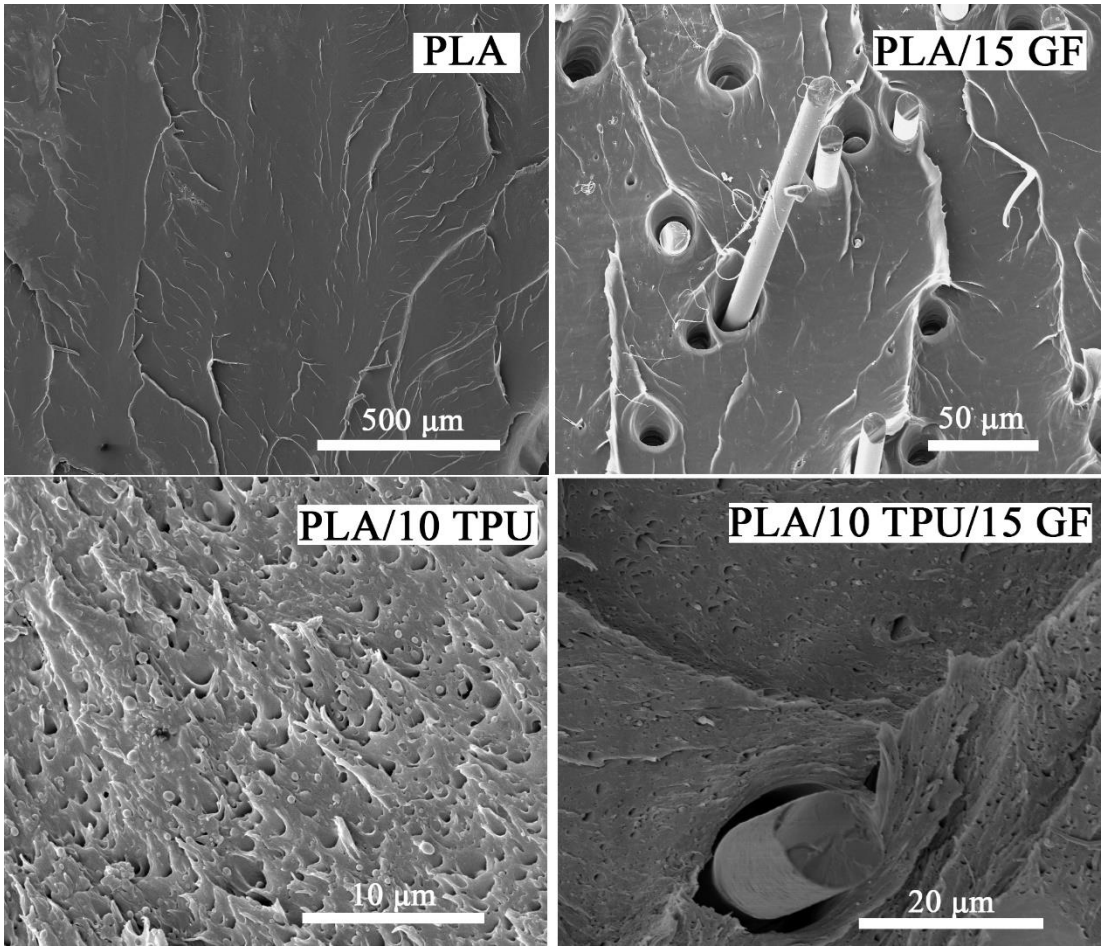

Figure 3.2 Higher magnification SEM fractographs showing micron sized TPU domains and interfacial debonding and pull-out of GF reinforcements

It is seen that increasing GF content increases tensile (σ_{TS}) and flexural strength (σ_{Flex}) of the PLA matrix up to 15 wt% GF. In this composition, increases in σ_{TS} and σ_{Flex} were 32% and 21%, respectively. Above this composition, i.e. 20 wt% GF, as discussed in the previous section, due to the decreased level of uniform distribution of GF reinforcements, strength values decreased slightly, but the values were still much higher compared to the strength values of neat PLA.

In terms of elastic modulus values both tensile modulus (E) and flexural modulus (E_{Flex}), increasing GF content resulted in again very significant increases in the modulus values of neat PLA. This time 15 wt% GF resulted in 48% and 100% increases in the values of E and E_{Flex}, respectively. Due to the very efficient stiffening action of GF reinforcements, use of 20 wt% GF increased modulus values even more.

The main reason to blend rather brittle polymers with thermoplastic elastomers is to improve their ductility and toughness. On the other hand, due to the "plasticizing" action of especially soft segments of thermoplastic elastomers, strength and modulus values of the polymer matrices decreases. Thus, Figures 3.3, 3.5 and Table 3.1 indicate that use of 10 wt% TPU blending resulted in 9% decreases in both tensile and flexural strength values; while the decreases were 13% and 16% in the tensile and flexural modulus values, respectively. However, it was observed that when PLA/10 TPU blend was reinforced with 15 wt% GF, then all these reduced strength and modulus values were recovered to above the values of neat PLA.

Therefore, it can be concluded that use of 15 wt% GF reinforcement resulted in optimum increases in the strength and elastic modulus of not only neat PLA but also PLA/10 TPU blend.

Table 3.1 Tensile Strength (σ_{TS}), Flexural Strength (σ_{Flex}), Tensile Modulus (E), Flexural Modulus (E_{Flex}) of the Specimens

Specimens	$\boldsymbol{\sigma_{TS}}$ **(MPa)**	$\boldsymbol{\sigma_{Flex}}$ **(MPa)**	$\boldsymbol{E}$ **(GPa)**	$\boldsymbol{E_{Flex}}$ **(GPa)**
PLA	58.6±1.4	97.9±1.3	2.85±0.08	3.60±0.07
PLA/5 GF	62.7±0.9	109.5±2.2	3.34±0.10	4.66±0.02
PLA/10 GF	71.6±0.9	114.0±2.6	3.70±0.26	5.69±0.08
PLA/15 GF	77.3±2.1	118.2±2.8	4.21±0.24	7.20±0.14
PLA/20 GF	76.0±2.6	104.4±2.9	4.35±0.28	7.98±0.16
PLA/10 TPU	53.4±1.4	88.9±1.4	2.49±0.07	3.03±0.11
PLA/10 TPU/15 GF	64.4±1.9	99.7±3.11	3.80±0.14	4.69±0.21

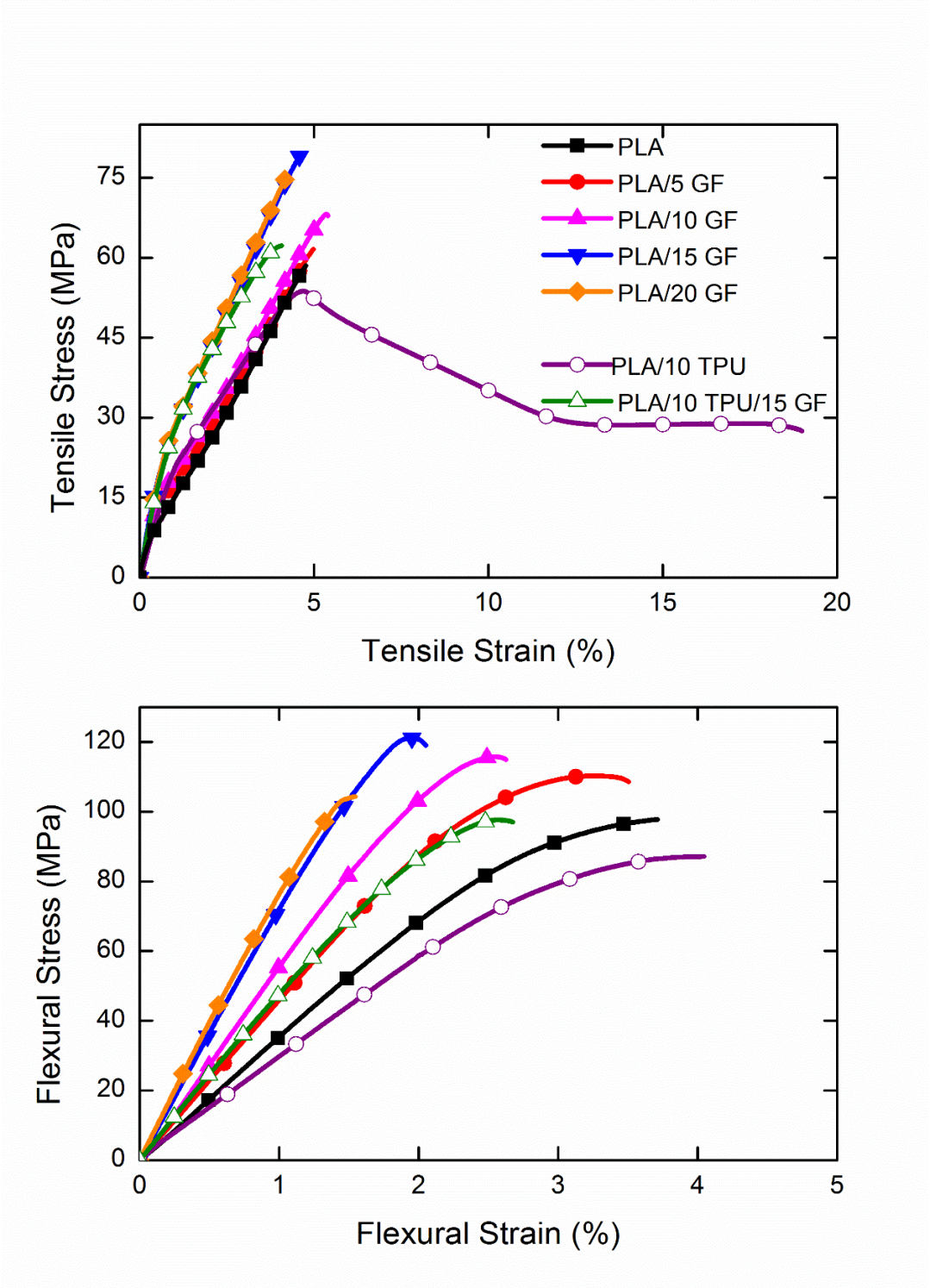

Figure 3.3 Stress-Strain curves of the specimens obtained during tensile and 3-point bending flexural tests

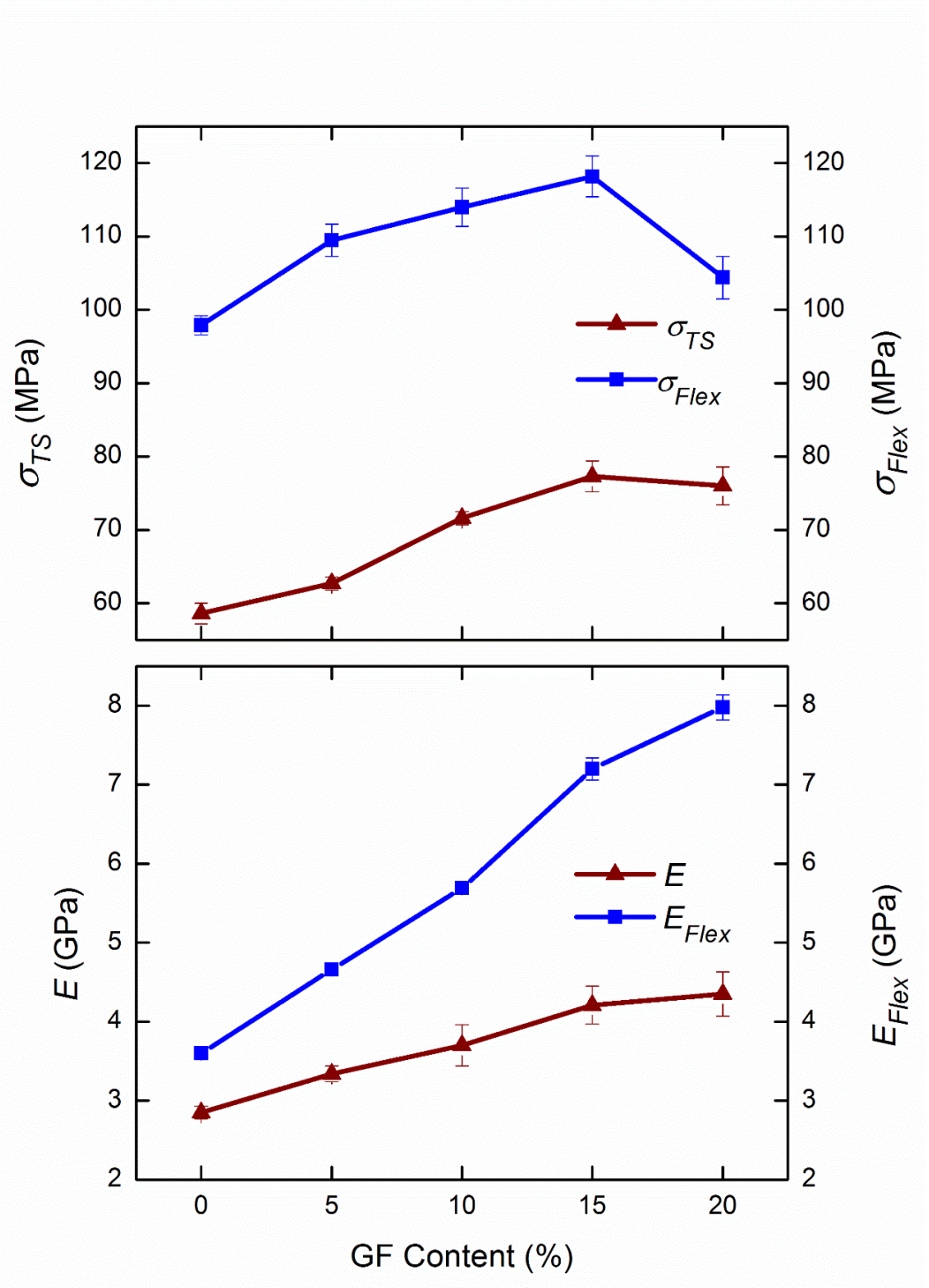

Figure 3.4 Effects of GF content on the strength and modulus values of the specimens

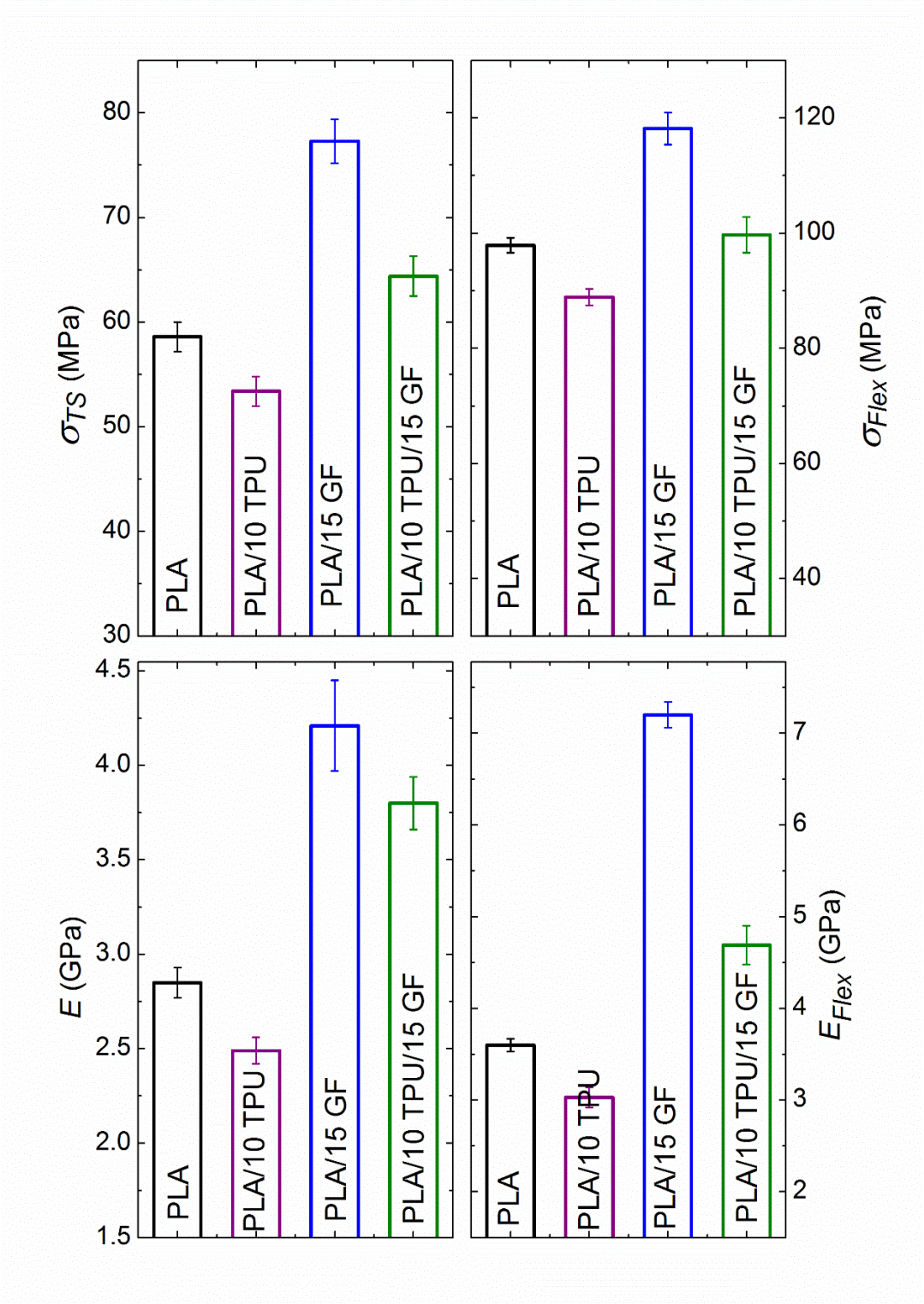

Figure 3.5 Effects of TPU blending on the strength and modulus of the specimens with and without GF reinforcement

3.1.3 Effects of GF and TPU on the Ductility and Fracture Toughness of PLA

Besides modulus and strength values, tension test gives information about the amount of plastic strain formed until fracture, in other words "% strain at break" which is regarded as "ductility" of materials. Figure 3.3 indicates that tensile stress-strain curves of neat PLA and PLA/GF composites were all rather linear having a plastic strain of around 5%, i.e. there is no significant contribution of GF in the ductility level of PLA matrix.

Figures 3.3, 3.6, 3.7 and Table 3.2 show that when PLA matrix was blended with 10 wt% TPU, due to its elastomeric nature, % strain at break (% ε_f) value increased enormously up to 18%, i.e. the improvement in ductility was more than three times.

The most important shortcoming of polylactide is its inherent brittleness; therefore, for most of the engineering applications enhanced improvement in toughness is essential. Consequently, in this study, fracture toughness tests (one of the most important parameter required for structural engineering applications) were conducted to investigate influences of GF reinforcements and TPU blending on the toughness of PLA. Results of this test, measuring the ability of the materials to withstand crack initiation and propagation, were evaluated in terms of both "Critical Stress Intensity Factor (K_{IC})" and "Critical Strain Energy Release Rate (G_{IC})" values, as given in Figures 3.6, 3.7 and Table 3.2.

SEM images in Figure 3.2 indicated that smooth fracture surface of neat PLA with very little plastic deformation lines transformed into rather rough fracture surfaces after both GF reinforcing and TPU blending. Therefore, Figures 3.6, 3.7 and Table 3.2 show that K_{IC} and G_{IC} fracture toughness values of neat PLA increased considerably.

It was observed that compared to the neat PLA the use of optimum 15 wt% GF content resulted in increased fracture toughness values as 21% in K_{IC} and 11% in G_{IC}. These improvements were due to the well-known toughening mechanisms of fiber

reinforcements defined as “crack deflection”, “debonding” and “fiber pull-out”, all leading to decreases in the propagation rates of cracks.

Figures 3.6, 3.7 and Table 3.2 also indicate that the highest improvement in the K_{IC} and G_{IC} fracture toughness values of neat PLA were achieved when blended with 10 wt% TPU, the increases being as much as 103% and 74%, respectively. This very efficient toughening mechanism due to the use of elastomeric materials is called “rubber toughening” or “shear yielding”, i.e. formation of large extend of plastic deformation before fracture. As shown in the SEM image of the PLA/10 TPU (Figure 3.2), very rough fracture surfaces around the micron sized TPU elastomeric domains represent large amount of plastic deformation which could absorb the energy required for crack initiation and also crack growth leading to fracture.

When PLA/10 TPU blend was reinforced with 15 wt% GF, it is seen that the performance of rubber toughening mechanism decreases substantially; however, the K_{IC} and G_{IC} fracture toughness values of this composition were still very high compared to neat PLA, and close to PLA/15 GF composites.

Therefore, it can be concluded that, although blending of neat PLA with 10 wt% TPU resulted in enormous improvement in K_{IC} and G_{IC} values, use of 15 wt% GF reinforcement with and without TPU resulted in similar level of increases. This means that, if the increases obtained in strength-modulus-toughness values of neat PLA by the use of optimum 15 wt% GF reinforcement were sufficient for an application, then there would be no need for an additional blending process with 10 wt% TPU.

Table 3.2 Tensile Strain at Break (ε_f) and Fracture Toughness (K_{IC} and G_{IC}) of the Specimens

Specimens	$\boldsymbol{\varepsilon_f}$ **(%)**	$\boldsymbol{K_{IC}}$ **(MPa√m)**	$\boldsymbol{G_{IC}}$ **(kJ/m^2)**
PLA	4.88±0.25	3.43±0.04	5.44±0.34
PLA/5 GF	5.81±0.66	3.87±0.12	6.39±0.32
PLA/10 GF	5.57±0.51	4.18±0.18	7.07±0.09
PLA/15 GF	5.24±0.42	4.16±0.10	6.96±0.01
PLA/20 GF	4.79±0.40	4.12±0.15	5.55±0.48
PLA/10 TPU	18.07±2.25	6.96±0.14	9.46±0.61
PLA/10 TPU/15 GF	4.21±0.41	4.85±0.15	6.84±0.11

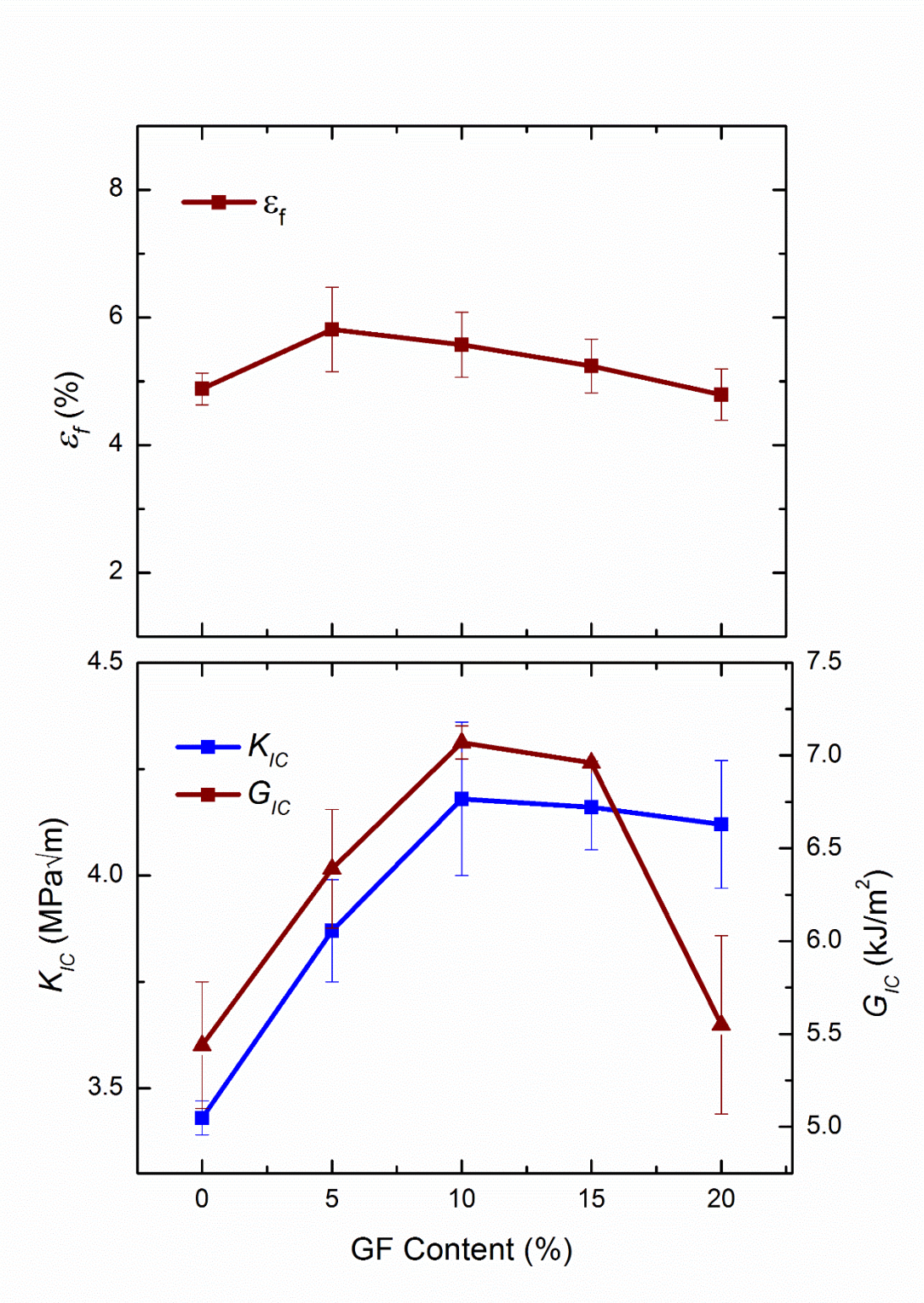

Figure 3.6 Effects of GF content on the ductility and fracture toughness of the specimens

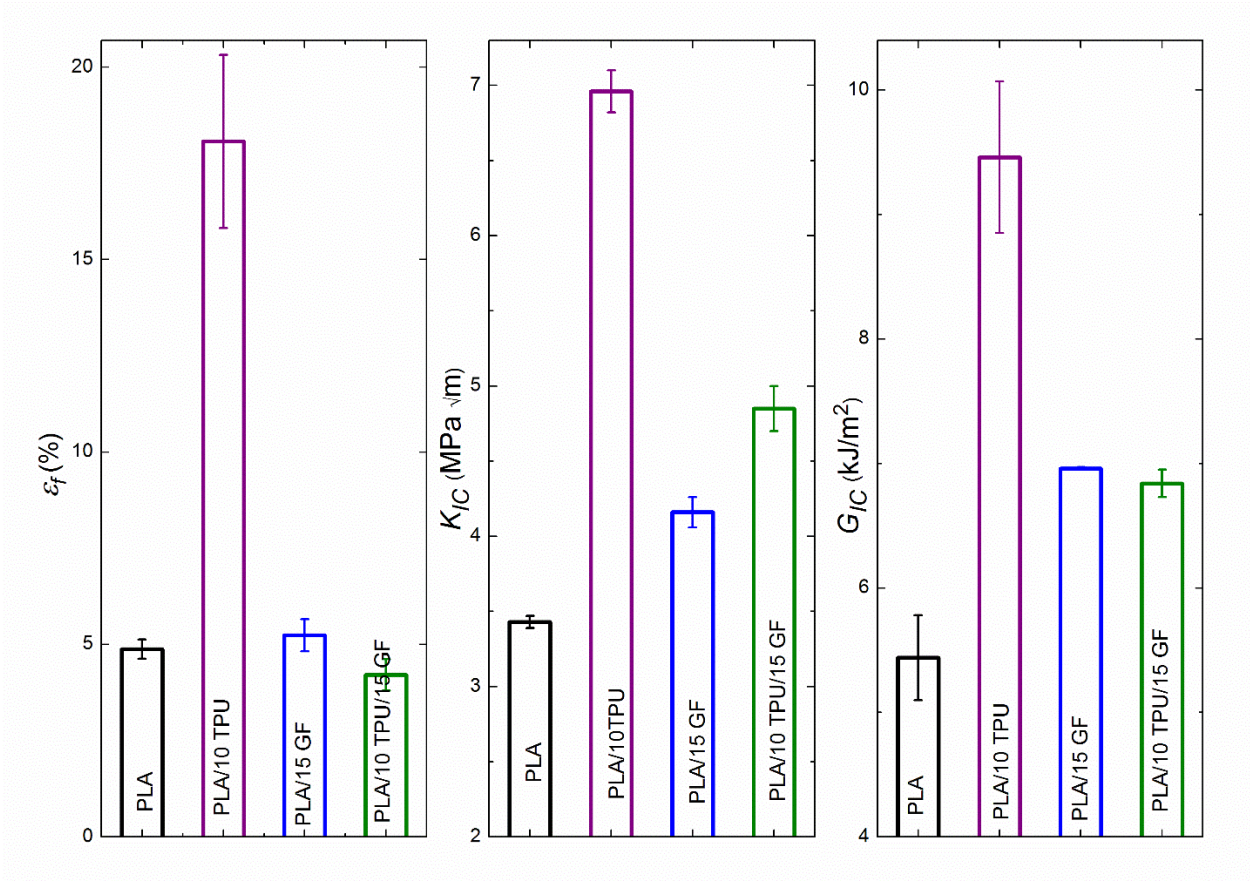

Figure 3.7 Effects of TPU blending on the ductility and fracture toughness of the specimens with and without GF reinforcement

3.1.4 Effects of GF and TPU on the Thermal Behavior of PLA

The first technique to investigate thermal properties of all specimens was DSC analyses. Thermograms of the first heating of the specimens were given in Figure 3.8, while the important transition temperatures; i.e. glass transition (T_g), cold crystallization (T_c) and melting (T_m) temperatures, were tabulated in Table 3.3 together with the enthalpy of melting (ΔH_m) and enthalpy of crystallization (ΔH_c) including percent crystallinity (X_c) of the PLA matrix. The relation used in calculation of percent crystallinity is given below; where w_{PLA} is the weight fraction of the PLA matrix and $\Delta H_m{}^o$ is the melting enthalpy of 100% crystalline PLA determined as 93 J/g in literature [118].

$$X_c = \frac{\Delta H_m - \Delta H_c}{w_{PLA}\ \Delta H_m^\circ} \times 100 \qquad \text{(Equation 1)}$$

It was observed that use of GF reinforcement resulted in no significant influences on the transition temperatures of PLA. Figure 3.8 and Table 3.3 reveal that transition temperatures remained in the narrow ranges of 63-65ºC for T_g, 118-122ºC for T_c and 148-150ºC for T_m. Use of TPU blending resulted in similar effects except certain decreases in T_c levels.

On the other hand, use of GF and TPU influenced enthalpies (both ΔH_m and ΔH_c) of the PLA significantly, which was reflected in the very high increased level of the crystallinity (X_c) of PLA. For instance, Table 3.3 reveals that use of 15 wt% GF with and without TPU increased crystallinity amount of neat PLA from 3.84% to 6.59% and 7.34%, respectively; that is an increase of almost two times.

As the second technique, thermogravimetric analyses (TGA) was conducted to determine the thermal degradation temperatures and %residue of each specimen. TG curves were given in Figure 3.9, while the data determined were tabulated in Table 3.4 as $T_{5\%}$, $T_{10\%}$ and $T_{25\%}$ representing the degradation temperatures at 5%, 10% and 25% mass losses; and T_{max} representing the temperature at maximum mass loss. In the table %residue of each specimen determined at 550ºC were also included. Table 3.4 revealed that use of GF reinforcement and TPU blending had no significant

contribution to the thermal degradation temperatures of PLA, while the %residue values were basically consistent with the GF content of the specimen composition.

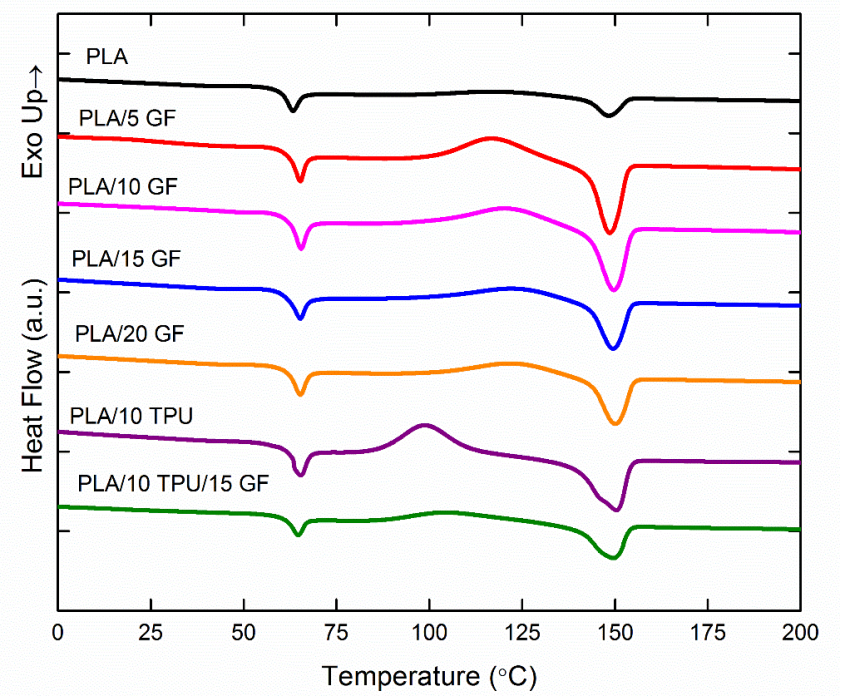

Figure 3.8 First heating DSC thermograms of the specimens

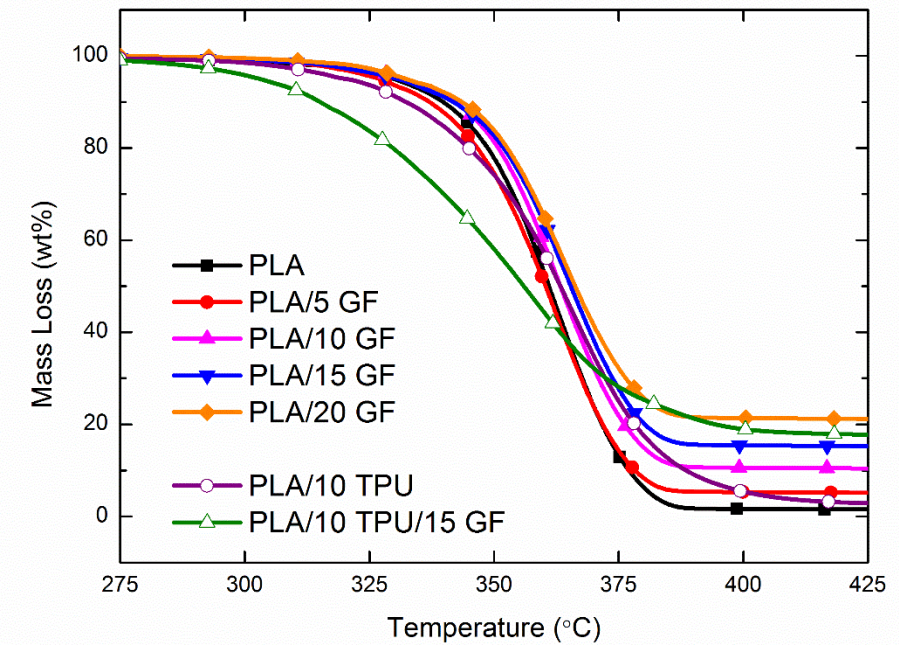

Figure 3.9 Thermogravimetric curves of the specimens

Table 3.3 Transition Temperatures (T_g, T_c, T_m), Enthalpies (ΔH_m, ΔH_c) and Crystallinity Percent (X_C) of the Specimens During DSC First Heating Profile

Specimens	T_g **(°C)**	T_c **(°C)**	T_m **(°C)**	ΔH_m **(J/g)**	ΔH_c **(J/g)**	X_C **(%)**
PLA	63.4	118.0	148.4	7.58	4.01	3.84
PLA/5 GF	65.2	116.3	148.6	25.2	19.9	6.45
PLA/10 GF	65.7	120.3	149.8	22.6	17.1	6.57
PLA/15 GF	65.4	122.2	149.4	17.1	11.2	7.34
PLA/20 GF	65.3	121.9	150.1	15.6	10.3	7.12
PLA/10 TPU	65.4	98.5	150.2	27.9	24.3	4.30
PLA/10 TPU/15 GF	64.7	104.2	149.4	15.9	11.3	6.59

Table 3.4 Thermal degradation temperatures ($T_{5\%}$, $T_{10\%}$, $T_{25\%}$) of the specimens at 5, 10 and 25 wt% mass losses, the maximum mass loss temperature (T_{max}) and %Residue at 550ºC

Specimens	**$T_{5\%}$ (°C)**	**$T_{10\%}$ (°C)**	**$T_{25\%}$ (°C)**	**T_{max} (°C)**	**%Residue at 550ºC**
PLA	330	340	352	367	1.05
PLA/5 GF	327	337	350	366	4.55
PLA/10 GF	332	342	354	367	10.21
PLA/15 GF	331	342	355	368	14.97
PLA/20 GF	332	344	356	368	20.96
PLA/10 TPU	320	332	349	369	1.82
PLA/10 TPU/15 GF	303	315	335	359	16.85

3.2 Effects of Shaping by 3D-Printing

3.2.1 Comparison of the Appearance and the Fracture Surface Morphology of the Specimens

Comparison of the macro level appearances of the injection molded and 3D-printed specimens were conducted by taking their photographic images. Figure 3.10 reveals that generally there were no significant differences in their macro level appearances. The most noticeable difference was, contrary to the 3D-printed neat PLA, injection molded PLA appeared to be very transparent. Because it is known that PLA has very low melt crystallization rate, in which its macromolecular chains do not have enough time to crystalize due to the very high cooling rate of injection molding resulting in a highly amorphous structure.

As would be discussed in the thermal behavior section, due to the lower cooling rate during 3D-printing, the neat PLA specimen had higher level of crystallinity. Moreover, due to the ±45º printing orientation, this specimen had a kind of slightly textured structure. In fact, this slightly textured structure was sensible by a finger touch on the surfaces of all 3D-printed specimens. Therefore, because of the scattered light transmission resulted from the more crystallinity amount and textured structure, 3D-printed neat PLA specimen appeared to be opaque.

Then, the differences in fracture surface morphology of the injection molded and 3D-printed specimens were investigated by SEM analysis as given in Figures 3.11 and 3.12. Figure 3.11 shows that there were no significant differences in the rather smooth fracture surfaces of the inherently brittle neat PLA specimens and the rather rough fracture surfaces of rubber toughened PLA/TPU specimens. Thus, as will be discussed in the next section, no significant differences were observed in the mechanical properties of the injection molded and 3D-printed specimens of both neat PLA and PLA/TPU blends.

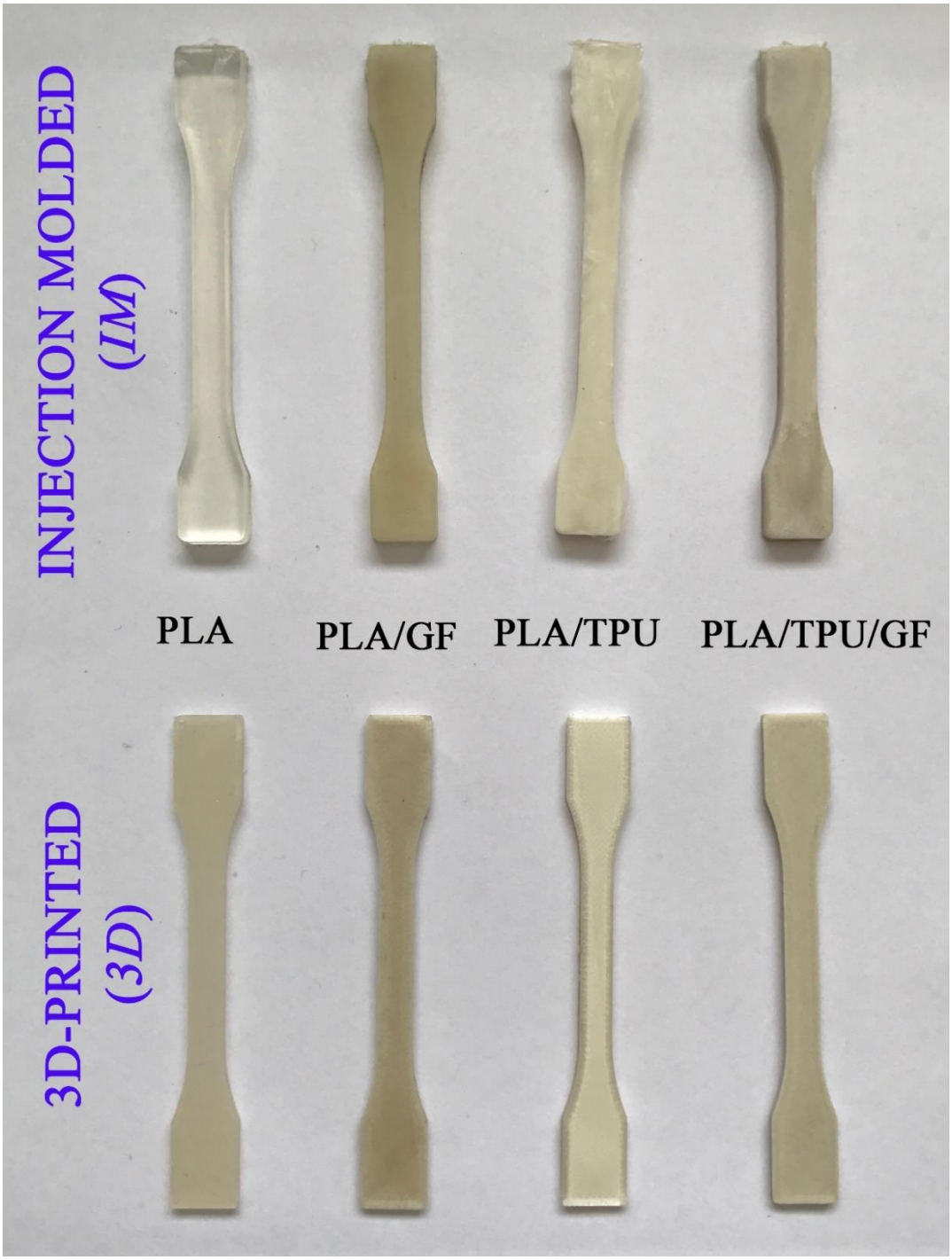

Figure 3.10 Photographic images comparing the macro level appearances of the specimens shaped by injection molding and 3D-printing

However, Figure 3.12 indicates that there were significant differences in terms of the orientation of the GF reinforcements in the fracture surfaces of injection molded and 3D-printed specimens of both PLA/GF and PLA/TPU/GF.

It is seen that almost all GF reinforcements were aligned perpendicular to the fracture plane of the injection molded specimens. Because, during injection molding pressure is applied parallel to the longitudinal direction of the test specimens leading to alignment along this direction.

During 3D-printing, since the equipment scans the specimen geometry with ±45º raster angle directions, Figure 3.12 shows that, in the 3D-printed specimens of PLA/GF and PLA/TPU/GF, some of the GF reinforcements were oriented to the fracture plane with +45º, while some of them were oriented with -45º.

Therefore, as will be discussed in the next section, due to these differences in the orientation of the GF reinforcements, significant changes were observed in the mechanical properties of the injection molded and 3D-printed specimens with GF reinforcements.

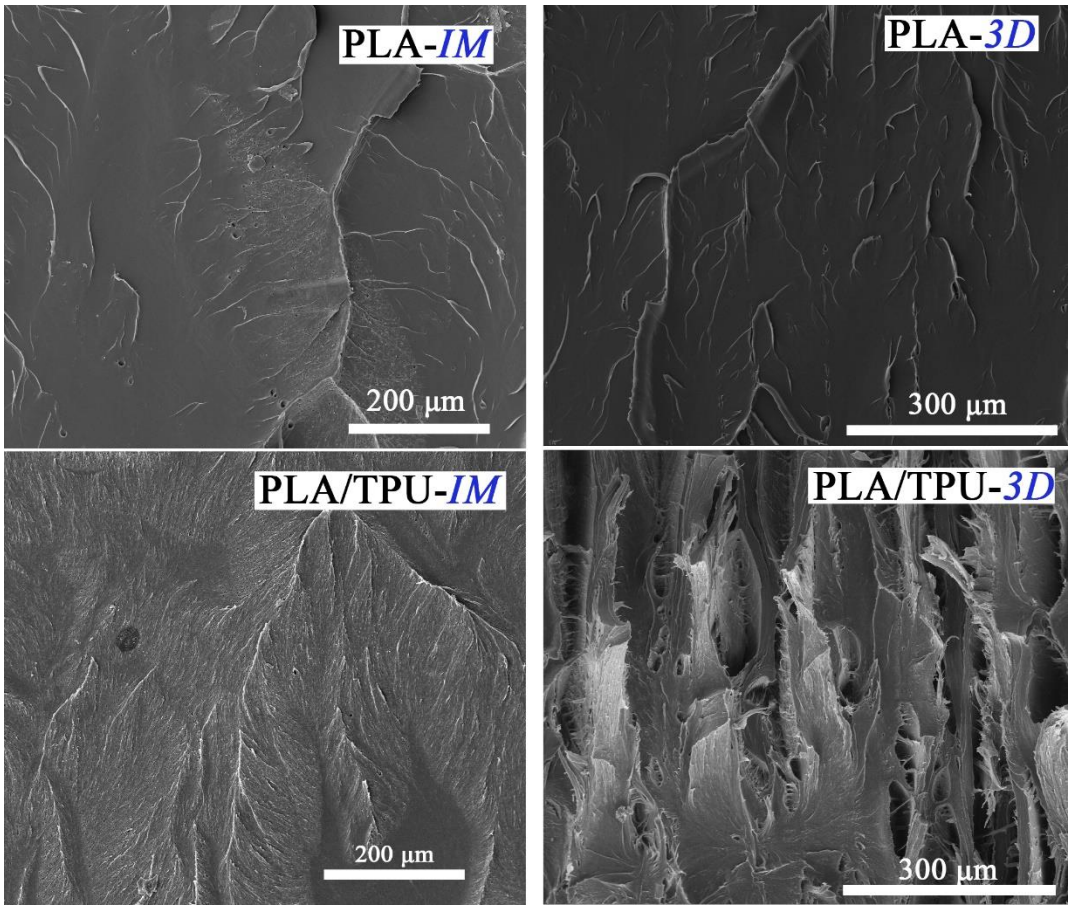

Figure 3.11 SEM images comparing the fracture surface morphology of the PLA and PLA/TPU specimens shaped by injection molding and 3D-printing

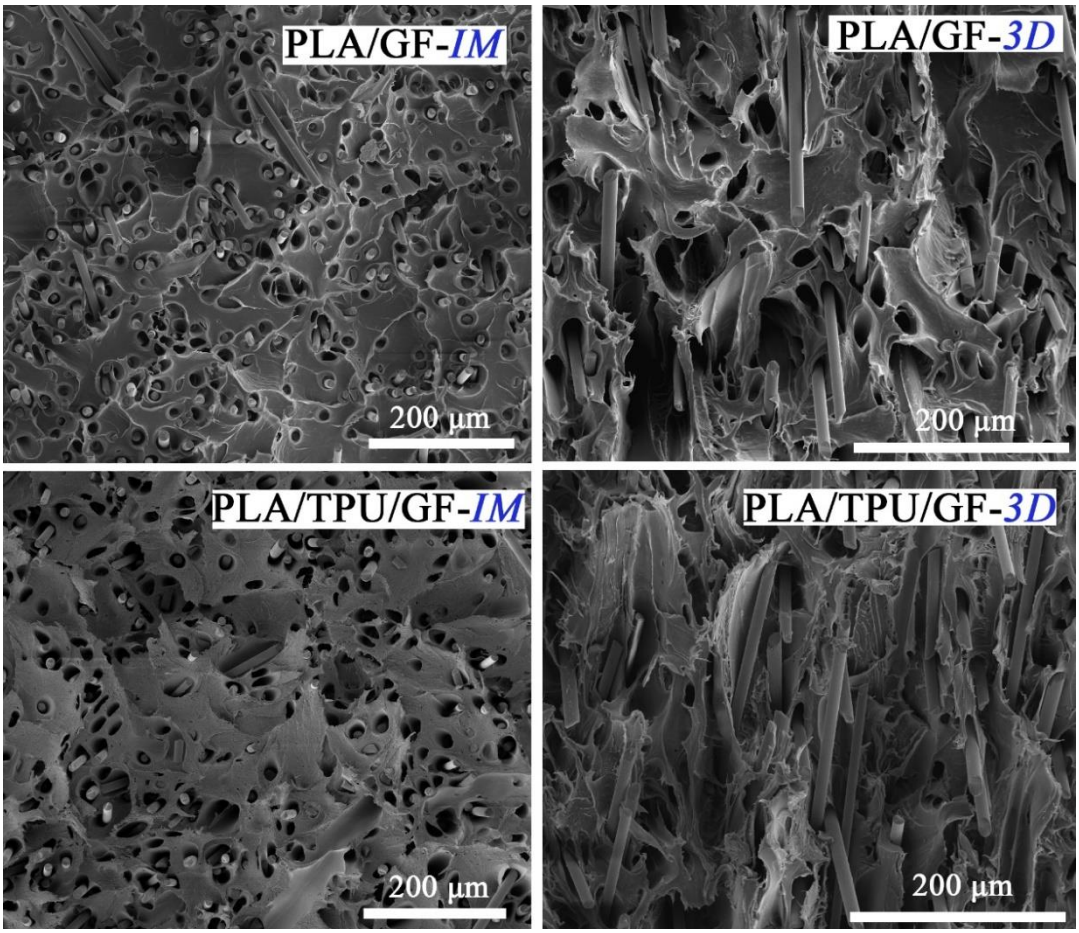

Figure 3.12 SEM images comparing the fracture surface morphology of the PLA/GF and PLA/TPU/GF specimens shaped by injection molding and 3D-printing

3.2.2 Comparison of the Mechanical Properties of the Specimens

In order to compare strength and elastic modulus values of the injection molded and 3D-printed specimens, both tension tests and three-point bending flexural tests were conducted. While "tensile stress-strain" curves and "flexural stress-strain" curves of all specimens are given in Figures 3.13 and 3.14, respectively; the values of "Tensile Strength (σ_{TS})" and "Tensile Modulus (E)" determined by tension tests; and values of "Flexural Strength (σ_{Flex})" and "Flexural Modulus (E_{Flex})" determined by bending tests are compared in Table 3.5. Moreover, influences of injection molding and 3D-printing shaping process on tensile and flexural strength values were compared in Figure 3.15; while tensile and flexural modulus values were compared in Figure 3.16.

These figures and Table 3.5 indicate that for the specimens of neat PLA and PLA/TPU blend, there were no influences of the injection molding and 3D-printing shaping processes on their strength values; because it was seen that both σ_{TS} and σ_{Flex} values of these specimens are almost equal.

Moreover, for these PLA and PLA/TPU specimens, elastic modulus values (both E and E_{Flex}) of the 3D-printed specimens were slightly higher than the injection molded specimens. For example; E and E_{Flex} of the 3D-printed specimens were both 9% higher for neat PLA; and 4% and 13% higher for PLA/TPU blend. These higher modulus values could be due to the stiffening action of the slightly textured structure formed during ±45º raster angle orientation of the 3D-printing.

On the other hand, Table 3.5 also shows that for the GF reinforced specimens; there were significant reductions in the strength and elastic modulus values of their 3D-printed specimens. For instance, the highest reductions in the strength and modulus of the PLA/GF specimens were 32% in σ_{Flex} and 41% in E_{Flex}; while reductions for the PLA/TPU/GF specimens were 30% in σ_{TS} and 20% in E values.

.

Table 3.5 Comparison of the Tensile Strength (σ_{TS}), Flexural Strength (σ_{Flex}), Tensile Modulus (E), Flexural Modulus (E_{Flex}) and Fracture Toughness (K_{IC} and G_{IC}) of the Injection Molded and 3D-Printed Specimens

Specimens	σ_{TS} **(MPa)**	σ_{Flex} **(MPa)**	E **(GPa)**	E_{Flex} **(GPa)**	K_{IC} **(MPa$\sqrt{m}$)**	G_{IC} **(kJ/m^2)**
PLA-*IM*	58.6±1.4	97.9±1.3	2.85±0.08	3.60±0.07	3.43±0.04	5.44±0.34
PLA-*3D*	58.4±0.3	97.2±1.4	3.11±0.03	3.93±0.21	5.03±0.20	7.32±0.66
PLA/TPU-*IM*	53.4±1.4	88.9±1.4	2.49±0.07	3.03±0.11	6.96±0.14	9.46±0.61
PLA/TPU-*3D*	52.3±1.9	88.3±1.5	2.59±0.02	3.42±0.16	8.74±0.14	11.30±1.43
PLA/GF-*IM*	77.3±2.1	118.2±2.8	4.21±0.24	7.20±0.14	4.16±0.10	6.96±0.11
PLA/GF-*3D*	52.1±2.3	80.1±3.1	3.75±0.16	4.25±0.37	3.27±0.20	6.37±0.29
PLA/TPU/GF-*IM*	64.4±1.9	99.7±3.1	3.80±0.14	4.69±0.21	4.85±0.15	6.84±0.12
PLA/TPU/GF-*3D*	45.2±1.3	80.6±3.2	3.03±0.32	3.83±0.24	5.70±0.37	8.84±0.23

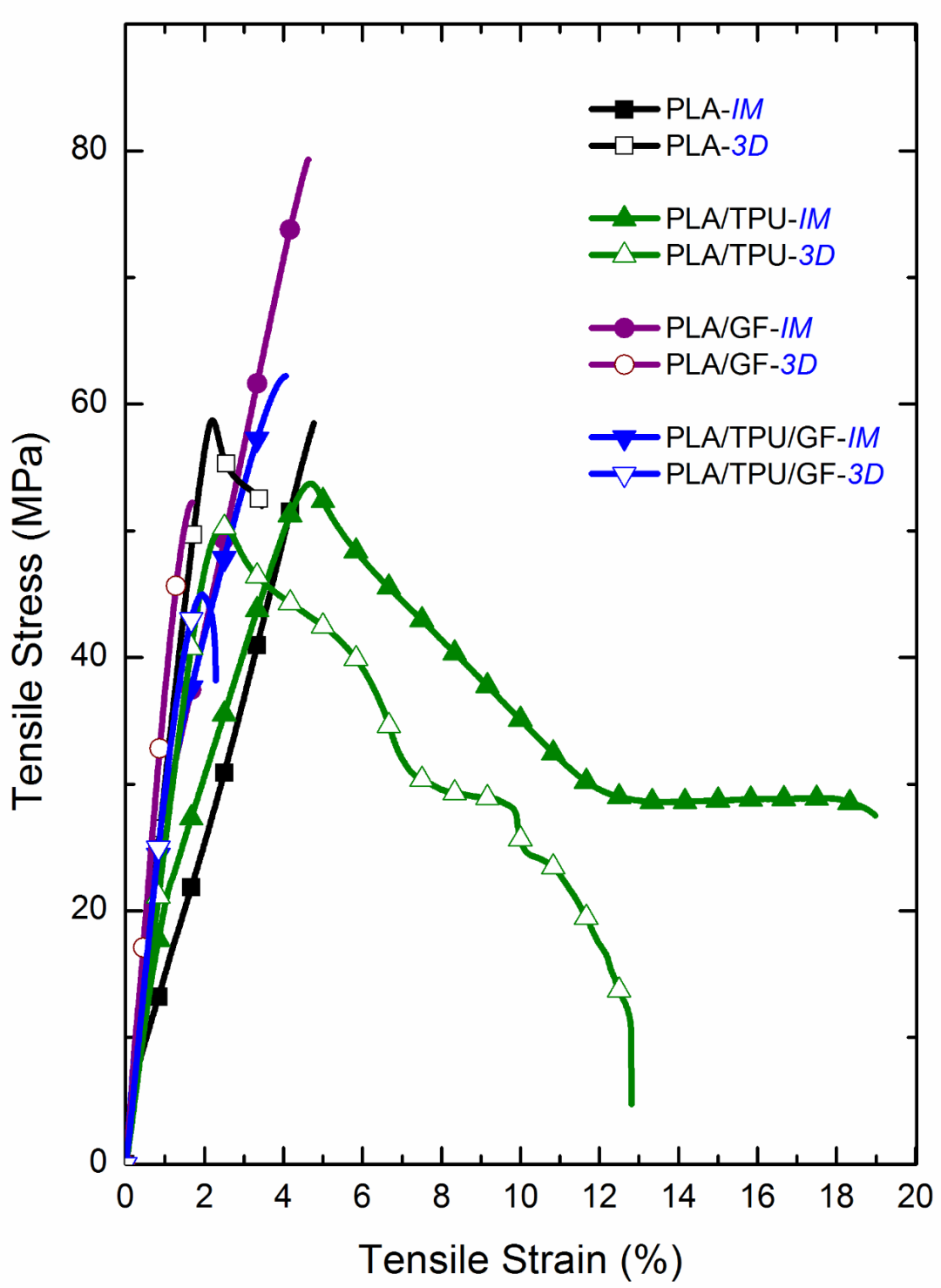

Figure 3.13 Comparison of the tensile stress-strain curves of the injection molded and 3D-printed specimens

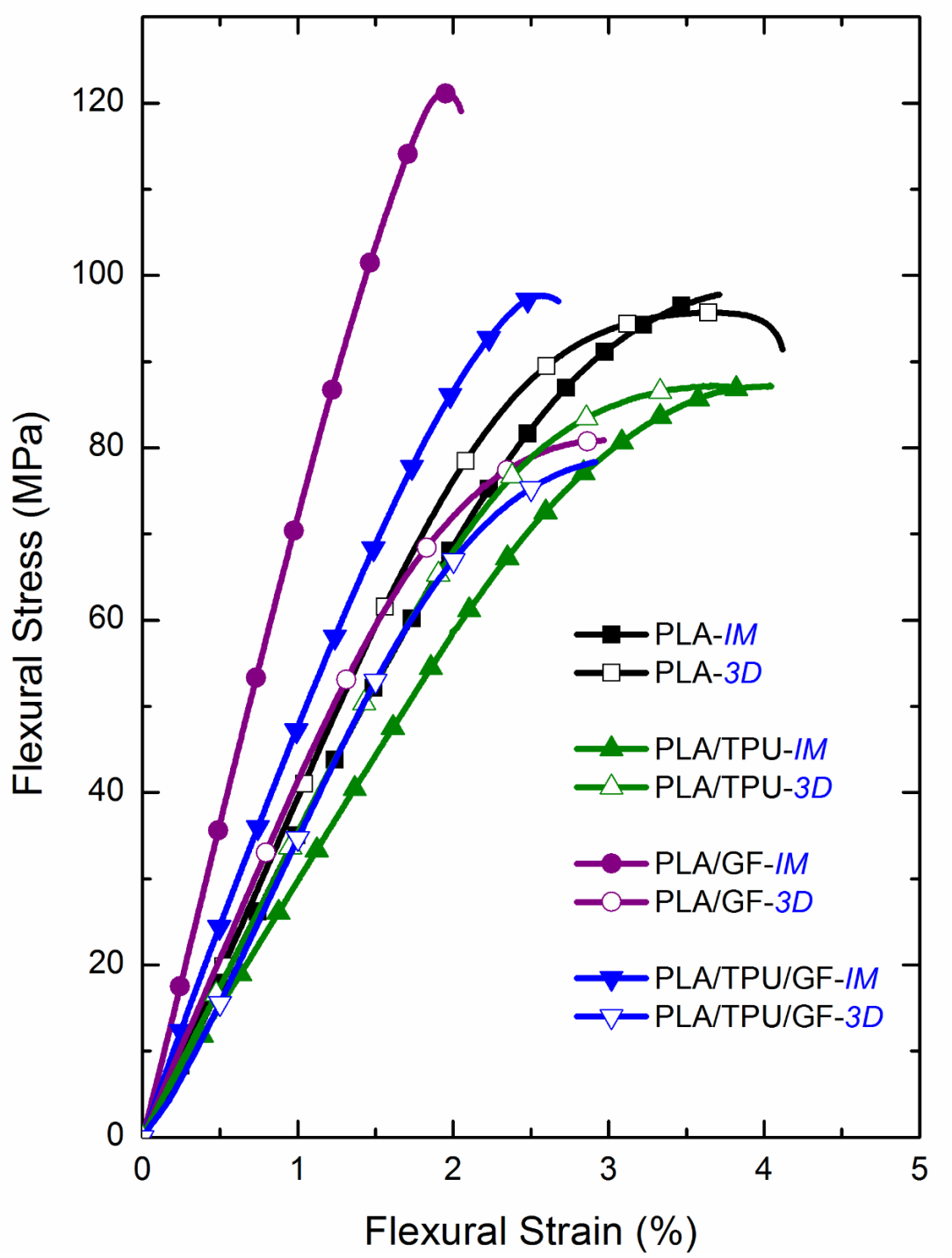

Figure 3.14 The comparison of the flexural stress-strain curves of the injection molded and 3D-printed specimens

As discussed in the SEM morphology analyses above, the main reason for these reductions could be due to the very different orientation of GF reinforcements; being almost all parallel to the longitudinal axis of the injection molded specimens leading to highly effective load transfer mechanism for strength and stiffening mechanism for modulus. In the 3D-printed specimens, ±45º oriented GF reinforcements resulted in decreased level of strengthening and stiffening mechanisms.

Since PLA is an inherently brittle biopolymer, measurement of its toughness becomes crucial. Thus, in order to compare fracture toughness values of the injection molded and 3D-printed specimens, their both "Critical Stress Intensity Factor (K_{IC})" and "Critical Strain Energy Release Rate (G_{IC})" values were determined, and compared in Table 3.5 and Figure 3.17. It is known that K_{IC} and G_{IC} values basically indicate the ability of materials to withstand crack initiation and propagation.

Table 3.5 and Figure 3.17 show that both fracture toughness values of the 3D-printed neat PLA and PLA/TPU specimens were again very beneficial compared to their injection molded specimens. The benefits in the K_{IC} and G_{IC} values of neat PLA were 47% and 35%, respectively; while these benefits were 26% and 19% for the PLA/TPU specimens, respectively. This behavior could be again due to the ±45º textured structure of the specimens leading to additional toughening mechanism of "crack deflection" in the textured body.

However, for the PLA/GF composites, fracture toughness values of the 3D-printed specimens were slightly lower compared to their injection molded specimens. Because crack deflection mechanism at the ±45º oriented GF reinforcements of 3D-printing would be lower compared to 90º oriented GF reinforcements in injection molding. This means that perpendicular GF reinforcements to the crack propagation plane would be much more effective in crack deflection and crack bowing mechanisms.

In the PLA/TPU/GF composite, fracture toughness values of the 3D-printed specimens were again beneficial compared to their injection molded specimens. This time the benefits of 3D-printing were 18% in K_{IC} and 29% in G_{IC}. Because in this specimen,

reduced crack deflection toughening effectiveness with ±45º oriented GF reinforcements were recovered by the enormous level of rubber toughening mechanism of TPU domains in the matrix.

Finally, in order to reveal %Benefits and %Reductions in the mechanical properties of the 3D-printed specimens compared to injection molded ones, Figure 3.18 was constructed. It can be concluded that use of 3D-printing in the shaping of neat PLA and PLA/TPU blend was generally very beneficial; on the other hand, due to the differences in the orientation of the GF reinforcements, there could be certain reductions in the mechanical performance od PLA/GF and PLA/TPU/GF.

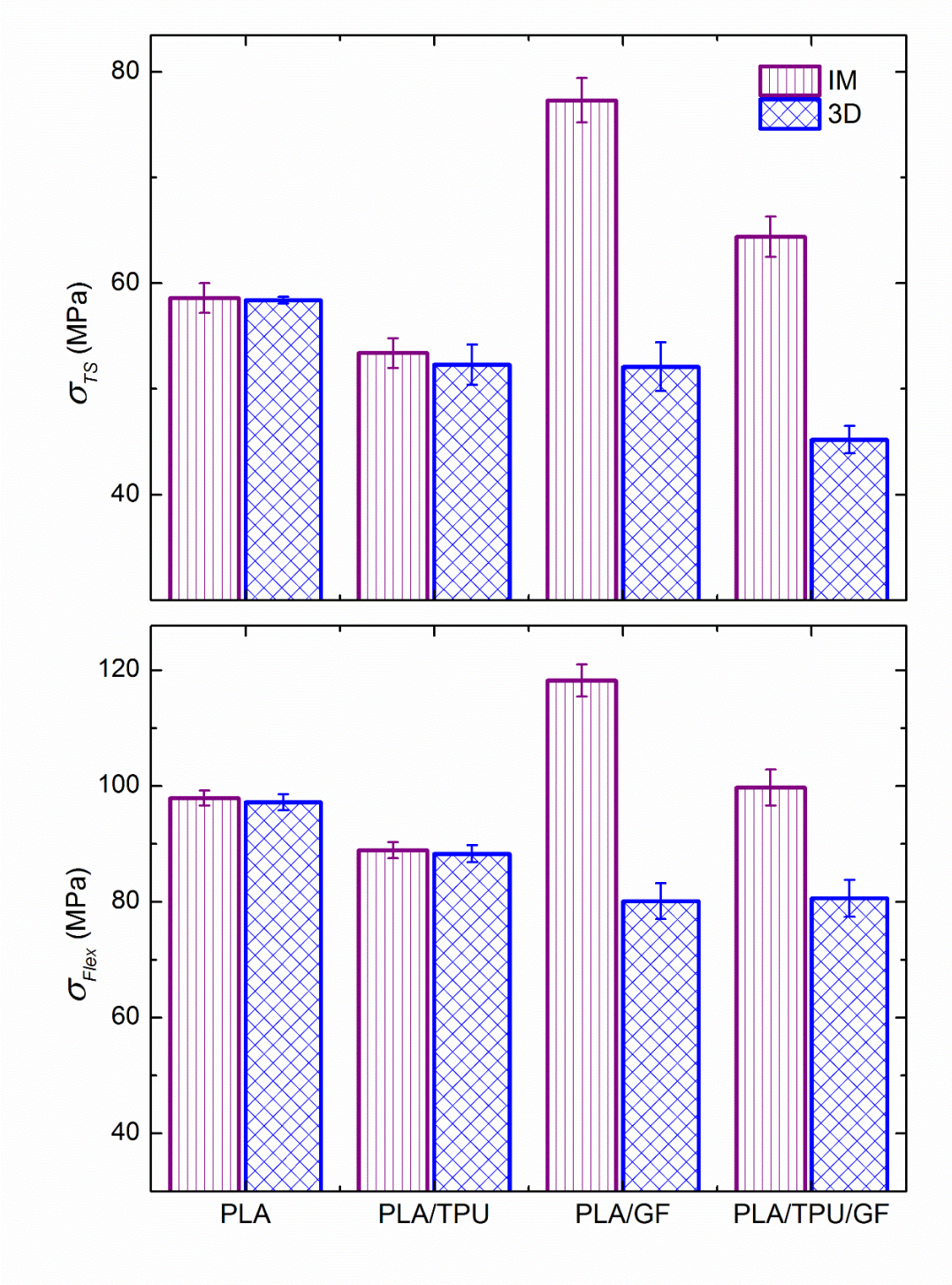

Figure 3.15 Comparison of the tensile strength and flexural strength of the injection molded and 3D-printed specimens

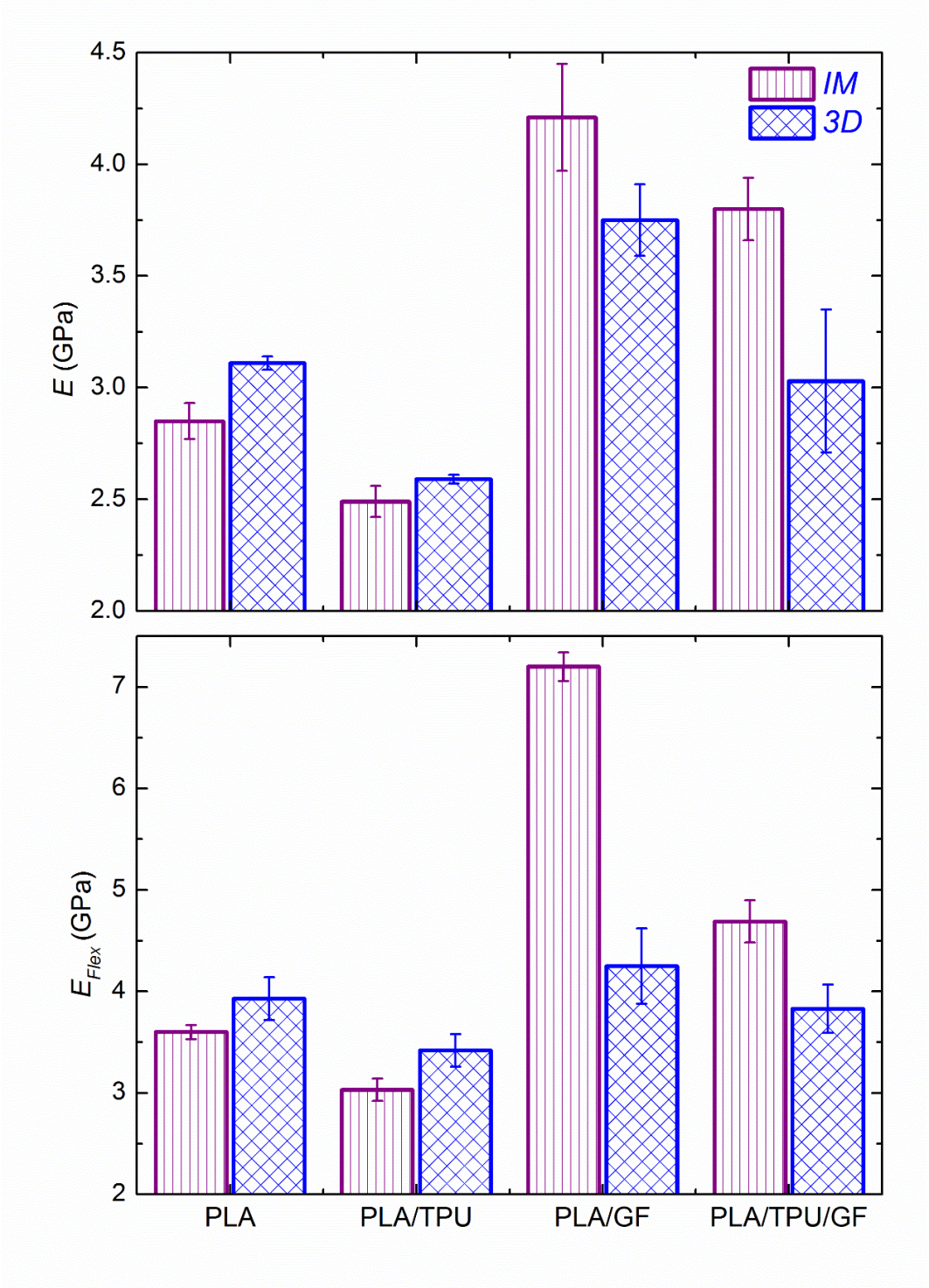

Figure 3.16 Comparison of the tensile modulus and flexural modulus of the injection molded and 3D-printed specimens

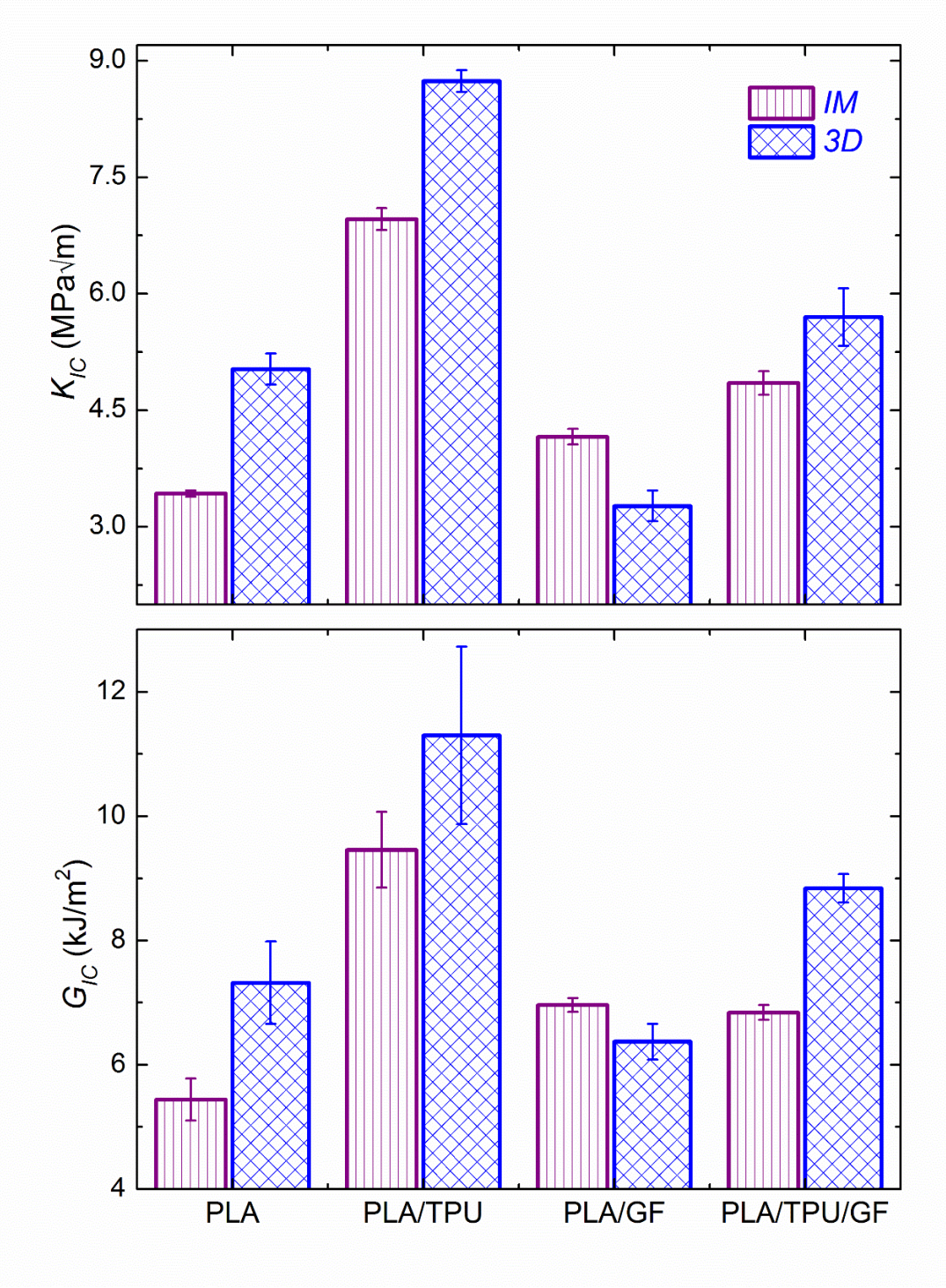

Figure 3.17 Comparison of the fracture toughness of the injection molded and 3D-printed specimens

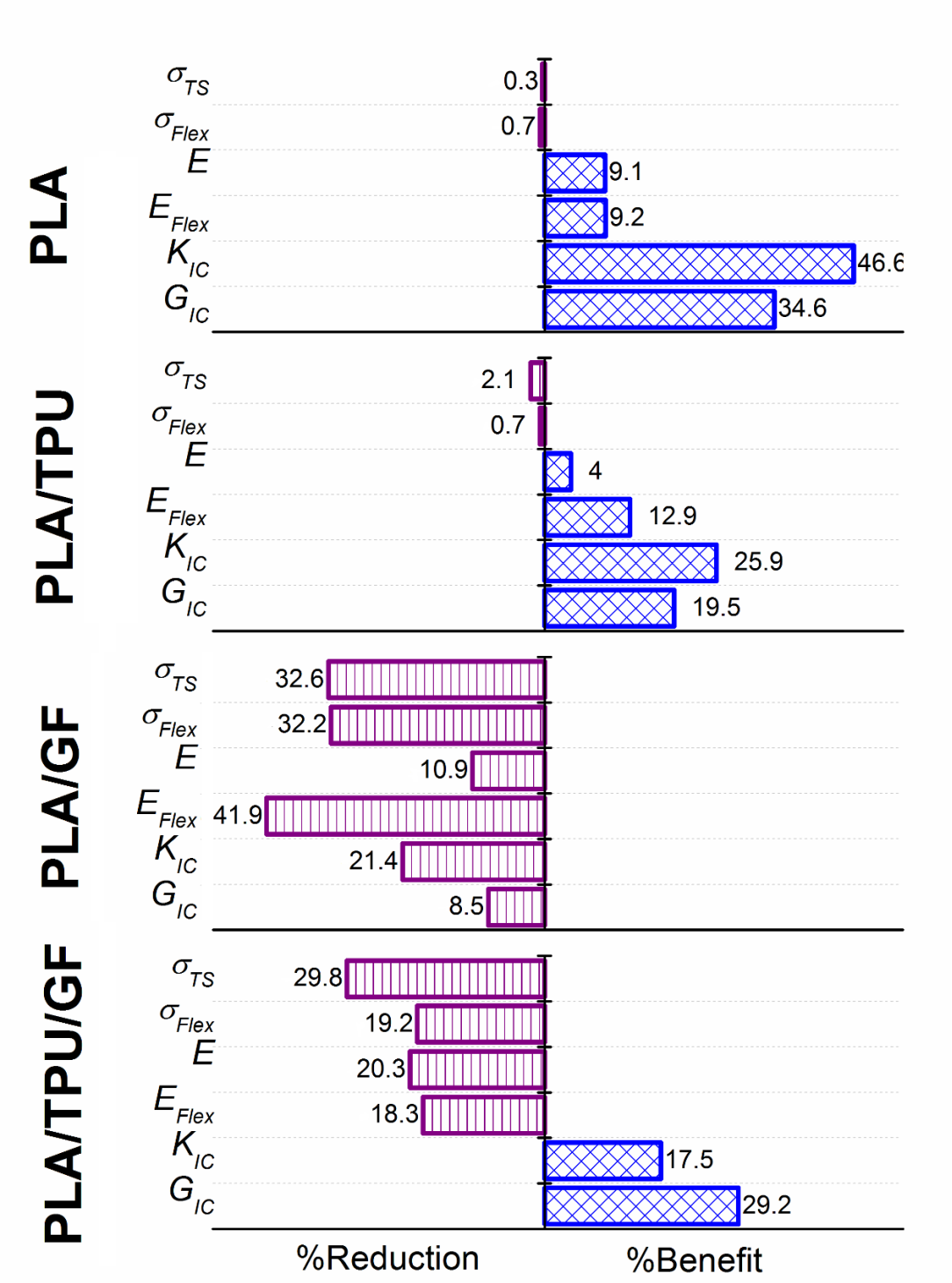

Figure 3.18 %Benefits and %Reductions in the mechanical properties of the 3D-printed specimens compared to injection molded specimens

3.2.3 Comparison of the Thermal Behavior of the Specimens

The first analyses to compare thermal behavior of the injection molded and 3D-printed specimens was DSC. First heating thermograms of the specimens were given in Figure 3.19, while the important transition temperatures; i.e. glass transition (T_g), cold crystallization (T_c) and melting (T_m) temperatures together with melting and crystallization enthalpies (ΔH_m and ΔH_c) including percent crystallinity (X_C) of the specimens were tabulated in Table 3.6. The relation used in calculation of percent crystallinity is given in section 3.1.4.

Table 3.6 and Figure 3.19 show that two shaping process used in this study do not lead to any differences in the transition temperatures (T_g, T_c, T_m) of the PLA based materials. Because it is seen that the values of all these transition temperatures of the injection molded and 3D-printed specimens are almost equal.

On the other hand, shaping by injection molding and 3D-printing has certain influences on the enthalpies and consequently on the crystallinity amount (X_C) of the specimens. For instance, % X_C of the injection molded PLA specimen is 3.84 while it is 5.27 for the 3D-printed one; similarly, these values are 4.30 and 6.33 for the for the PLA/TPU blend, respectively. This could be interpreted that cooling rate during 3D-printing is rather lower than the cooling rate during injection molding; so that macromolecular PLA chains have more time to crystallize during 3D-printing.

However, Table3.6 also indicates that crystallinity amount of the GF reinforced specimens (both PLA/GF and PLA/TPU/GF) shaped by 3D-printing were lower than their injection molded specimens. Because these high aspect ratio GF reinforcements could hinder the conformational mobility of the PLA chains to crystallize.

Table 3.6 Comparison of the Transition Temperatures (T_g, T_c, T_m), Enthalpies (ΔH_m, ΔH_c) and Crystallinity Percent (X_C) of the Injection Molded and 3D-Printed Specimens During DSC First Heating

Specimens	T_g **(°C)**	T_c **(°C)**	T_m **(°C)**	ΔH_m **(J/g)**	ΔH_c **(J/g)**	X_C **(%)**
PLA-*IM*	63.4	118.0	148.4	7.58	4.01	3.84
PLA-*3D*	63.6	120.5	149.7	18.5	13.6	5.27
PLA/TPU-*IM*	65.4	98.5	150.2	27.9	24.3	4.30
PLA/TPU-*3D*	65.3	102.7	150.4	23.8	18.5	6.33
PLA/GF-*IM*	65.4	122.2	149.4	17.1	11.2	7.34
PLA/GF-*3D*	65.1	116.3	148.6	25.5	21.9	4.55
PLA/TPU/GF-*IM*	64.7	104.2	149.4	15.9	11.3	6.59
PLA/TPU/GF-*3D*	64.3	103.2	147.7	19.1	15.2	5.59

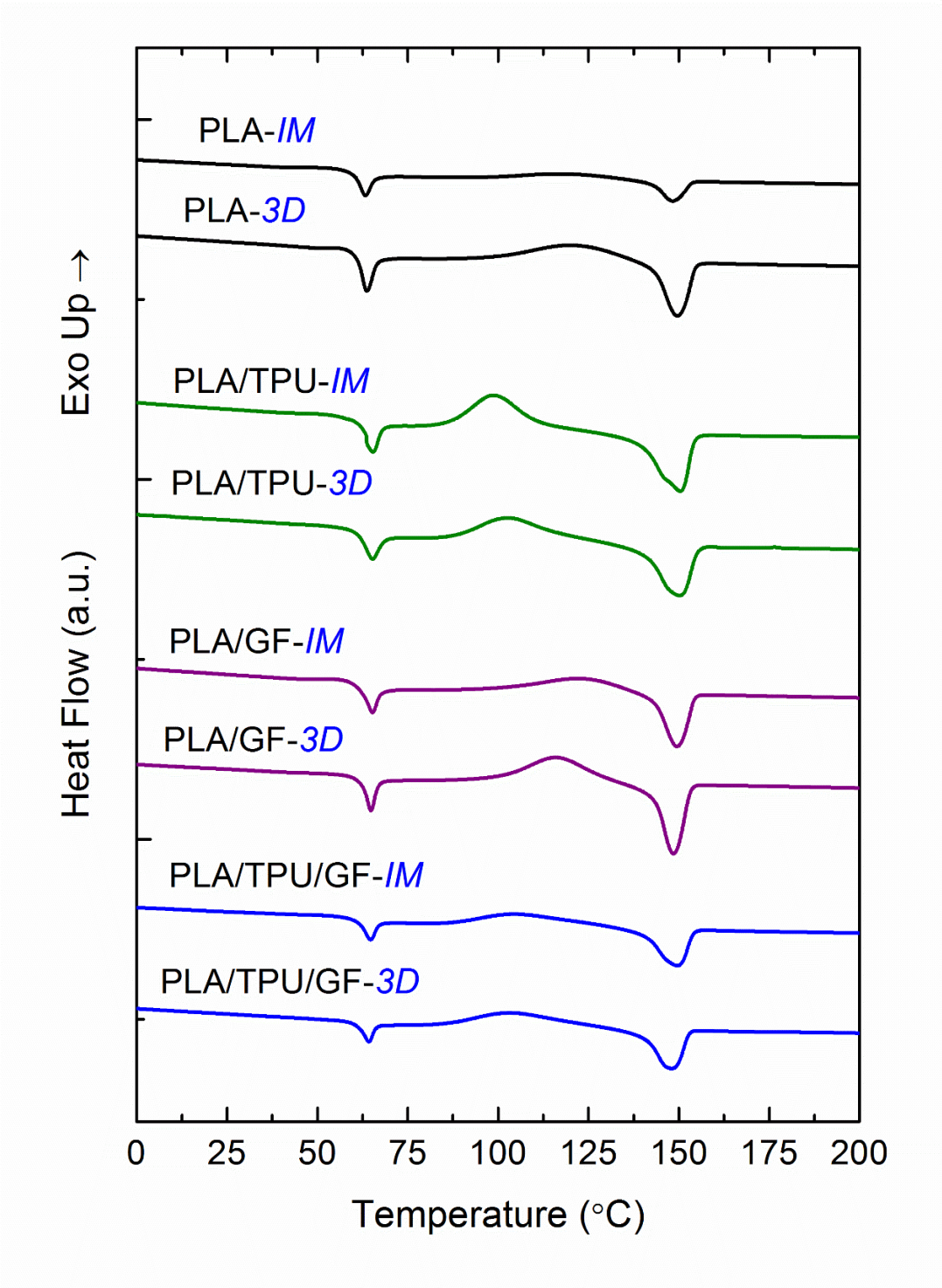

Figure 3.19 Comparison of the first heating DSC thermograms of the injection molded and 3D-printed specimens

The second analyses to compare thermal behavior of the injection molded and 3D-printed specimens was TGA. Thermogravimetric curves of the specimens were given in Figure 3.20, while the data determined were tabulated in Table 3.7 as $T_{5\%}$, $T_{10\%}$ and $T_{25\%}$ representing the thermal degradation temperatures of the samples at 5, 10 and 25% mass losses, and T_{max} representing the temperature at maximum mass loss. In the table %residue of each specimen determined at 550ºC were also included. Table 3.7 and Figure 3.20 revealed that shaping by injection molding and 3D-printing had no influences on the thermal degradation temperatures of all PLA based materials, because it is seen that all values are almost equal.

Table 3.7 Comparison of the Thermal degradation temperatures (T5%, T10%, T25%) of the Injection Molded and 3D-Printed specimens at 5, 10 and 25 wt% mass losses, the maximum mass loss temperature (Tmax) and %Residue at 550ºC

Specimens	**$T_{5\%}$ (°C)**	**$T_{10\%}$ (°C)**	**$T_{25\%}$ (°C)**	**T_{max} (°C)**	**%Residue at 550ºC**
PLA-*IM*	330	340	352	367	1.05
PLA-*3D*	328	338	350	366	0.82
PLA/TPU-*IM*	320	332	349	369	1.82
PLA/TPU-*3D*	314	325	343	365	1.62
PLA/GF-*IM*	331	342	355	368	14.97
PLA/GF-*3D*	322	335	349	366	13.22
PLA/TPU/GF-*IM*	303	315	335	359	16.85
PLA/TPU/GF-*3D*	306	317	337	366	18.34

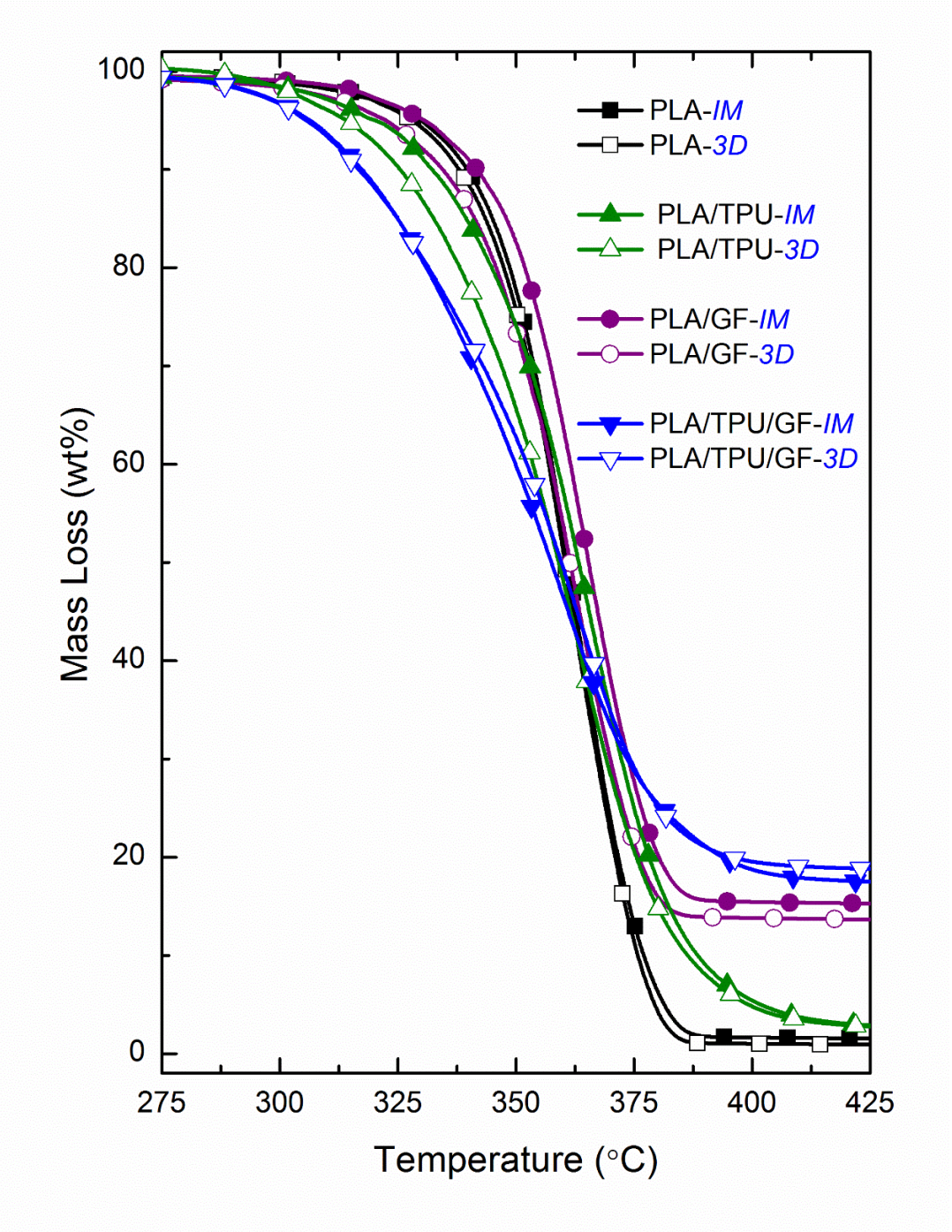

Figure 3.20 Comparison of the thermogravimetric curves of the injection molded and 3D-printed specimens

3.3 Effects of Weathering

3.3.1 Alteration in the Color

One of the main problem in the outdoor applications of polymeric components is their color change with sunlight exposure. Therefore, in this study, alterations in color of the specimens after each accelerated weathering period were evaluated first visually by the photographic images (Figure 3.21) and then quantitatively by determining CEILAB color space parameters via diffused reflectance analyses (DRA) (Table 3.8).

It is seen in Figure 3.21 that the neat PLA specimen appears very transparent; because, as will be discussed in the thermal behavior section, PLA has no ability to crystallize due to the very high cooling rate of the injection molding process resulting in a high level of amorphous structure. However, during accelerated weathering test, the temperature in the unit is 70ºC in each UV-irradiation cycle, which is sufficient for the start of cold crystallization of PLA. Thus, just after 100h period, due to the increased level of crystallinity level, neat PLA specimen becomes “white”. Figure 3.21 shows that, whiteness of PLA specimen increases slightly with further weathering periods.

Similarly, the quantitative color parameters in Table 3.8 revealed that, the most significant change occurs in the values of L* parameter which represents “whiteness”. It is seen that increasing the weathering period increases the L* parameter, and consequently the total color change parameter of ΔE*.

By the addition of 15 wt% GF into the PLA matrix, Figure 1 indicates that the color of the composite specimen becomes a kind of slightly yellowish grey. After each accelerated weathering period, the greyness and yellowness level of the specimens fade away, becoming more and more light grey.

The visual observation of the PLA/GF composite specimens were also consistent with the quantitative color parameters. Table 1 shows that the values of +b* color parameter representing “yellowness” decreases with increasing weathering period; i.e. the

yellowish color tone of the specimens fade away. Similarly, L* color parameter of the composite specimens increases with increasing weathering period; i.e. the greyness color tone decreases leading to final appearance of the specimen as light grey color.

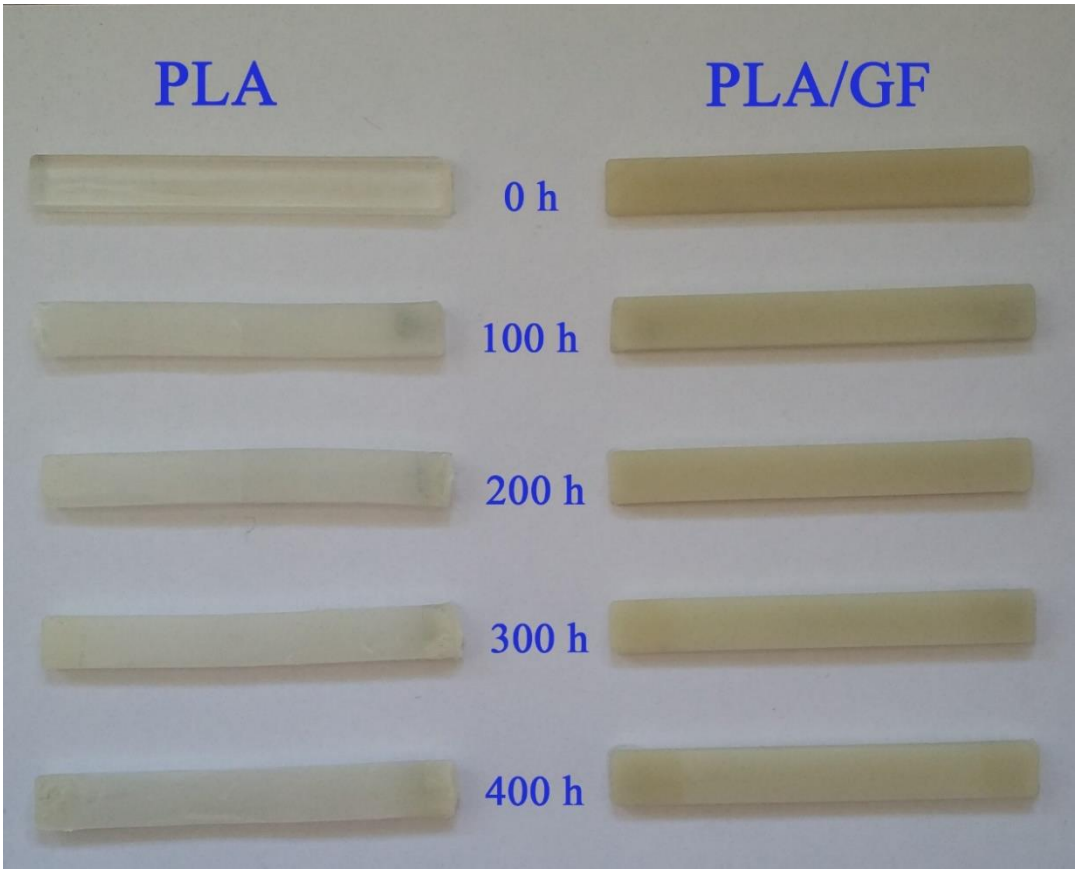

Figure 3.21 Alterations in the photographic images of the specimens after each accelerated weathering period

3.3.2 Alteration in the Chemical Structure

It is known that the UV-irradiation and moisture cycles during the accelerated weathering leads to deterioration in the chemical structure of PLA matrix especially in the form of molecular weight (MW) decrease via chain scission reactions. Therefore, as the first chemical analyses technique, static light scattering (SLS) spectrometry was conducted to determine the level of molecular weight reduction of PLA matrix after each weathering period. SLS spectrometry results in Figure 3.22 show that the weight average molecular weight (M_w) of the unweathered PLA matrix drops drastically from

$3.7x10^5$ down to $1.3x10^5$ just after only 100h weathering period; and this value almost diminishes to 0.1 $x10^5$ after 400h accelerated weathering. As will be discussed in the mechanical properties section later, these reductions in M_w of the PLA matrix resulted in significant losses especially in the strength and toughness of the specimens.

Table 3.8 Alterations in the CIELAB color space parameters (L*, a*, b*) and total color change (ΔE*) values of the specimens after each accelerated weathering period

Specimens	***L****	***a****	***b****	**Δ*E****
PLA-0h	24.63	-0.31	-0.64	
PLA-100h	38.15	-0.54	-3.72	13.87
PLA-200h	39.69	-0.73	-4.02	16.62
PLA-300h	48.97	-0.68	-3.40	25.23
PLA-400h	49.14	-0.64	-4.12	33.17
PLA/GF-0h	48.45	-1.43	4.42	
PLA/GF-100h	55.16	-1.95	3.57	6.79
PLA/GF-200h	56.62	-1.92	3.46	8.24
PLA/GF-300h	59.14	-1.86	3.34	10.76
PLA/GF-400h	59.87	-1.94	3.22	11.50

Secondly, in order to observe alterations in the chemical bond structure of the specimens after each accelerated weathering period; ATR-FTIR analyses were also conducted. Those spectra for the neat PLA specimens after each accelerated weathering are given in Figure 3.23. In the literature [7] it is well established that the chemical bond structure of PLA has basically six distinctive IR bands.

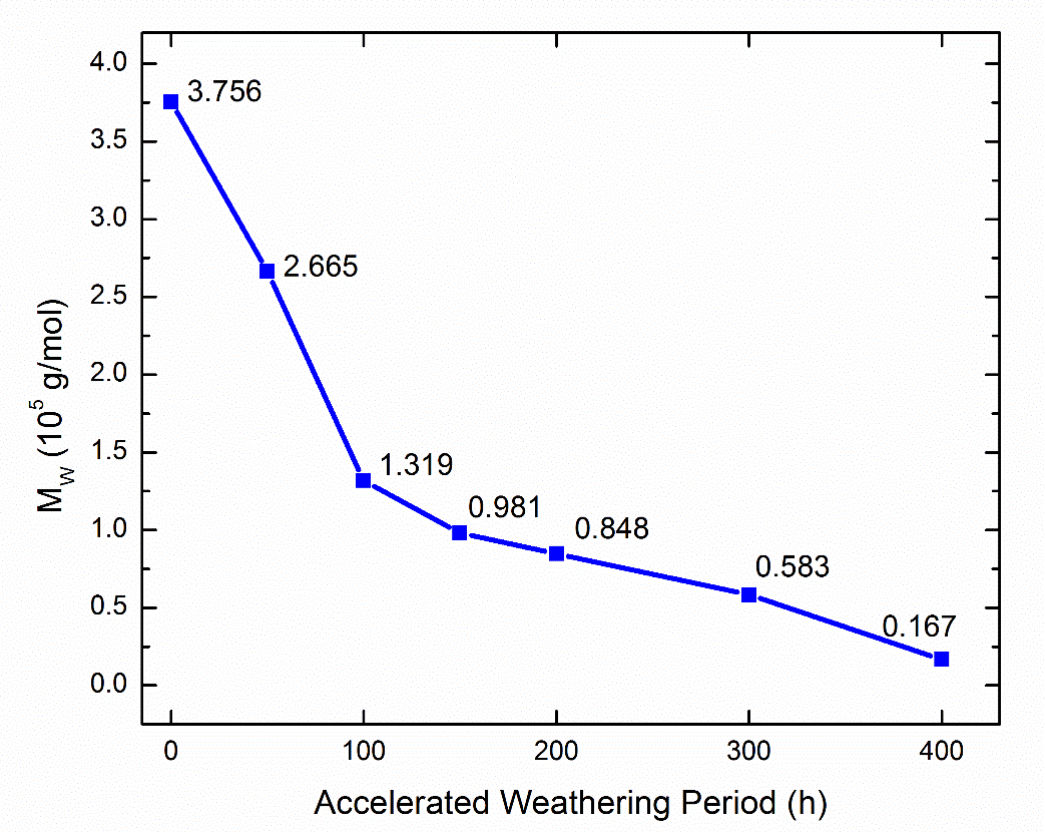

Figure 3.22 Alterations in the weight average molecular weight of the PLA matrix after each accelerated weathering period

The first spectra in Figure 2.33 shows that all these typical bands were observed for the unweathered PLA matrix (PLA-0h); i.e. C-C stretching peak at 866 cm^{-1}; C-O stretching peaks at 1080 cm^{-1} and 1262 cm^{-1}; C-H deformation peak at 1370 cm^{-1}; CH_3 bending absorption at 1451 cm^{-1}; C=O ester carbonyl stretching groups at 1748 cm^{-1}; and C-H stretching peaks at 2879 cm^{-1}, 2946 cm^{-1} and 2995 cm^{-1}.

It has been discussed [119]–[121] that the most significant deterioration of UV-irradiation is the "chain scission" especially at the C-C and C-O bonds of the ester backbone structure of PLA by a photon absorption. The mechanism is generally called as "photolysis", or as the type of degradation reactions; "Norrish II type photo-cleavage reaction" and "photo-oxidation reaction". Thus, Figure 3.23 indicates that, due to the significant level of chain scissions in the ester backbone structure of PLA, IR intensities of not only C-C and C-O stretching peaks but also all other typical peaks of unweathered PLA specimen (0h) decrease significantly with increasing accelerated

weathering period. It is seen that these peaks almost all faded away becoming very broad after 400h accelerated weathering.

It has been stated [121] that photolysis of PLA via Norrish II type photo-cleavage reaction leading to decreased molecular weight by chain scission results in the formation of C=C double bonds and hydroperoxide (O-H) at the new PLA chain terminals. Thus, it is seen in Figure 3.23 that, even after 100h weathering period, these new peaks of C=C and O-H appears at 2147 cm^{-1} and 3742 cm^{-1}, respectively. Apart from new peak formations, it is known [83] that, chain scissions via photolysis reactions also lead to shifting of the IR peaks of the typical PLA bands to lower wavenumbers. For instance, Figure 3.23 reveals that, after weathering, the C-O stretching peaks shifted from 1080 cm^{-1} to 1025 cm^{-1}, and 1262 cm^{-1} to 1091 cm^{-1}; while the C=O carbonyl stretching peaks shifted from 1749 cm^{-1} to 1743 cm^{-1}.

Apart from UV-irradiation steps, during accelerated weathering tests, there were also moisture (condensation) steps leading to not only swelling and plasticizing of PLA matrix, but also significant level of chemical degradation called as “hydrolysis”. During hydrolysis, it was stated that especially C-O ester linkages of PLA structure experience cleavage, leading to again significant decreases in molecular weight [83, 85, 119].

It was also explained [119] that products of the hydrolysis and photolysis reactions are rather similar. Thus, the alterations in the IR spectra of the weathered specimens discussed above would be valid also for the hydrolysis.

In the IR spectra of the PLA/GF composite specimens after each weathering period, very broad unclear peaks were obtained. This could be due to the very high amount of inorganic glass structure (15 wt% GF) obscuring the IR transmittance, so that it was not possible to discussed the alterations in the spectra of these specimens. However, it can be pointed out that there would be the same photolysis and hydrolysis reactions discussed above in the PLA matrix of the GF reinforced composite specimens.

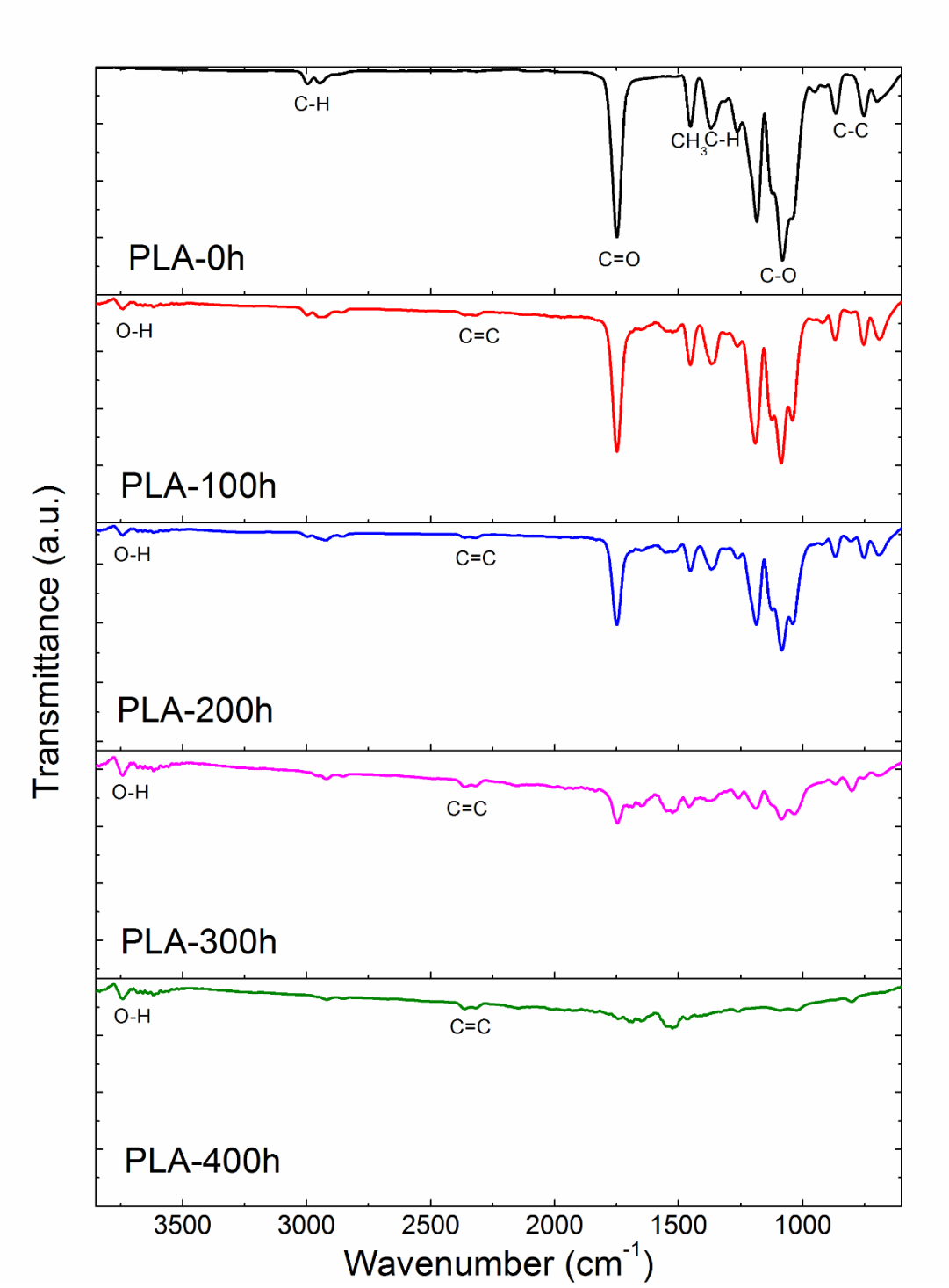

Figure 3.23 Alterations in the ATR-FTIR spectra of the neat PLA specimens after each accelerated weathering period

3.3.3 Alteration in the Fracture Surface Morphology

In order to observe alterations in the fracture surface morphology of the specimens, their fracture toughness test specimens were investigated under SEM after each accelerated weathering period. In Figure 3.24, SEM images of neat PLA and PLA/GF specimens after each accelerated weathering period. It is seen that neat PLA specimen, being inherently brittle material, has rather very smooth fracture surface before weathering. On the other hand, after weathering, due to the significant chemical structure deteriorations of photolysis and hydrolysis reactions, extensive number of voids, cracks and cleavages appeared on the fracture surface.

For the neat PLA/GF composite specimen, Figure 3.24 shows that apart from the pull-out holes of the GF reinforcements, the number of voids, cracks and cleavages in its PLA matrix were not so severe compared to neat PLA specimen. Thus, as will be discussed in the mechanical properties sections below, reductions in the mechanical properties of the PLA/GF specimen, due to weathering degradations, were not as drastic as the reductions of the neat PLA specimen.

3.3.4 Alteration in the Mechanical Properties

Alterations in the mechanical properties of the neat PLA and PLA/GF composite specimens after each accelerated weathering periods were first evaluated by tension tests and 3-point bending tests. The resultant “tensile stress- strain” and “flexural stress- strain” curves are given in Figure 3.25 and 3.26, respectively; while the tensile and flexural modulus (E and E_{Flex}) values, together with tensile and flexural strengths (σ_{TS} and σ_{Flex}) values are tabulated in Table 3.9. Moreover, effects of increasing accelerated weathering periods on these strength and modulus values were illustrated in Figure 3.27.

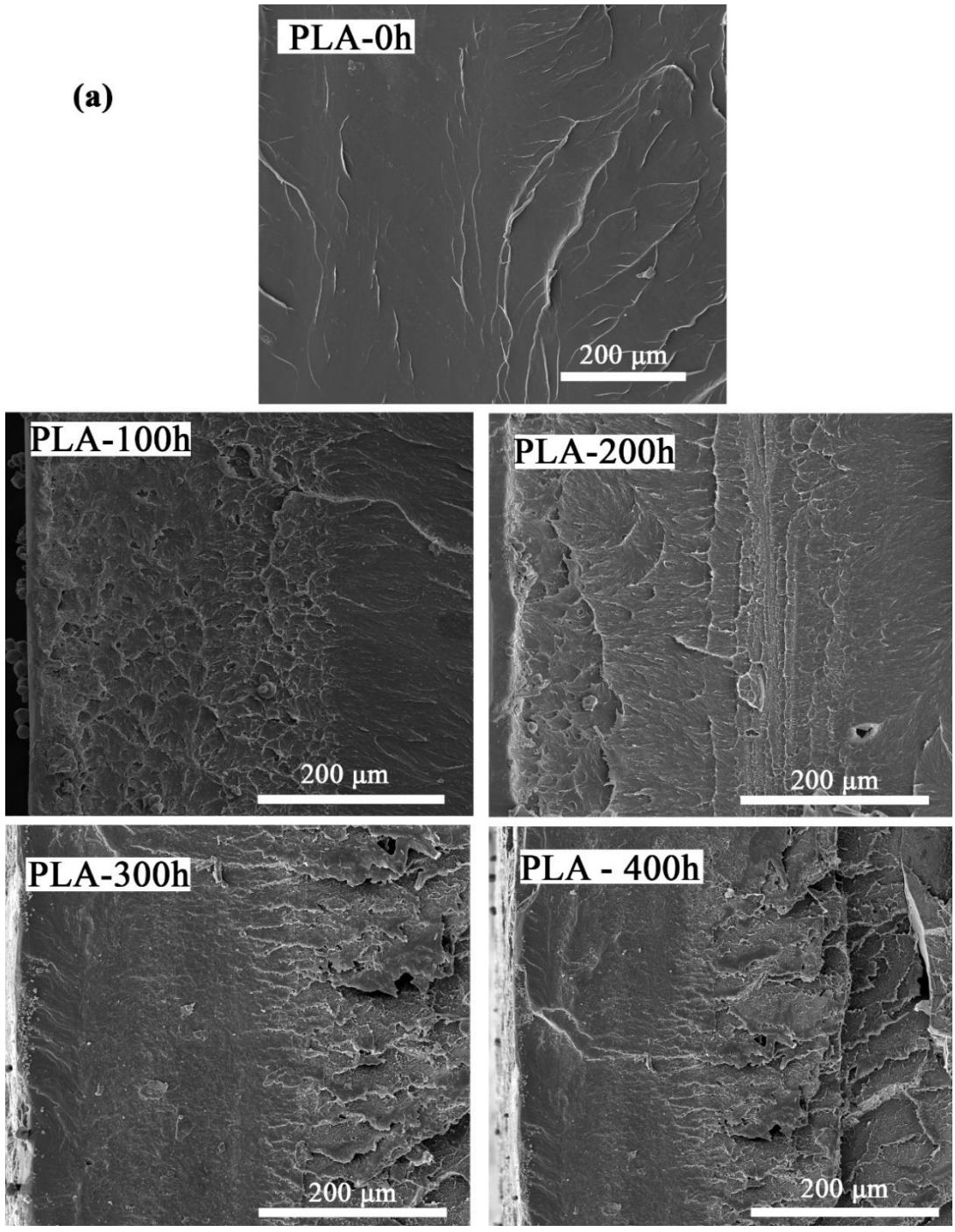

Figure 3.24 Alterations in the SEM images of the fracture surface morphology of the specimens after each accelerated weathering period (a) neat PLA, (b) PLAGF composite

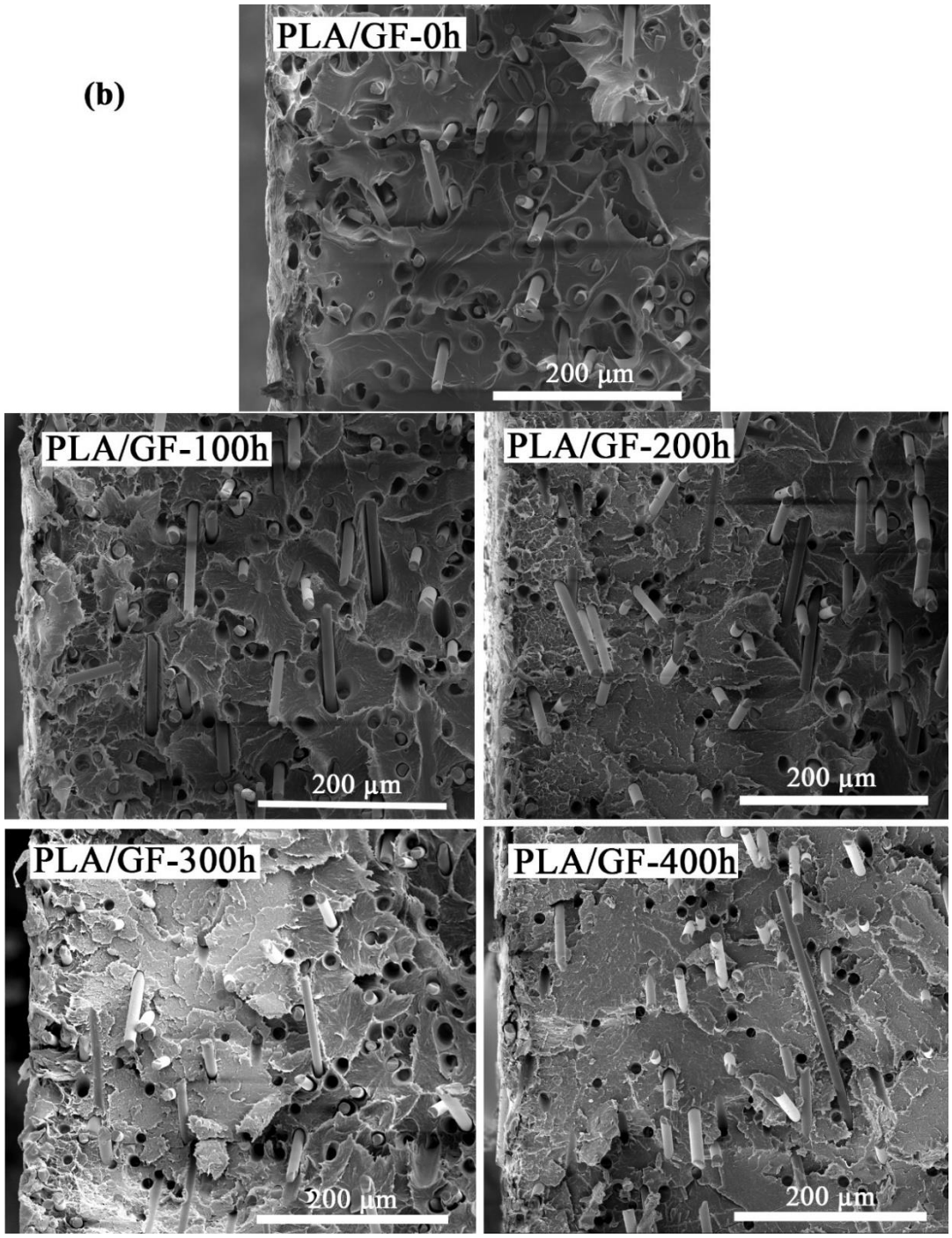

Figure 3.24 (Continued)

It is seen in Table 3.9 and Figure 3.27 that, during the initial accelerated weathering periods of 50h and 100h, there were slight increases in the elastic modulus (both E and E_{Flex}) of the neat PLA and PLA/GF composite specimens. These increases were due to the increased crystallinity amount of their PLA matrices. Because, as will be discussed in the thermal behavior section, during UV-irradiation cycles of weathering tests, the temperature of the unit is 70ºC, which is sufficient for the start of cold crystallization of PLA macromolecular chains.

On the other hand, beyond accelerated weathering period of 150h, detrimental effects of photolysis and hydrolysis reactions were more dominant compared to the stiffening action of increased crystallinity; thus, elastic modulus (E and E_{Flex}) values of the specimens started to decline gradually.

Reductions in the elastic modulus values of the neat PLA specimens after 400h weathering period were important; being 16% in E_{Flex} and an enormous drop of 54% in E. However, due to the very efficient stiffening actions of GF reinforcements, there were almost no deteriorations in the elastic modulus of the PLA/GF composite specimens; i.e. E and E_{Flex} values of unweathered (0h) and weathered (400h) PLA/GF specimens were almost the same.

Table 3.9 and Figure 3.27 also shows that, although increased crystallinity amount after 50h and 100h increased strength of the composite specimen slightly, generally increasing accelerated weathering periods decreased strength (both σ_{TS} and σ_{Flex}) values of the neat PLA and PLA/GF composite specimens. Because, strengthening action of the higher crystallinity amount was not sufficient to keep the strength values of the specimens from the very detrimental extensive chain scission actions of the weathering degradation reactions mentioned before.

It was observed that, after 400h weathering period, reductions in the strength of the neat PLA were more severe, being as much as 92% in σ_{TS} and 70% in σ_{Flex}; while for the PLA/GF composite specimen only 34% in σ_{TS} and 46% in σ_{Flex}.

Table 3.9 Alterations in the Tensile Modulus (E), Flexural Modulus (E_{Flex}), Tensile Strength (σ_{TS}) and Flexural Strength (σ_{Flex}) of the specimens after each accelerated weathering period

Specimens	***E* (GPa)**	***E*$_{Flex}$ (GPa)**	**σ_{TS} (MPa)**	**σ_{Flex} (MPa)**
PLA-0h	2.85±0.08	3.60±0.07	58.6±1.4	97.9±1.3
PLA-50h	2.89±0.16	4.58±0.09	51.6±1.1	93.0±1.9
PLA-100h	2.86±0.18	4.51±0.01	39.1±0.6	82.8±0.2
PLA-150h	2.73±0.09	4.21±0.04	29.5±1.2	57.7±2.7
PLA-200h	2.43±0.13	4.12±0.13	22.8±1.5	52.3±0.6
PLA-300h	1.98±0.29	3.95±0.04	11.7±1.2	35.7±3.4
PLA-400h	1.32±0.16	3.03±0.11	4.8±0.4	28.9±2.8
PLA/GF-0h	4.21±0.24	7.20±0.14	77.3±2.1	118.2±2.8
PLA/GF-50h	4.30±0.13	7.29±0.07	77.7±1.2	135.7±1.1
PLA/GF-100h	4.77±0.34	7.34±0.08	82.0±2.7	130.4±1.7
PLA/GF-150h	4.60±0.38	7.28±0.08	77.3±2.5	110.2±2.2
PLA/GF-200h	4.39±0.22	7.21±0.07	65.7±3.6	105.2±2.4
PLA/GF-300h	4.26±0.24	7.19±0.07	56.4±2.9	89.7±2.0
PLA/GF-400h	4.19±0.31	7.14±0.22	51.4±3.9	63.9±1.4

Benefits in the strength values of the PLA/GF specimen was due to the inorganic strong glass structure of the GF reinforcements having almost no chemical degradation during weathering periods. Therefore, even after 400h weathering period, GF reinforcements keep their significant composite strengthening mechanisms of “load transfer from the matrix” and “decreased mobility of the matrix chains”.

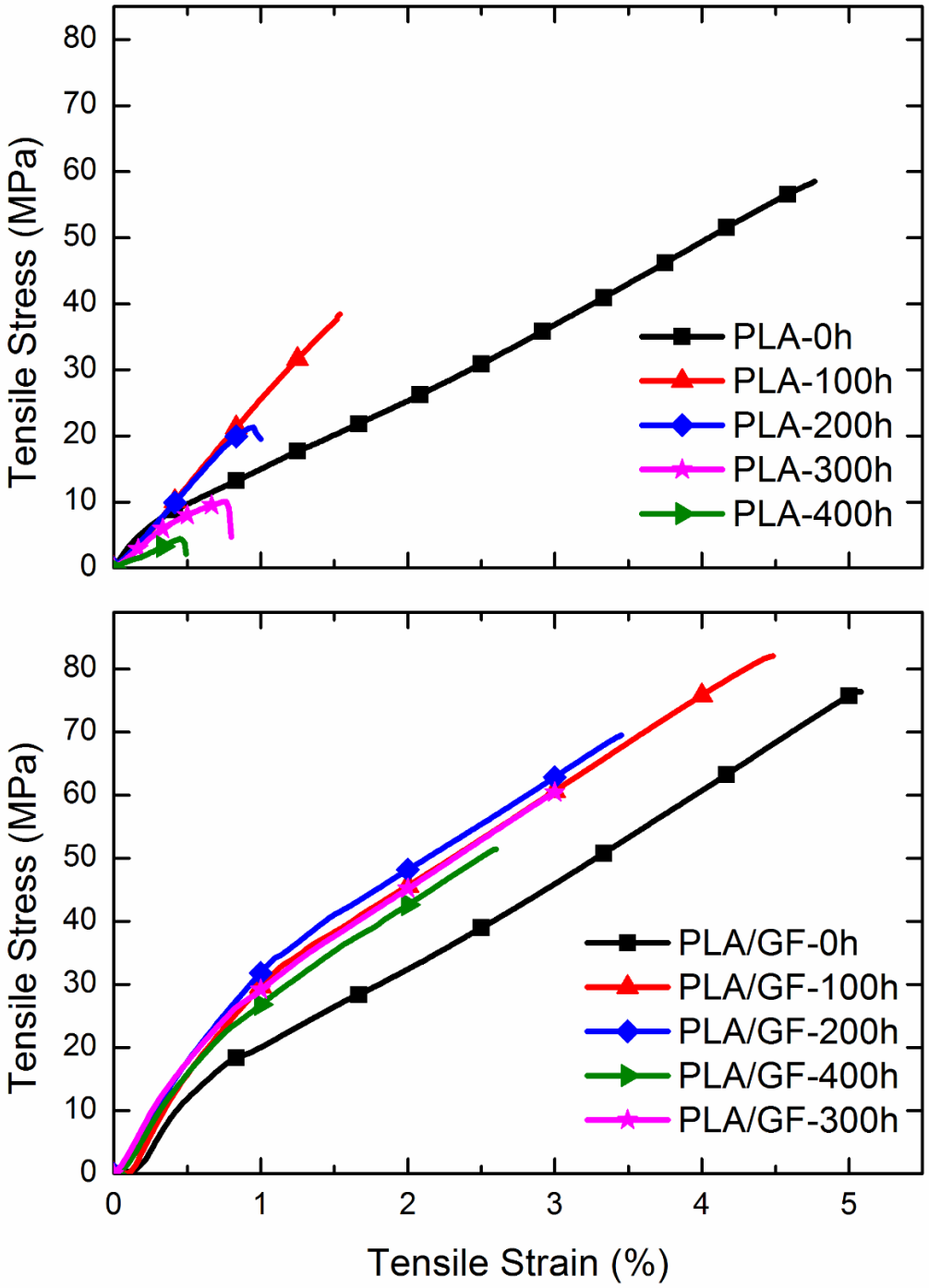

Figure 3.25 Alterations in the tensile stress-strain curves of the specimens after each accelerated weathering period

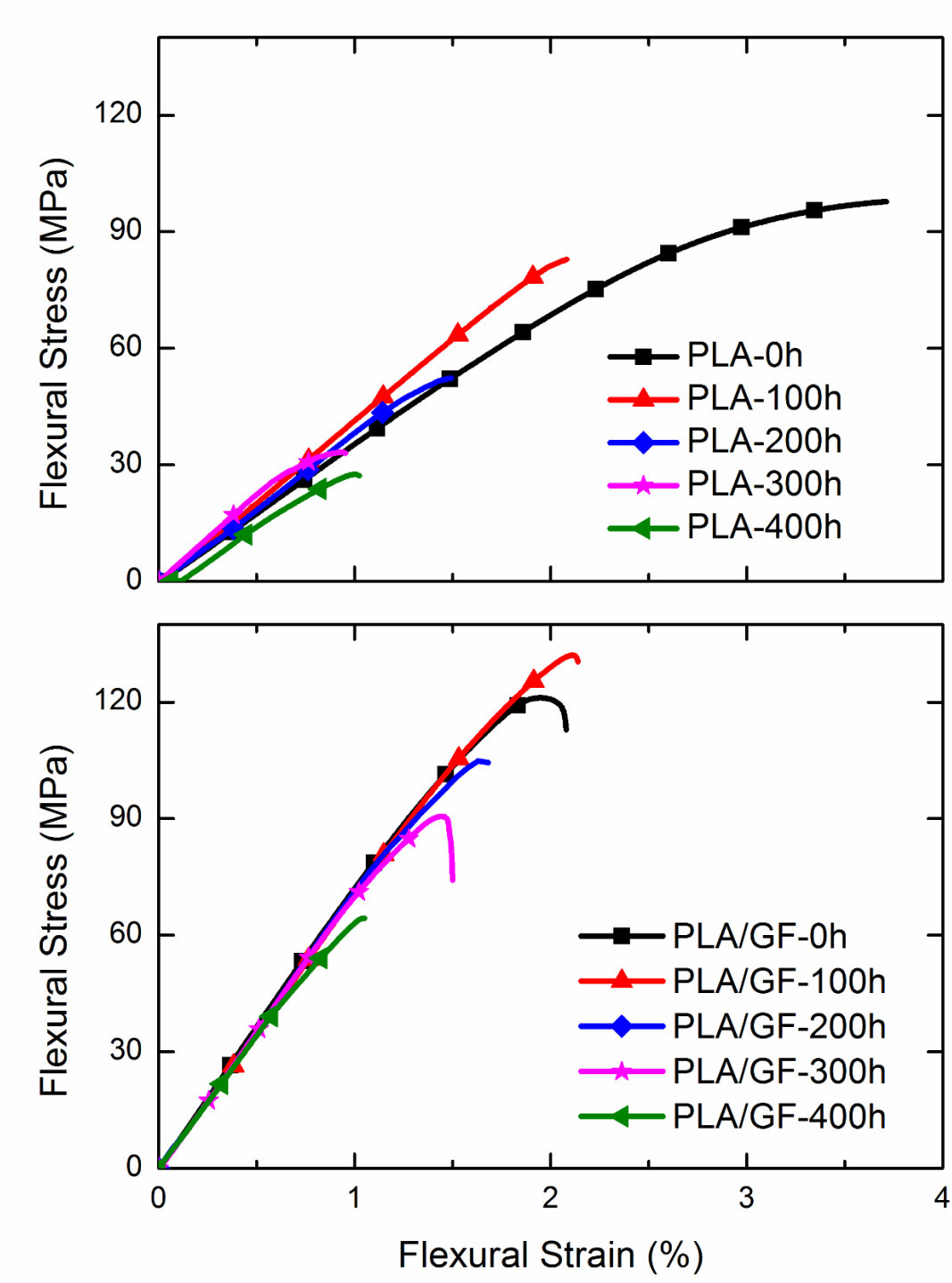

Figure 3.26 Flexural stress-strain curves of the neat PLA and its GF biocomposite specimens before and after each accelerated weathering period

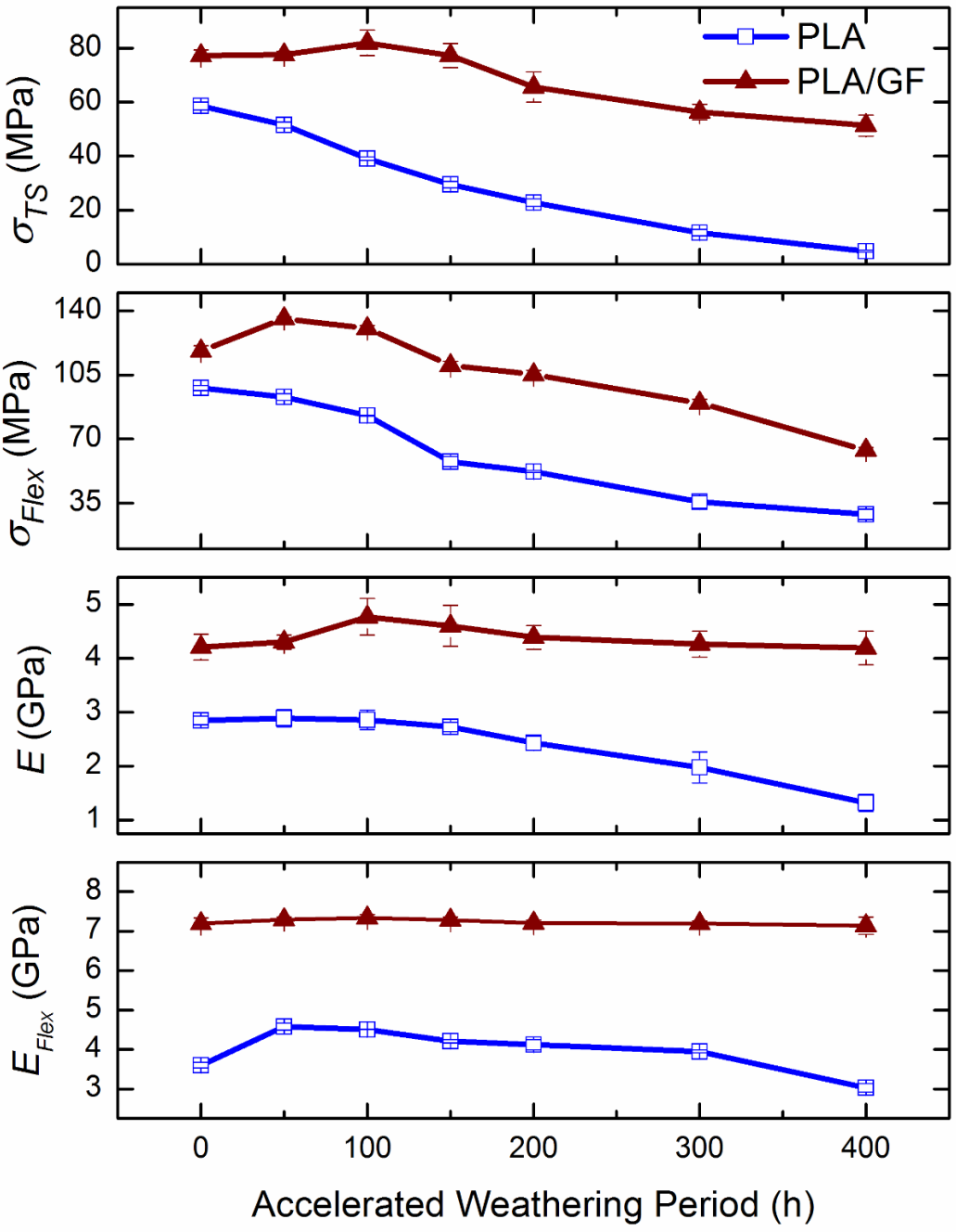

Figure 3.27 Effects of accelerated weathering periods on the flexural and tensile strength and flexural and tensile modulus of the specimens

Alterations in the ductility, i.e. ability of the materials to have plastic deformation until fracture, were determined from the stress-strain curves of the specimens during tension test (Figure 3.25), and the values in terms of "percent final strain at break" ($\%\varepsilon_f$) were tabulated in Table 3; while effects of each accelerated weathering period on the ductility of the specimens were evaluated in Figure 3.28.

Table 3.10 and Figure 3.28 indicate that, due to the similar reasons discussed above, ductility ($\%\varepsilon_f$) values of the specimens decreased parallel to the increasing weathering periods. After 400h weathering, it is seen that the reduction in the ductility of neat PLA specimen was again severe being as much as 91%, while the ductility reduction in the PLA/GF composite specimens was 50%.

Alteration in the fracture toughness, i.e. ability of the molecules to hinder crack initiation and propagation leading to fracture, of the specimens were determined in terms of "Critical Stress Intensity Factor (K_{IC})" and "Critical Strain Energy Release Rate (G_{IC})" values as given in Table 3.10. Effects of each accelerated weathering period on the fracture toughness values were evaluated in Figure 3.28.

Table 3.10 and Figure 3.28 reveal that, although increased crystallinity amount only after 50h increased fracture toughness of the neat PLA specimen very slightly; normally, increasing accelerated weathering period resulted in successive decreases in the values of fracture toughness (both K_{IC} and G_{IC}) of the neat PLA and PLA/GF composite specimens.

Again, reductions in the fracture toughness values of the neat PLA were more critical compared to the reductions in the PLA/GF composite. For instance, reductions in the K_{IC} and G_{IC} values of neat PLA were 41% and 55%; while these reductions for the PLA/GF were 36% and 41%, respectively.

Benefit in the fracture toughness values of the PLA/GF specimens was, as discussed above, due to the no influences of weathering degradation on the inorganic glass structure of GF reinforcements; keeping them to function effectively in the composite

toughening mechanisms of not only “crack deflection” and “crack bowing”, but also “debonding” and “fiber pull-out”.

Finally, in order to reveal benefits of using PLA/GF composite rather than neat PLA, all the mechanical properties of these two specimens before weathering (0h) and after 400h of accelerated weathering are tabulated in Table 3.11. Note that benefits of using PLA/GF-0h and PLA/GF-400h composite specimens compared to PLA-0h and PLA-400h specimens are tabulated in terms of “% benefit at 0h” and “% benefit at 400h”, respectively.

According to the data given in Table 3.11 it can be deduced that in terms of mechanical properties, use of PLA with 15 wt% GF is extremely beneficial not only under normal conditions, but also under severe atmospheric weathering conditions, i.e. not only for “indoor applications” but also for “outdoor applications”.

For example, flexural modulus and strength (E_{Flex} and σ_{Flex}) were 100% and 39% beneficial before weathering, but after weathering these benefits were 136% and 167%, respectively. Benefits in K_{IC} fracture toughness before and after weathering were 21% and 32%, respectively.

It should be also pointed out that benefits of PLA/GF composite specimen were not only due to the very effective stiffening, strengthening, toughening actions of the GF reinforcements discussed above, it should be also due to the “barrier” actions of the high aspect ratio short glass fibers decreasing the very detrimental effects of the photolysis and hydrolysis reactions on the PLA matrix.

Table 3.10 Alterations in the Tensile Strain at Break (ε_f) and Fracture Toughness (K_{IC} and G_{IC}) of the specimens after each accelerated weathering period

Specimens	ε_f **(%)**	K_{IC} **(MPa√m)**	G_{IC} **(kJ/m²)**
PLA	4.88±0.25	3.43±0.04	5.44±0.34
PLA-50h	2.39±0.19	3.50±0.04	5.94±0.16
PLA-100h	1.51±0.15	3.37±0.01	4.93±0.64
PLA-150h	1.18±0.10	3.03±0.06	4.24±0.72
PLA-200h	1.08±0.09	2.68±0.05	3.45±0.54
PLA-300h	0.88±0.22	2.53±0.12	3.16±0.78
PLA-400h	0.45±0.04	2.02±0.11	2.44±0.52
PLA/GF	5.24±0.10	4.16±0.10	6.06±0.11
PLA/GF-50h	5.04±0.05	4.14±0.05	5.09±0.42
PLA/GF-100h	4.82±0.24	4.12±0.12	4.99±0.13
PLA/GF-150h	4.64±0.64	3.96±0.15	4.85±0.61
PLA/GF-200h	3.35±0.26	3.80±0.13	4.73±0.11
PLA/GF-300h	2.71±0.24	3.59±0.11	4.22±0.29
PLA/GF-400h	2.64±0.12	2.67±0.22	3.56±0.50

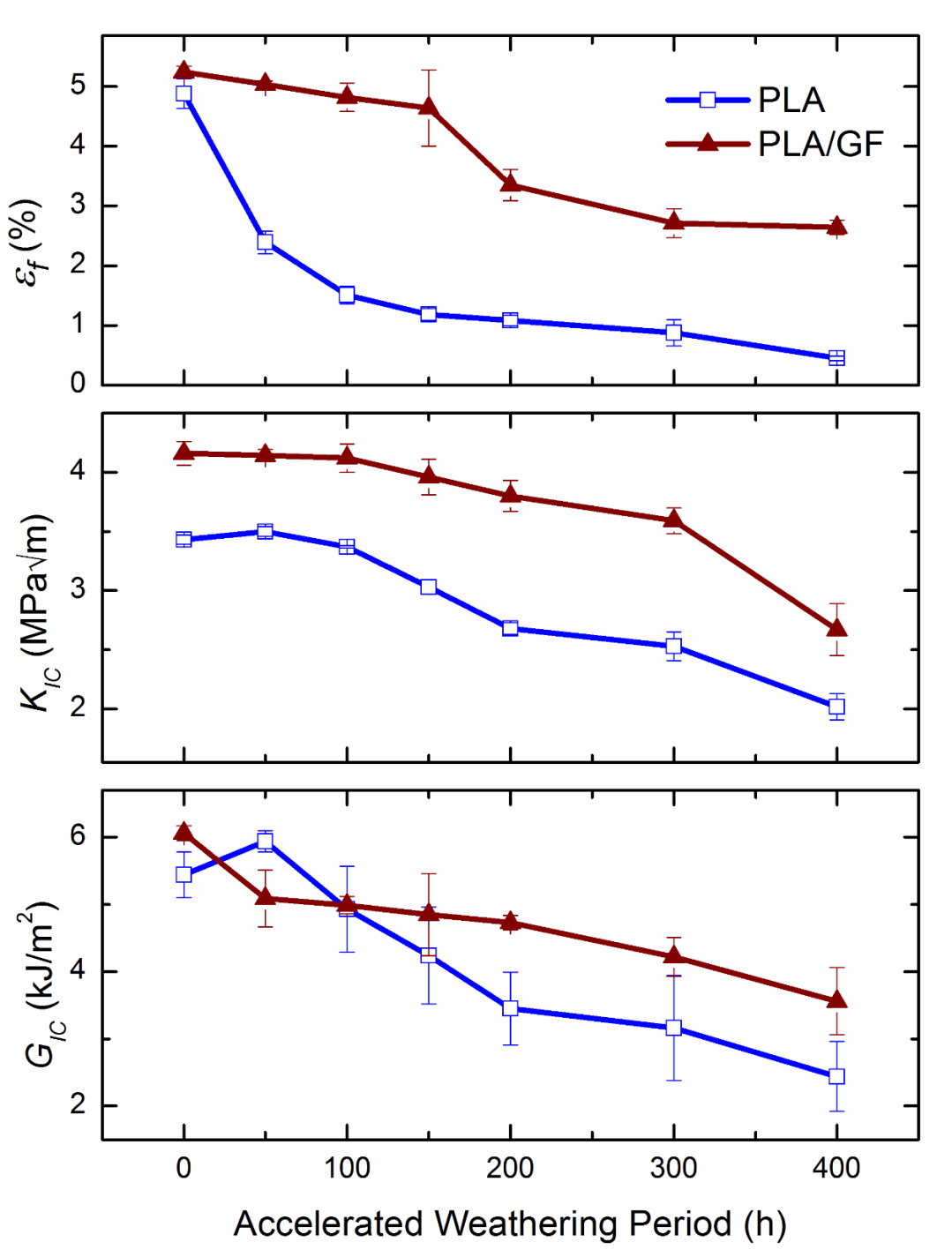

Figure 3.28 Effects of accelerated weathering periods on the ductility and fracture toughness of the specimens

Table 3.11 Comparison of the mechanical properties of neat PLA and PLA/GF composite specimens before (0 h) and after (400 h) accelerated weathering used to determine the "% benefit" (percent increase in the values) of the composite specimen at 0 h and 400 h

Mechanical Properties	**PLA at 0h**	**PLA/GF at 0h**	**Benefits at 0h**	**PLA at 400h**	**PLA/GF at 400h**	**Benefits at 400h**
Tensile Modulus E (GPa)	2.85	4.21	48**%**	1.32	4.19	217**%**
Flexural Modulus E_{Flex} (GPa)	3.60	7.20	100**%**	3.03	7.14	136**%**
Tensile Strength σ_{TS} (MPa)	58.6	77.3	32**%**	4.8	51.4	971**%**
Flexural Strength σ_{Flex} (MPa)	97.9	135.7	39**%**	28.9	63.9	167**%**
Tensile Strain at Break ε_f (%)	4.48	5.24	7**%**	0.45	2.64	487**%**
Fracture Toughness K_{IC} (MPa$\sqrt{m}$)	3.43	4.16	21**%**	2.02	2.67	32**%**
Fracture Toughness G_{IC} (kJ/m^2)	5.44	6.06	11**%**	2.44	3.56	32**%**

3.3.5 Alteration in the Thermal Properties

Differential scanning calorimetry (DSC) analyses and thermogravimetric analyses (TGA) were carried out to observe the alterations in the thermal properties of neat PLA and PLA/ GF composite specimens before and after each accelerated weathering period.

First heating DSC thermograms of the specimens were given in Figure 3.29, while the important transition temperatures, i.e. glass transition (T_g), cold crystallization (T_c), melting (T_m) temperatures, the enthalpy of melting (ΔH_m) and crystallization (ΔH_c) including percent crystallinity (X_c) values were tabulated in Table 3.12. The relation used in calculation of percent crystallinity is given in section 3.1.4.

Table 3.12 and Figure 3.29 point out that there were no significant alterations in the glass transition and melting temperatures of the PLA matrices of the specimens. The most significant alteration was the loss of the exothermic cold crystallization (ΔH_c) peaks in the first heating profiles of the accelerated weathered PLA and PLA/GF specimens. Because it is known that PLA has inherently very slow crystallization rate. Since cooling rate of the injection molding process, used for shaping of the specimens, was very fast; PLA chains had no sufficient time to crystallize. For these unweathered (0h) specimens, crystallinity amount (X_c) was only 3.84% for neat PLA, and 7.34% for PLA/GF specimens.

On the other hand, during accelerated weathering tests, since the temperature of the unit at each UV-irradiation cycle was 70ºC, macromolecular chains in the PLA matrices of the specimens had sufficient energy and time required for the conformational mobility of cold crystallization. Therefore, Table 3.12 reveals that after each accelerated weathering period, crystallinity amount of the specimens increased significantly, e.g. reaching to 47.31% for PLA-400h and 43.66% for PLA/GF-400h.

It should be also noted that, another reason for the increase of the crystallinity could be due to severe chain scission actions of the photolysis and hydrolysis reactions.

Because, these rather short chains of PLA matrices would have more conformational mobility required for the higher level of crystallinity.

Alterations in the thermogravimetric analyses of the specimens after each accelerated weathering period were evaluated in the form of TG curves in Figure 3.30; and in terms of the thermal degradation temperatures $T_{5\%}$, $T_{10\%}$, $T_{25\%}$ representing the temperatures at which the 5, 10, 25 wt% mass losses, and T_{max} representing the temperature at maximum mass loss in Table 3.13. In this table, %residue of each specimen determined at 550ºC were also included.

Although, Table 3.13 indicates that there were certain reductions (by 10º-20ºC) in the onset temperatures of thermal degradation, i.e. in the values of $T_{5\%}$ and $T_{10\%}$ of the specimens after accelerated weathering periods, there was almost no change in the T_{max} degradation temperature of the specimens.

Table 3.13 also reveals that, even after 400h weathering, %residue of the PLA/GF composite specimens remain unchanged. This could be interpreted that photolysis and hydrolysis reactions of the weathering degradation resulted in no change in the inorganic glass structure of these 15 wt% GF reinforcements.

Table 3.12 Alterations in the transition temperatures (T_g, T_c, T_m), enthalpies (ΔH_m, ΔH_c) and crystallinity percent (X_C) of the specimens after each accelerated weathering period obtained during DSC first heating profile

Specimens	T_g **(°C)**	T_c **(°C)**	T_m **(°C)**	ΔH_m **(J/g)**	ΔH_c **(J/g)**	X_C **(%)**
PLA	63.4	118	148.4	7.5	4.01	3.84
PLA-50h	66.1	-	151.2	30.5	-	32.81
PLA-100h	65.3	-	151.0	34.2	-	36.77
PLA-150h	65.2	-	151.3	35.4	-	38.06
PLA-200h	65.1	-	152.1	38.3	-	41.18
PLA-300h	66.4	-	150.3	40.4	-	43.44
PLA-400h	66.5	-	150.2	44.1	-	47.31
PLA/GF	65.4	122.2	149.4	17.1	11.2	7.34
PLA/GF-50h	65.1	-	150.1	32.1	-	34.52
PLA/GF-100h	65.1	-	150.3	33.5	-	36.02
PLA/GF-150h	66.3	-	150.4	33.8	-	36.34
PLA/GF-200h	67.3	-	150.5	35.7	-	38.39
PLA/GF-300h	66.5	-	150.5	36.4	-	39.14
PLA/GF-400h	66.8	-	151.1	40.6	-	43.66

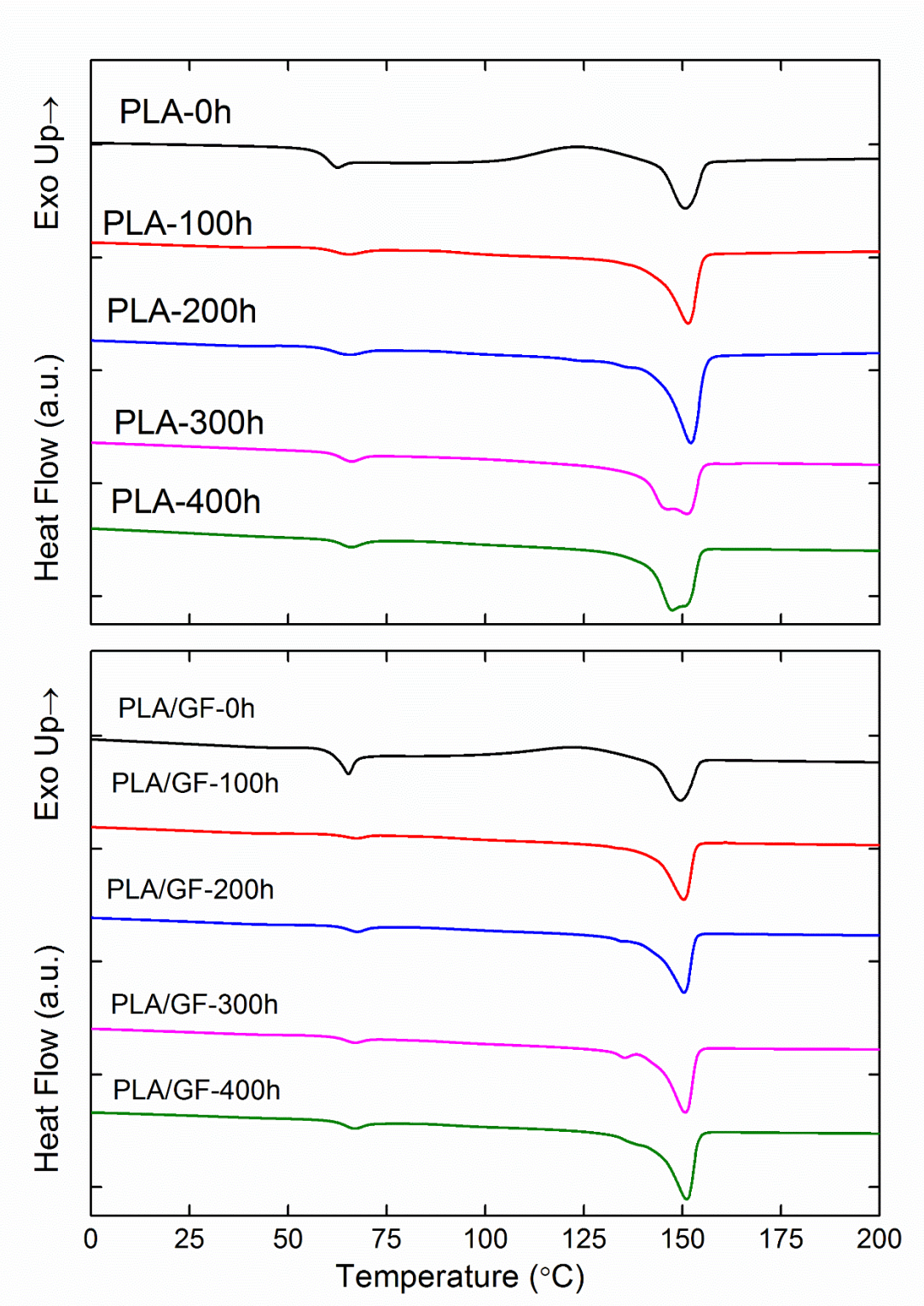

Figure 3.29 Alterations in the first heating DSC thermograms of the specimens after each accelerated weathering period

Table 3.13 Alterations in the thermal degradation temperatures ($T_{5\%}$, $T_{10\%}$, $T_{25\%}$) of the specimens at 5, 10 and 25 wt% mass losses and the maximum mass loss temperature (T_{max}) and %Residue at 550ºC after each accelerated weathering period

Specimens	$T_{5\%}$ **(°C)**	$T_{10\%}$ **(°C)**	$T_{25\%}$ **(°C)**	T_{max} **(°C)**	***%Residue at 550ºC***
PLA-0h	330	340	352	367	1.05
PLA-50h	321	333	347	365	0.97
PLA-100h	327	339	352	367	1.11
PLA-150h	326	339	352	367	0.98
PLA-200h	326	338	352	367	1.18
PLA-300h	319	333	350	368	0.96
PLA-400h	312	327	345	366	0.95
PLA/GF-0h	331	342	355	368	14.97
PLA/GF-50h	313	328	346	365	14.36
PLA/GF-100h	320	331	348	366	14.70
PLA/GF-150h	320	332	348	366	14.73
PLA/GF-200h	324	336	352	367	15.15
PLA/GF-300h	320	332	350	366	15.51
PLA/GF-400h	317	331	349	366	15.27

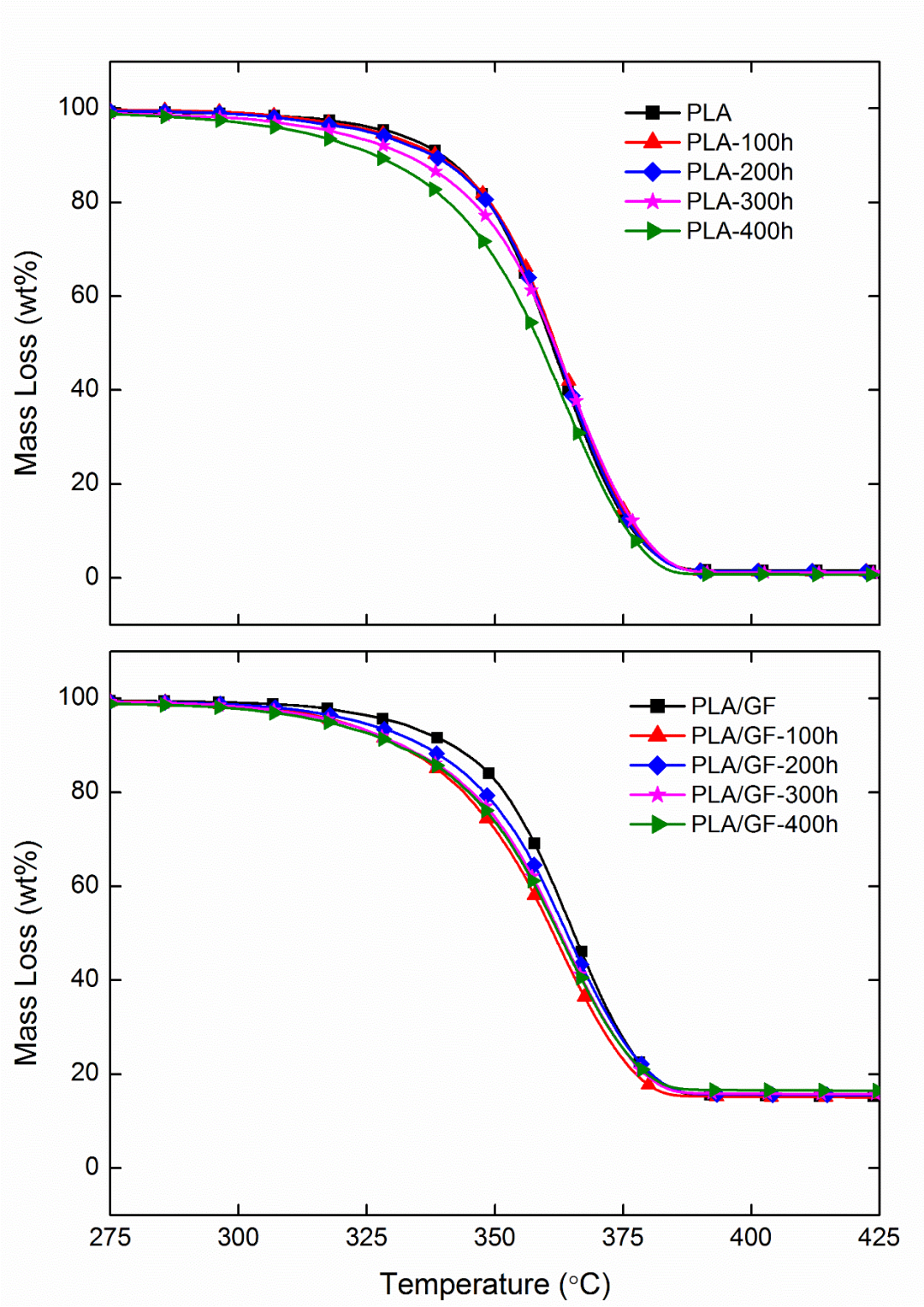

Figure 3.30 Alterations in the thermogravimetric curves of the specimens after each accelerated weathering period

CHAPTER 4

CONCLUSIONS

The main conclusions drawn from the three different parts of this thesis can be summarized as follows:

(i) Effects of GF Content and TPU Elastomer Blending

- SEM analyses revealed that up to 15 wt% content, silane sized GF reinforcements were rather uniformly distributed in the matrices of both neat PLA and PLA/TPU blend. Beyond that content, level of uniformity decreased, consequently mechanical properties started to decrease. SEM images also showed that there was no uniform distribution problem of micron-sized TPU domains in the PLA matrix.

- Tensile and flexural tests indicated that due to the very efficient strengthening and stiffening actions of GF reinforcements, all strength and elastic modulus values of PLA increased. For instance, use of 15 wt% GF resulted in 32% and 21% rises in tensile strength (σ_{TS}) and flexural strength (σ_{Flex}); while 48% and 100% rises in tensile modulus (E) and flexural modulus (E_{Flex}) values of the neat PLA, respectively.

- Due to the plasticizing action of the soft segments of thermoplastic elastomers, use of 10 wt% TPU blending resulted in certain decreases in the strength and modulus values of PLA. On the other hand, when this PLA/TPU blend was reinforced with 15 wt% GF, then all these reduced strength and modulus values were recovered.

- Ductility measurements in terms of % strain at break (%ε_f) values and fracture toughness tests in terms of K_{IC} and G_{IC} values pointed out that due to the elastomeric nature of TPU and its very efficient rubber toughening mechanisms, blending of PLA with 10 wt% TPU resulted in more than three times increase in ductility; and 103% and 74% increases in K_{IC} and G_{IC} fracture toughness values, respectively.

- Due to the toughening mechanisms of fiber reinforcements; crack deflection, debonding and fiber pull-out, use of optimum 15 wt% GF content also resulted in increased fracture toughness values as 21% in K_{IC} and 11% in G_{IC}. When TPU blending and GF reinforcement were used together, the performance of rubber toughening mechanism decreases; however, the K_{IC} and G_{IC} fracture toughness values of this composition were still very high compared to neat PLA, and close to PLA/15 GF composites.

- Therefore, it can be concluded that, although blending of PLA with 10 wt% TPU resulted in enormous improvement in K_{IC} and G_{IC} values, use of 15 wt% GF reinforcement with and without TPU resulted in similar level of increases. That is, if the increases obtained in strength-modulus-toughness values of neat PLA by the use of optimum GF reinforcement were sufficient for an application, then there would be no need for an additional TPU blending.

- Thermal analyses by DSC and TGA indicated that use of GF reinforcement and TPU blending had no significant contribution to the transition temperatures and thermal degradation temperatures of PLA. However, first heating DSC thermograms revealed that crystallinity amount of PLA would be increased almost two times due to especially heterogeneous nucleation site actions of GF reinforcements and fine sized TPU domains.

(ii) Effects of Shaping by 3D-Printing

- Photographic images revealed that generally there was no significant difference in the macro level appearances of the injection molded and 3D-printed PLA blend and

composite specimens. The most noticeable difference was for the neat PLA specimen. Due to the highly amorphous structure, injection molded neat PLA was very transparent. Contrarily, due to the more crystallinity amount and textured structure, 3D-printed neat PLA specimen appeared to be opaque.

- SEM analysis illustrated that there was no significant difference in the fracture surface morphology of the injection molded and 3D-printed neat PLA and blend specimens. The most significant difference was in terms of the orientation of the GF reinforcements in PLA composite specimens. In the injection molded specimens almost all GF reinforcements were aligned perpendicular to the fracture plane. Contrarily, in the 3D-printed specimens, due to the ±45º raster angle printing directions, some of the GF reinforcements were oriented to the fracture plane with +45º, while some of them are oriented with -45º.

- Tensile and flexural tests indicated that for the neat PLA and blend specimens, there were no influences of the injection molding and 3D-printing shaping process on their strength values; being almost equal. Moreover, due to the stiffening action of the slightly textured structure formed during 3D-printing, elastic modulus values of the 3D-printed specimens were even slightly higher than the injection molded specimens.

- On the other hand, due to the lower efficiency of the ±45º oriented GF reinforcements in the strengthening and stiffening mechanisms, there were significant reductions in the strength and elastic modulus values of the 3D-printed composite specimens, being as much as 32% in strength and 41% in modulus values compared to injection molded specimens.

- Fracture toughness tests indicated that 3D-printed neat PLA and blend specimens were also very beneficial compared to their injection molded specimens; these benefits in the fracture toughness values being as much as 47% for neat PLA and 26% for PLA/TPU blend. This behavior could be again due to the ±45º textured structure of the specimens leading to additional toughening mechanism of “crack deflection” in the textured body.

- However, due to lower efficiency of the ±45º oriented GF reinforcements in the composite toughening mechanisms of crack deflection and crack bowing; fracture toughness values of the 3D-printed PLA/GF composite specimens were slightly lower compared to their injection molded specimens.

- In the PLA/TPU/GF composite, fracture toughness values of the 3D-printed specimens were again beneficial as much as 29% compared to their injection molded specimens. Because in this specimen, reduced effectiveness of the crack deflection toughening mechanism with ±45º oriented GF reinforcements were recovered by the enormous level of rubber toughening mechanism of TPU domains in the matrix.

- TGA analyses revealed that specimen shaping by injection molding and 3D-printing processes have no effects on the thermal degradation temperatures of the PLA based materials. Similarly, DSC analyses indicated that they have also no effects on the transition temperatures of all specimens; but there are certain influences on the crystallinity amount. For instance, due to the rather lower cooling rate during 3D-printing compared to the very fast cooling rate of injection molding, crystallinity amount of the neat PLA specimen increased from 3.84% to 5.27%.

(iii) Effects of Weathering

- Visual photographic images and quantitative color space parameters via diffused reflectance analyses (DRA) indicated that before weathering neat PLA specimen appears very transparent due to its highly amorphous structure, while it becomes white due to certain level of crystallization during weathering. These analyses also indicated that yellowish grey color of the PLA/GF composite specimens fade away by the weathering degradation.

- Static light scattering (SLS) spectrometry revealed that weathering periods resulted in structural deterioration of the PLA matrix especially in the form of drastic

decrease in molecular weight from $3.7x10^5$ down to $0.1x10^5$ via chain scission reactions; which was reflected as significant losses in the mechanical properties.

- ATR-FTIR analyses showed that the main degradation mechanism of UV-irradiation cycles was “photolysis” in terms of “Norrish II type photo-cleavage reaction” and “photo-oxidation reaction”; while the main degradation mechanism of moisture (condensation) cycles was “hydrolysis”.

- Fracture surface morphology observations via SEM analysis indicated that weathering degradation mechanisms resulted in extensive number of voids, cracks and cleavages on the fracture surface of the specimens.

- Mechanical tests revealed that although there were slight increases in some mechanical properties of the specimens during the initial weathering periods of 50h and 100h due to the increased crystallinity amount of their PLA matrices; normally beyond 150h all mechanical properties decreased with increasing weathering periods.

- It was observed that reductions in the mechanical properties (strength-modulus-toughness) of the neat PLA were much more critical compared to the reductions in the PLA/GF composite. For instance, the reduction in the tensile strength of the neat PLA specimen was as much as 92%; while that reduction for the PLA/GF specimen was only 34%.

- Benefits in the mechanical properties of the PLA/GF composite specimen were due to the inorganic strong glass structure of the GF reinforcements having almost no chemical degradation during weathering periods. Therefore, even after 400h weathering period, GF reinforcements kept their actions in the composite strengthening-stiffening-toughening mechanisms.

- DSC analyses indicated that he most significant alteration during weathering was the higher amount of crystallinity. Because, during UV-irradiation cycles at 70ºC,

macromolecular chains in the PLA matrices of the specimens had sufficient energy and time required for the conformational mobility of cold crystallization.

- TGA analyses also revealed that even after 400h weathering period, %residue of the PLA/GF composite specimens remain unchanged. This could be interpreted that photolysis and hydrolysis reactions of the weathering degradation resulted in no change in the inorganic glass structure of the GF reinforcements.

REFERENCES

[1] M. R. N. Fazita *et al.*, "Green Composites Made of Bamboo Fabric and Poly (Lactic) Acid for Packaging Applications—A Review," *Materials (Basel).*, vol. 9, no. 6, p. 435, Jun. 2016.

[2] M. Hasan, A. Hassan, and Z. Zakaria, "Poly(Lactic Acid) Hybrid Green Composites," in *Biodegradable Green Composites*, John Wiley & Sons, Inc, 2016, pp. 149–166.

[3] L. T. Sin, A. R. Rahmat, W. A. W. A. Rahman, L. T. Sin, A. R. Rahmat, and W. A. W. A. Rahman, "5 – Mechanical Properties of Poly(lactic Acid)," in *Polylactic Acid PLA Biopolymer Technology and Applications*, Elsevier, 2013, pp. 177–219.

[4] J. Odent, J.-M. Raquez, and P. Dubois, "Highly Toughened Polylactide-Based Materials through Melt-Blending Techniques," in *Biodegradable Polyesters*, Wiley-VCH Verlag GmbH & Co. KGaA, 2015, pp. 235–274.

[5] H. Tsuji, "Poly(Lactic Acid)," in *Bio-Based Plastics: Materials and Applications*, John Wiley & Sons Ltd, 2013, pp. 171–239.

[6] A. P. Gupta and V. Kumar, "New emerging trends in synthetic biodegradable polymers – Polylactide: A critique," *Eur. Polym. J.*, vol. 43, no. 10, pp. 4053–4074, 2007.

[7] S. Domenek and V. Ducruet, "Characteristics and Applications of PLA," in *Biodegradable and Biobased Polymers for Environmental and Biomedical Applications*, John Wiley & Sons, Inc., 2016, pp. 171–224.

[8] T. Sathishkumar, S. Satheeshkumar, and J. Naveen, "Glass fiber-reinforced polymer composites - a review," *J. Reinf. Plast. Compos.*, vol. 33, no. 13, pp. 1258–1275, Jul. 2014.

[9] V. M. Karbhari, "The Nature of E-Glass Fibers," in *Rehabilitation of Pipelines Using Fiber-Reinforced Polymer (FRP) Composites*, Elsevier, 2015.

[10] J. M. Stickel and M. Nagarajan, “Glass Fiber-Reinforced Composites: From Formulation to Application,” *Int. J. Appl. Glas. Sci.*, vol. 3, no. 2, pp. 122–136, Jun. 2012.

[11] F. T. Wallenberger, J. C. Watson, and H. Li, “Glass Fibers,” in *ASM Handbook, Vol.21: Composites,* ASM International, 2001, pp. 27–34.

[12] J. G. Drobny, “9 - Thermoplastic Polyurethane Elastomers BT - Handbook of Thermoplastic Elastomers (Second Edition),” in *Plastics Design Library*, Oxford: William Andrew Publishing, 2014, pp. 233–253.

[13] D. J. Martin, A. F. Osman, Y. Andriani, and G. A. Edwards, “11 - Thermoplastic polyurethane (TPU)-based polymer nanocomposites,” in *Advances in Polymer Nanocomposites*, F. Gao, Ed. Woodhead Publishing, 2012, pp. 321–350.

[14] S. Thomas and R. Stephen, Eds., *Rubber Nanocomposites: Preparation, Properties, and Applications*. Chichester, UK: John Wiley & Sons, Ltd, 2010.

[15] I. Gibson, D. W. Rosen, and B. Stucker, *Additive Manufacturing Technologies*. Boston, MA: Springer US, 2010.

[16] M. J. Cotteleer, “3D Opportunity: Additive Manufacturing Paths to Performance, Innovation, and Growth,” *Deloitte Review*, 2014. [Online]. Available: http://simt.com/uploads/4881/SIMT_AM_Conference_Keynote.pdf. [Accessed: 27-Nov-2015].

[17] IDC, “3D printing market distribution worldwide in 2016, by use case,” *Statista - The Statistics Portal*, 2017. [Online]. Available: https://www.statista.com/statistics/661876/worldwide-3d-printing-market-by-use-case/.

[18] J. Izdebska, S. Thomas, D. J. Thomas, and T. C. Claypole, “18 – 3-D Printing,” in *Printing on Polymers*, 2016, pp. 293–306.

[19] L. Columbus, “The State of 3D Printing 2016,” *Forbes*, 2016.

[20] O. S. Carneiro, A. F. Silva, and R. Gomes, “Fused deposition modeling with polypropylene,” *Mater. Des.*, vol. 83, pp. 768–776, 2015.

[21] “Filaments.directory - 3D Printer Filament Trends : July 2017.” [Online]. Available: https://www.filaments.directory/en/trends#statistics. [Accessed: 23-Jul-2017].

[22] I. C. McNeill and H. A. Leiper, “Degradation studies of some polyesters and polycarbonates—2. Polylactide: Degradation under isothermal conditions, thermal degradation mechanism and photolysis of the polymer,” *Polym. Degrad. Stab.*, vol. 11, no. 4, pp. 309–326, Jan. 1985.

[23] W. Sakai and N. Tsutsumi, “Photodegradation and Radiation Degradation,” in *Poly(Lactic Acid)*, Hoboken, NJ, USA: John Wiley & Sons, Inc., 2010, pp. 413–421.

[24] E. Ikada, “Photo- and Bio-degradable Polyesters. Photodegradation Behaviors of Aliphatic Polyesters,” *J. Photopolym. Sci. Technol.*, vol. 10, no. 2, pp. 265–270, 1997.

[25] W. L. Tham, B. T. Poh, Z. A. Mohd Ishak, and W. S. Chow, “Water Absorption Kinetics and Hygrothermal Aging of Poly(lactic acid) Containing Halloysite Nanoclay and Maleated Rubber,” *J. Polym. Environ.*, vol. 23, no. 2, pp. 242–250, Jun. 2015.

[26] M. Hakkarainen and A. Finne-Wistrand, “Polylactide,” in *Handbook of Engineering and Speciality Thermoplastics*, John Wiley & Sons, Inc., 2011, pp. 349–376.

[27] P. Haque *et al.*, “Interfacial properties of phosphate glass fibres/PLA composites: Effect of the end functionalities of oligomeric PLA coupling agents,” *Compos. Sci. Technol.*, vol. 70, no. 13, pp. 1854–1860, 2010.

[28] I. Ahmed *et al.*, “Composites for bone repair: phosphate glass fibre reinforced PLA with varying fibre architecture,” *J Mater Sci Mater Med*, vol. 22, no. 8, pp. 1825–1834, 2011.

[29] P. Haque *et al.*, “Influence of compatibilizing agent molecular structure on the mechanical properties of phosphate glass fiber-reinforced PLA composites,” *J. Polym. Sci. Part A Polym. Chem.*, vol. 48, no. 14, pp. 3082–3094, 2010.

[30] M. S. Hasan, I. Ahmed, A. J. Parsons, G. S. Walker, and C. A. Scotchford, “The influence of coupling agents on mechanical property retention and long-term cytocompatibility of phosphate glass fibre reinforced PLA composites,” *J Mech Behav Biomed Mater*, vol. 28, pp. 1–14, 2013.

[31] I. Ahmed, P. S. Cronin, E. A. Abou Neel, A. J. Parsons, J. C. Knowles, and C. D. Rudd, “Retention of mechanical properties and cytocompatibility of a phosphate-based glass fiber/polylactic acid composite,” *J Biomed Mater Res B Appl Biomater*, vol. 89, no. 1, pp. 18–27, 2009.

[32] N. Han *et al.*, “Influence of screw holes and gamma sterilization on properties of phosphate glass fiber-reinforced composite bone plates,” *J Biomater Appl*, vol. 27, no. 8, pp. 990–1002, 2013.

[33] R. M. Felfel, I. Ahmed, A. J. Parsons, and C. D. Rudd, “Bioresorbable screws reinforced with phosphate glass fibre: manufacturing and mechanical property characterisation,” *J Mech Behav Biomed Mater*, vol. 17, pp. 76–88, 2013.

[34] R. M. Felfel, I. Ahmed, A. J. Parsons, G. Palmer, V. Sottile, and C. D. Rudd, “Cytocompatibility, degradation, mechanical property retention and ion release profiles for phosphate glass fibre reinforced composite rods,” *Mater Sci Eng C Mater Biol Appl*, vol. 33, no. 4, pp. 1914–1924, 2013.

[35] R. M. Felfel, I. Ahmed, A. J. Parsons, G. S. Walker, and C. D. Rudd, “In vitro degradation, flexural, compressive and shear properties of fully bioresorbable composite rods,” *J Mech Behav Biomed Mater*, vol. 4, no. 7, pp. 1462–1472, 2011.

[36] R. M. Felfel, I. Ahmed, A. J. Parsons, and C. D. Rudd, “Bioresorbable composite screws manufactured via forging process: pull-out, shear, flexural and degradation characteristics,” *J Mech Behav Biomed Mater*, vol. 18, pp. 108–122, 2013.

[37] M. S. Mohammadi, I. Ahmed, N. Muja, C. D. Rudd, M. N. Bureau, and S. N. Nazhat, “Effect of phosphate-based glass fibre surface properties on thermally

produced poly(lactic acid) matrix composites," *J Mater Sci Mater Med*, vol. 22, no. 12, pp. 2659–2672, 2011.

[38] M. S. Hasan, I. Ahmed, A. Parsons, G. Walker, and C. Scotchford, "Cytocompatibility and Mechanical Properties of Short Phosphate Glass Fibre Reinforced Polylactic Acid (PLA) Composites: Effect of Coupling Agent Mediated Interface," *J Funct Biomater*, vol. 3, no. 4, pp. 706–725, 2012.

[39] L. Lin, C. Deng, G. Lin, and Y. Wang, "Mechanical Properties, Heat Resistance and Flame Retardancy of Glass Fiber-Reinforced PLA-PC Alloys Based on Aluminum Hypophosphite," *Polym. Plast. Technol. Eng.*, vol. 53, no. 6, pp. 613–625, 2014.

[40] X. Lu *et al.*, "Morphology and properties of bio-based poly (lactic acid)/high-density polyethylene blends and their glass fiber reinforced composites," *Polym. Test.*, vol. 54, pp. 90–97, 2016.

[41] M. S. Huda, L. T. Drzal, A. K. Mohanty, and M. Misra, "Chopped glass and recycled newspaper as reinforcement fibers in injection molded poly(lactic acid) (PLA) composites: A comparative study," *Compos. Sci. Technol.*, vol. 66, no. 11–12, pp. 1813–1824, 2006.

[42] A. Jaszkiewicz, A. K. Bledzki, and P. Franciszczak, "Improving the mechanical performance of PLA composites with natural, man-made cellulose and glass fibers a comparison to PP counterparts," *Polymery*, vol. 58, no. 6, pp. 435–442, 2013.

[43] R. Jaratrotkamjorn, C. Khaokong, and V. Tanrattanakul, "Toughness enhancement of poly(lactic acid) by melt blending with natural rubber," *J. Appl. Polym. Sci.*, vol. 124, no. 6, pp. 5027–5036, 2012.

[44] C. Zhang *et al.*, "Thermal, mechanical and rheological properties of polylactide toughened by expoxidized natural rubber," *Mater. Des.*, vol. 45, pp. 198–205, 2013.

[45] N. Bitinis, R. Verdejo, P. Cassagnau, and M. A. Lopez-Manchado, "Structure and properties of polylactide/natural rubber blends," *Mater. Chem. Phys.*, vol. 129, no. 3, pp. 823–831, 2011.

[46] S. Yıldız, B. Karaağaç, and G. Ozkoc, “Thoughening of poly(lactic acid) with silicone rubber,” *Polym. Eng. Sci.*, vol. 54, no. 9, pp. 2029–2036, Sep. 2014.

[47] C. Kaynak and Y. Meyva, “Use of maleic anhydride compatibilization to improve toughness and other properties of polylactide blended with thermoplastic elastomers,” *Polym. Adv. Technol.*, vol. 25, no. 12, pp. 1622–1632, Dec. 2014.

[48] F. Feng and L. Ye, “Morphologies and mechanical properties of polylactide/thermoplastic polyurethane elastomer blends,” *J. Appl. Polym. Sci.*, vol. 119, no. 5, pp. 2778–2783, Mar. 2011.

[49] R. Yu, L. Zhang, Y. Feng, R. Zhang, and J. Zhu, “Improvement in toughness of polylactide by melt blending with bio-based poly(ester)urethane,” *Chinese J. Polym. Sci.*, vol. 32, no. 8, pp. 1099–1110, 2014.

[50] Y.-Y. Shi *et al.*, “Super Toughened Poly(L-lactide)/Thermoplastic Polyurethane Blends Achieved by Adding Dicumyl Peroxide,” *Polym. Plast. Technol. Eng.*, vol. 53, no. 13, pp. 1344–1353, Sep. 2014.

[51] Y. Shi *et al.*, “Super toughening of the poly(l-lactide)/thermoplastic polyurethane blends by carbon nanotubes,” *RSC Adv.*, vol. 3, no. 48, pp. 26271–26282, 2013.

[52] Y. Zhou, L. Luo, W. Liu, G. Zeng, and Y. Chen, “Preparation and Characteristic of PC/PLA/TPU Blends by Reactive Extrusion,” *Adv. Mater. Sci. Eng.*, vol. 2015, 2015.

[53] J.-J. Han and H.-X. Huang, “Preparation and characterization of biodegradable polylactide/thermoplastic polyurethane elastomer blends,” *J. Appl. Polym. Sci.*, vol. 120, no. 6, pp. 3217–3223, Jun. 2011.

[54] S. Jia, Z. Wang, Y. Zhu, L. Chen, and L. Fu, “Composites of poly(lactic) acid/thermoplastic polyurethane/mica with compatibilizer: morphology, miscibility and interphase,” *RSC Adv.*, vol. 5, no. 120, pp. 98915–98924, 2015.

[55] Z.-W. Liu *et al.*, "Mechanical and thermal properties of thermoplastic polyurethane-toughened polylactide-based nanocomposites," *Polym. Compos.*, vol. 35, no. 9, pp. 1744–1757, Sep. 2014.

[56] L. Zhang *et al.*, "Free radical competitions in polylactide/bio-based thermoplastic polyurethane/ free radical initiator ternary blends and their final properties," *Polymer (Guildf).*, vol. 64, pp. 69–75, 2015.

[57] F. Yu and H.-X. Huang, "Simultaneously toughening and reinforcing poly (lactic acid)/thermoplastic polyurethane blend via enhancing interfacial adhesion by hydrophobic silica nanoparticles," *Polym. Test.*, vol. 45, pp. 107–113, 2015.

[58] F. Zhao, H.-X. Huang, and S.-D. Zhang, "Largely toughening biodegradable poly(lactic acid)/thermoplastic polyurethane blends by adding MDI," *J. Appl. Polym. Sci.*, vol. 132, no. 48, p. n/a-n/a, Dec. 2015.

[59] Z. Liu, Y. Luo, H. Bai, Q. Zhang, and Q. Fu, "Remarkably Enhanced Impact Toughness and Heat Resistance of poly(l-Lactide)/Thermoplastic Polyurethane Blends by Constructing Stereocomplex Crystallites in the Matrix," *ACS Sustain. Chem. Eng.*, vol. 4, no. 1, pp. 111–120, Jan. 2016.

[60] J. Dai, H. Bai, Z. Liu, L. Chen, Q. Zhang, and Q. Fu, "Stereocomplex crystallites induce simultaneous enhancement in impact toughness and heat resistance of injection-molded polylactide/polyurethane blends," *RSC Adv.*, vol. 6, no. 21, pp. 17008–17015, 2016.

[61] E. Oliaei, B. Kaffashi, and S. Davoodi, "Investigation of structure and mechanical properties of toughened poly(l -lactide)/thermoplastic poly(ester urethane) blends," *J. Appl. Polym. Sci.*, vol. 133, no. 15, p. n/a-n/a, Apr. 2016.

[62] H. Hong *et al.*, "Preparation, rheological properties and primary cytocompatibility of TPU/PLA blends as biomedical materials," *J. Wuhan Univ. Technol. Sci. Ed.*, vol. 31, no. 1, pp. 211–218, 2016.

[63] E. Oliaei and B. Kaffashi, "Investigation on the properties of poly(l-lactide)/thermoplastic poly(ester urethane)/halloysite nanotube composites

prepared based on prediction of halloysite nanotube location by measuring free surface energies," *Polymer (Guildf).*, vol. 104, pp. 104–114, 2016.

[64] M. Shanler and P. Basiliere, "Hype Cycle for 3D Printing, 2015," *Gartner*, 2015. [Online]. Available: https://www.gartner.com/doc/3100228/hype-cycle-d-printing-. [Accessed: 25-Nov-2015].

[65] G. Postiglione, G. Natale, G. Griffini, M. Levi, and S. Turri, "Conductive 3D microstructures by direct 3D printing of polymer/carbon nanotube nanocomposites via liquid deposition modeling," *Compos. Part A Appl. Sci. Manuf.*, vol. 76, pp. 110–114, 2015.

[66] S. Guo, X. Yang, M.-C. Heuzey, and D. Therriault, "3D printing of a multifunctional nanocomposite helical liquid sensor," *Nanoscale*, vol. 7, no. 15, pp. 6451–6456, 2015.

[67] D. Drummer, S. Cifuentes-Cuéllar, and D. Rietzel, "Suitability of PLA/TCP for fused deposition modeling," *Rapid Prototyp. J.*, vol. 18, no. 6, pp. 500–507, 2012.

[68] T. Serra, M. A. Mateos-Timoneda, J. A. Planell, and M. Navarro, "3D printed PLA-based scaffolds," *Organogenesis*, vol. 9, no. 4, pp. 239–244, Oct. 2013.

[69] N. Sa'ude, M. H. I. Ibrahim, M. Ibrahim, and N. S. Badrishah, "Sustainable Natural Bio Composite for FDM Feedstocks," in *Machine Design and Manufacturing Engineering III*, 2014, vol. 607, pp. 65–69.

[70] A. Le Duigou, M. Castro, R. Bevan, and N. Martin, "3D printing of wood fibre biocomposites: From mechanical to actuation functionality," *Mater. Des.*, vol. 96, pp. 106–114, 2016.

[71] Q. Chen, J. D. Mangadlao, J. Wallat, A. De Leon, J. K. Pokorski, and R. C. Advincula, "3D Printing Biocompatible Polyurethane/Poly(lactic acid)/Graphene Oxide Nanocomposites: Anisotropic Properties," *ACS Appl. Mater. Interfaces*, vol. 9, no. 4, pp. 4015–4023, 2017.

[72] T. Serra, M. Ortiz-Hernandez, E. Engel, J. A. Planell, and M. Navarro, "Relevance of PEG in PLA-based blends for tissue engineering 3D-printed

scaffolds," *Mater. Sci. Eng. C*, vol. 38, pp. 55–62, 2014.

[73] M. Franchetti and C. Kress, "An economic analysis comparing the cost feasibility of replacing injection molding processes with emerging additive manufacturing techniques," *Int. J. Adv. Manuf. Technol.*, vol. 88, no. 9–12, pp. 2573–2579, Feb. 2017.

[74] C. Huber *et al.*, "3D print of polymer bonded rare-earth magnets, and 3D magnetic field scanning with an end-user 3D printer," *Appl. Phys. Lett.*, vol. 109, no. 16, p. 162401, Oct. 2016.

[75] A. T. Miller, D. L. Safranski, K. E. Smith, D. G. Sycks, R. E. Guldberg, and K. Gall, "Fatigue of injection molded and 3D printed polycarbonate urethane in solution," *Polymer (Guildf).*, vol. 108, pp. 121–134, 2017.

[76] Z. Weng, J. Wang, T. Senthil, and L. Wu, "Mechanical and thermal properties of ABS/montmorillonite nanocomposites for fused deposition modeling 3D printing," *Mater. Des.*, vol. 102, pp. 276–283, 2016.

[77] C. Zhang, C. Man, W. Wang, L. Jiang, and Y. Dan, "Degradation of Poly(L-lactide) Films under Ultraviolet Irradiation and Water Bath," *Polym. Plast. Technol. Eng.*, vol. 50, no. 8, pp. 810–817, 2011.

[78] A. V Janorkar, A. T. Metters, and D. E. Hirt, "Degradation of poly(L-lactide) films under ultraviolet-induced photografting and sterilization conditions," *J. Appl. Polym. Sci.*, vol. 106, no. 2, pp. 1042–1047, 2007.

[79] P. Stloukal *et al.*, "Assessment of the interrelation between photooxidation and biodegradation of selected polyesters after artificial weathering," *Chemosphere*, vol. 88, no. 10, pp. 1214–1219, Aug. 2012.

[80] S. Bocchini, K. Fukushima, A. Di Blasio, A. Fina, A. Frache, and F. Geobaldo, "Polylactic Acid and Polylactic Acid-Based Nanocomposite Photooxidation," *Biomacromolecules*, vol. 11, no. 11, pp. 2919–2926, 2010.

[81] S. Dopico-García *et al.*, "Insight into industrial PLA aging process by complementary use of rheology, HPLC, and MALDI," *Polym. Adv. Technol.*,

vol. 24, no. 8, pp. 723–731, Aug. 2013.

[82] H. Tsuji, K. Ikarashi, and N. Fukuda, “Poly(l-lactide): XII. Formation, growth, and morphology of crystalline residues as extended-chain crystallites through hydrolysis of poly(l-lactide) films in phosphate-buffered solution,” *Polym. Degrad. Stab.*, vol. 84, no. 3, pp. 515–523, Jun. 2004.

[83] H. Shinzawa, M. Nishida, T. Tanaka, and W. Kanematsu, “Accelerated Weathering-Induced Degradation of Poly(Lactic Acid) Fiber Studied by Near-Infrared (NIR) Hyperspectral Imaging,” *Appl. Spectrosc.*, vol. 66, no. 4, pp. 470–474, Apr. 2012.

[84] A. Copinet, C. Bertrand, S. Govindin, V. Coma, and Y. Couturier, “Effects of ultraviolet light (315 nm), temperature and relative humidity on the degradation of polylactic acid plastic films,” *Chemosphere*, vol. 55, no. 5, pp. 763–773, May 2004.

[85] M. Deroiné *et al.*, “Accelerated ageing of polylactide in aqueous environments: Comparative study between distilled water and seawater,” *Polym. Degrad. Stab.*, vol. 108, pp. 319–329, Oct. 2014.

[86] F. R. Beltrán, V. Lorenzo, M. U. de la Orden, and J. Martínez-Urreaga, “Effect of different mechanical recycling processes on the hydrolytic degradation of poly(l-lactic acid),” *Polym. Degrad. Stab.*, vol. 133, pp. 339–348, Nov. 2016.

[87] R. N. Darie, S. Vlad, N. Anghel, F. Doroftei, T. Tamminen, and I. Spiridon, “New PP/PLA/cellulose composites: effect of cellulose functionalization on accelerated weathering behavior (accelerated weathering behavior of new PP/PLA/cellulose composites),” *Polym. Adv. Technol.*, vol. 26, no. 8, pp. 941–952, Aug. 2015.

[88] D. Van Cong, N. T. T. Trang, N. V. Giang, T. D. Lam, and T. Hoang, “Effect of TiO2-Crystal Forms on the Photo-Degradation of EVA/PLA Blend Under Accelerated Weather Testing,” *J. Electron. Mater.*, vol. 45, no. 5, pp. 2536–2546, May 2016.

[89] E. Hablot, S. Dharmalingam, D. G. Hayes, L. C. Wadsworth, C. Blazy, and R. Narayan, “Effect of Simulated Weathering on Physicochemical Properties and

Inherent Biodegradation of PLA/PHA Nonwoven Mulches," *J. Polym. Environ.*, vol. 22, no. 4, pp. 417–429, Dec. 2014.

[90] I. Moura, G. Botelho, and A. V. Machado, "Characterization of EVA/PLA Blends When Exposed to Different Environments," *J. Polym. Environ.*, vol. 22, no. 1, pp. 148–157, Mar. 2014.

[91] D. Van Cong *et al.*, "Studies on the Degradation of Poly(Ethylene-co-vinylacetate)/Polylactides/TiO2 Nanocomposites Under Accelerated Weathering," *J. Nanosci. Nanotechnol.*, vol. 16, no. 9, pp. 9612–9620, Sep. 2016.

[92] I. Spiridon, O. M. Paduraru, M. F. Zaltariov, and R. N. Darie, "Influence of Keratin on Polylactic Acid/Chitosan Composite Properties. Behavior upon Accelerated Weathering," *Ind. Eng. Chem. Res.*, vol. 52, no. 29, pp. 9822–9833, Jul. 2013.

[93] R. Acioli-Moura and X. S. Sun, "Thermal degradation and physical aging of poly(lactic acid) and its blends with starch," *Polym. Eng. Sci.*, vol. 48, no. 4, pp. 829–836, Apr. 2008.

[94] I. Spiridon, K. Leluk, A. M. Resmerita, and R. N. Darie, "Evaluation of PLA–lignin bioplastics properties before and after accelerated weathering," *Compos. Part B Eng.*, vol. 69, pp. 342–349, 2015.

[95] B. S. Ndazi and S. Karlsson, "Characterization of hydrolytic degradation of polylactic acid/rice hulls composites in water at different temperatures," *Express Polym. Lett.*, vol. 5, no. 2, pp. 119–131, 2011.

[96] W. Yang, F. Dominici, E. Fortunati, J. M. Kenny, and D. Puglia, "Effect of lignin nanoparticles and masterbatch procedures on the final properties of glycidyl methacrylate-g-poly (lactic acid) films before and after accelerated UV weathering," *Ind. Crops Prod.*, vol. 77, pp. 833–844, 2015.

[97] V. P. Sajna, S. K. Nayak, and S. Mohanty, "Weathering and Biodegradation Study on Graft Copolymer Compatibilized Hybrid Bionanocomposites of Poly(Lactic Acid)," *J. Mater. Eng. Perform.*, vol. 25, no. 7, pp. 2895–2906, 2016.

[98] I. Spiridon, R. N. Darie, and H. Kangas, “Influence of fiber modifications on PLA/fiber composites. Behavior to accelerated weathering,” *Compos. Part B Eng.*, vol. 92, pp. 19–27, 2016.

[99] I. Spiridon, R. Nicoleta, D. Nita, M. Kozlowski, A. Nechita, and R. G. Ursu, “Influence of Accelerated Waethering on the Performance of Polylactic Acid based Materials,” *Cellul. Chem. Technol. Cellul. Chem. Technol*, vol. 50, pp. 5–6, 2016.

[100] O. Gil-Castell *et al.*, “Impact of hydrothermal ageing on the thermal stability, morphology and viscoelastic performance of PLA/sisal biocomposites,” *Polym. Degrad. Stab.*, vol. 132, pp. 87–96, Oct. 2016.

[101] C. Man *et al.*, “Poly (lactic acid)/titanium dioxide composites: Preparation and performance under ultraviolet irradiation,” *Polym. Degrad. Stab.*, vol. 97, no. 6, pp. 856–862, Jun. 2012.

[102] M. Pluta, M. Murariu, M. Alexandre, A. Galeski, and P. Dubois, “Polylactide compositions. The influence of ageing on the structure, thermal and viscoelastic properties of PLA/calcium sulfate composites,” *Polym. Degrad. Stab.*, vol. 93, no. 5, pp. 925–931, May 2008.

[103] G. Gorrasi, C. Milone, E. Piperopoulos, M. Lanza, and A. Sorrentino, “Hybrid clay mineral-carbon nanotube-PLA nanocomposite films. Preparation and photodegradation effect on their mechanical, thermal and electrical properties,” *Appl. Clay Sci.*, vol. 71, pp. 49–54, 2013.

[104] A. Finniss, S. Agarwal, and R. Gupta, “Retarding hydrolytic degradation of polylactic acid: Effect of induced crystallinity and graphene addition,” *J. Appl. Polym. Sci.*, vol. 133, no. 43, Nov. 2016.

[105] A. Buzarovska and A. Grozdanov, “Biodegradable poly(L-lactic acid)/TiO2 nanocomposites: Thermal properties and degradation,” *J. Appl. Polym. Sci.*, vol. 123, no. 4, pp. 2187–2193, Feb. 2012.

[106] W. Chávez-Montes, G. González-Sánchez, and S. Flores-Gallardo, “Poly-Lactide/Exfoliated C30B Interactions and Influence on Thermo-Mechanical

Properties Due to Artificial Weathering," *Polymers (Basel).*, vol. 8, no. 4, p. 154, Apr. 2016.

[107] W. Chávez-Montes, G. González-Sánchez, E. López-Martínez, P. de Lira-Gómez, L. Ballinas-Casarrubias, and S. Flores-Gallardo, "Effect of Artificial Weathering on PLA/Nanocomposite Molecular Weight Distribution," *Polymers (Basel).*, vol. 7, no. 4, pp. 760–776, Apr. 2015.

[108] M.-Y. Jo, Y. J. Ryu, J. H. Ko, and J.-S. Yoon, "Hydrolysis and thermal degradation of poly(L -lactide) in the presence of talc and modified talc," *J. Appl. Polym. Sci.*, vol. 129, no. 3, pp. 1019–1025, Aug. 2013.

[109] Y. Liu, W. Chen, and H.-I. Kim, "Synthesis, Characterization, and Hydrolytic Degradation of Polylactide/Poly(ethylene glycol)/Nano-silica Composite Films," *J. Macromol. Sci. Part A*, vol. 49, no. 4, pp. 348–354, Apr. 2012.

[110] M. Gardette, S. Thérias, J.-L. Gardette, M. Murariu, and P. Dubois, "Photooxidation of polylactide/calcium sulphate composites," *Polym. Degrad. Stab.*, vol. 96, no. 4, pp. 616–623, Apr. 2011.

[111] C. Kaynak and B. Sarı, "Accelerated weathering performance of polylactide and its montmorillonite nanocomposite," *Appl. Clay Sci.*, vol. 121, pp. 86–94, 2016.

[112] C. Kaynak and I. Kaygusuz, "Consequences of accelerated weathering in polylactide nanocomposites reinforced with halloysite nanotubes," *J. Compos. Mater.*, vol. 50, no. 3, pp. 365–375, Feb. 2016.

[113] C. Kaynak and A. R. Erdogan, "Mechanical and thermal properties of polylactide/talc microcomposites: before and after accelerated weathering," *Polym. Adv. Technol.*, vol. 27, no. 6, pp. 812–822, Jun. 2016.

[114] C. Kaynak and B. Dogu, "Effects of Accelerated Weathering in Polylactide Biocomposites Reinforced with Microcrystalline Cellulose," *Int. Polym. Process.*, vol. 31, no. 4, pp. 410–422, Aug. 2016.

[115] K. Tanaka, M. Miyamura, Y. Okamoto, T. Katayama, T. Katayama, and S. Yoshikawa, "Influence of Annealing Process on Crystallinity of Glass Fiber Reinforced Easily Degradable PLA Composites," *Key Eng. Mater.*, vol. 627, pp. 169–172, 2014.

[116] K. Y. Tshai, A. B. Chai, I. Kong, M. E. Hoque, and K. H. Tshai, “Hybrid Fibre Polylactide Acid Composite with Empty Fruit Bunch: Chopped Glass Strands,” *J. Compos.*, vol. 2014, pp. 1–7, 2014.

[117] Y. Meyva and C. Kaynak, “Toughening of Polylactide by Bio-Based and Petroleum-Based Thermoplastic Elastomers,” *Int. Polym. Process.*, vol. 30, no. 5, pp. 593–602, 2015.

[118] E. W. Fischer, H. J. Sterzel, and G. Wegner, “Investigation of the structure of solution grown crystals of lactide copolymers by means of chemical reactions,” *Kolloid-Zeitschrift und Zeitschrift für Polym.*, vol. 251, no. 11, pp. 980–990, 1973.

[119] M. Niaounakis, *Biopolymers : reuse, recycling, and disposal*. Elsevier Science, 2013.

[120] A. Araújo, G. L. Botelho, M. Silva, and A. V. Machado, “UV Stability of Poly(Lactic Acid) Nanocomposites,” *J. Mater. Sci. Eng. B*, vol. 3, no. 2, pp. 75–83, 2013.

[121] D. Ishikawa *et al.*, “High-speed monitoring of the crystallinity change in poly(lactic acid) during photodegradation by using a newly developed wide area NIR imaging system (Compovision),” *Anal. Bioanal. Chem.*, vol. 407, no. 2, pp. 397–403, Jan. 2015.